8-2015

Quantification of Variable Rate Irrigation Benefits and Spatial Variability in Root Zone Water Holding Capacity

Tsz Him Lo
University of Nebraska-Lincoln, tszhimlo@huskers.unl.edu

QUANTIFICATION OF VARIABLE RATE IRRIGATION BENEFITS AND SPATIAL VARIABILITY IN ROOT ZONE WATER HOLDING CAPACITY

by

Tsz Him Lo

A THESIS

Presented to the Faculty of

The Graduate College at the University of Nebraska

In Partial Fulfillment of Requirements

For the Degree of Master of Science

Major: Agricultural and Biological Systems Engineering

Under the Supervision of Professor Derek M. Heeren

Lincoln, Nebraska

August, 2015

QUANTIFICATION OF VARIABLE RATE IRRIGATION BENEFITS AND SPATIAL VARIABILITY IN ROOT ZONE WATER HOLDING CAPACITY

Tsz Him Lo, M.S.

University of Nebraska, 2015

Adviser: Derek Heeren

Variable rate irrigation (VRI) investment decisions require field-specific knowledge of benefits. The objective of this research was to help producers and consultants consider and quantify potential benefits of VRI. First, a conceptual model was developed for evaluating the public and/or private gain from adopting VRI where irrigation water supply is non-restrictive. Potential benefits were classified into three categories and were attributed to ten reasons. In the Central Plains at current prices, a small improvement in corn (maize) yield would make a large contribution to VRI profitability. Second, the potential irrigation withdrawal reduction from adapting VRI to spatial heterogeneity of root zone water holding capacity (*R*)—one particular benefit of VRI—was estimated for 49,224 center pivot irrigated fields in Nebraska. On each of these fields, the amount of *R* that is unutilized by conventional irrigation but can be mined annually by VRI was calculated from the statewide gridded Soil Survey Geographic database (gSSURGO). Over 51 mm of potential withdrawal reduction from this application of VRI was found on 2% of the analyzed fields. Third, based on field research, a method of conducting a field characterization of *R* was recommended for refining estimates of those withdrawal reductions and for informing VRI management. Field capacity (FC) was observationally determined by measuring in-situ soil water

content after the wet soil has had time to drain following substantial precipitation, and *R* was spatially predicted by regression with a densely known auxiliary variable. As compared with FC values computed from gSSURGO and pedotransfer function outputs, FC values computed according to the observational method were more effective in accounting for observed soil moisture patterns at the study site. The field characterization of *R*, therefore, may be advantageous on fields where the expected profit from mining unutilized *R* with VRI exceeds the cost of characterization. Future research should present field demonstrations of VRI profitability, provide guidance on VRI management, and produce transferable methods for and field-specific results of quantifying VRI benefits.

ACKNOWLEDGEMENTS

God, thank you for always carrying me with Your grace. You are my everything. Without You, I am and can do nothing.

Mom and Dad, thank you for always guiding me, supporting me, and praying for me. Thank you for never giving up on me despite all my failures. Thank you for enabling me to pursue my dream in this distant land.

Dr. Heeren, thank you for being my academic and spiritual mentor. Thank you for your example, your encouragement, and your prayers. Thank you for giving me freedom when I needed to roam and setting boundaries when I needed to focus.

Drs. Heeren, Luck, Martin, Eisenhauer, and Mateos, thank you for all the time and expertise you have unhesitatingly contributed to my research as my advisory committee.

Keith, Burdette, Alan, and Tyler, thank you for being a research team that was patient with and even made up for my mistakes and my inexperience. I could not have asked for more.

Our farmer-cooperators, thank you for being more generous and more accommodating than I could have ever imagined. It was truly a pleasure to work with you.

Drs. Arkebauer and Martin, thank you for generously lending us your research equipment.

Drs. Arkebauer, Franz, Irmak, Muñoz-Arriola, Walter-Shea, Yang, and Zygielbaum, thank you for our research discussions, which I found to be thought-provoking.

Drs. Eisenhauer, Erickson, Ferguson, Heeren, Klopfenstein, Luck, MacDonald, Martin, Marx, Suyker, Walter-Shea, Wardlow, Watson, and Weller, thank you for the knowledge and experience that you have shared through your courses.

Teresa of Biological Systems Engineering, Terri of Graduate Studies, and the International Student and Scholar Office staff, thank you for doing what you do day after day.

Officemates, thank you for your company and your enrichment of my past two years.

Chinese Christian Church of Lincoln, thank you for being my family here.

GRANT INFORMATION

This research was supported by the Water, Energy and Agriculture Initiative, which was made possible with funding from the Nebraska Corn Board, the Nebraska Soybean Board, the Agricultural Research Division at the University of Nebraska-Lincoln (UNL) and Nebraska Public Power District through the Nebraska Center for Energy Sciences Research at UNL.

TABLE OF CONTENTS

LIST OF FIGURES

LIST OF TABLES

CHAPTER 1: GENERAL INTRODUCTION AND CONCEPTUAL MODEL

1.1. Background and Justification

After over two decades of engineering innovation (Evans et al., 2013), variable rate irrigation (VRI; i.e., site-specific center pivot irrigation) has emerged as an effective and convenient means of customizing irrigation to parts of a field. With VRI, the application depth, intensity, and timing in as well as the spatial extent of each management zone can now be controlled at levels of precision that had been infeasible in the large fields of modern agriculture. However, adoption of this powerful technology has been slow. Evans et al. (2013) estimated that less than 500 speed control VRI systems and less than 200 more advanced VRI systems have been installed, and not all of them are being used to implement VRI for crop production.

Literature on the factors hindering VRI adoption points to the importance of economics (Evans and King, 2012; Evans et al., 2013). An opportunity for researchers in this context is providing guidance on VRI investment analysis. On one hand, researchers can encourage producers and service providers to consider all potential benefits of VRI. On the other hand, researchers can develop methods of estimating the magnitude of those benefits. With such guidance, producers can proceed to evaluate VRI investments in an informed manner.

1.2. Consideration of All VRI Potential Benefits

1.2.1. Conceptual Model

Diverse benefits of VRI have been enumerated in the literature. The conceptual model presented in this subsection serves as a clear and organized framework for

considering potential benefits when irrigation water supply is not restrictive. In this setting, fields were assumed to be currently managed to produce the best total yield under the constraints of conventional irrigation (CI; i.e., non-site-specific center pivot irrigation). An alternative conceptual model may be more appropriate when irrigation water supply is restrictive instead.

The impact of VRI benefits can reach beyond field boundaries. For example, reducing nitrogen (N) leaching with VRI not only decreases fertilizer budgets but may also improve the quality of drinking water and the environment. To evaluate the financial profitability of VRI, the quantities in the conceptual model should be parameterized to represent the private component of the benefits (i.e., changes in producers' revenue and expenses). However, to evaluate the overall gain from VRI, the quantities in the conceptual model should be parameterized to include the public component of the benefits (i.e., changes in societal and environmental well-being) as well.

In this conceptual model, VRI benefits were classified into three categories and attributed to ten reasons (table 1.1).

Table 1.1. Three categories of and ten reasons for VRI benefits where irrigation water supply is non-restrictive.

Categories of VRI benefits	Reasons for VRI benefits
ΔW = reduction of public and private cost of irrigation	*a* = avoidance areas
ΔX = reduction of public and private cost of agrochemicals (both material and application)	*e* = variable evapotranspiration
	f = variable crop water production function
	h = variable natural hydrological inputs
	k = first span sprinklers
	m = variable rate chemigation
ΔY = increase of public and private benefit of yield	*p* = variable pressure
	q = variable irrigation runoff potential
	r = variable root zone water holding capacity
	s = saturated areas

The reasons for VRI benefits are clarified below:

- Areas with no crop do not need to be irrigated or chemigated. With VRI, these areas can be skipped when irrigating or chemigating (Sadler et al., 2005).
- Evapotranspiration (ET) may be spatially heterogeneous when vegetation status and/or microclimate are different among a uniformly managed crop. ET may be spatially heterogeneous also when crops of diverse planting dates, maturity lengths, and/or species (Jensen and Haise, 1963) are grown concurrently on one field. With VRI, irrigation can be adjusted to match these differences in crop water use.
- Crop water production functions for the same season may be spatially heterogeneous within a field (Sadler et al., 2002). With VRI, each management zone can receive its profit-maximizing amount of seasonal irrigation. The impact of such management is expected to be the greatest for crops whose yield quantity (e.g., cotton; Grimes et al., 1969) or quality (e.g., winegrape; Matthews and Anderson, 1988) is maximized under mild deficit irrigation and is declined under full irrigation even when soils are not saturated.
- Natural hydrology may be spatially heterogeneous, causing differences in the amount of water that is added to the managed root zone by processes such as capillary rise, subsurface lateral flow, and infiltration of direct natural precipitation and of run-on. With VRI, irrigation can compensate for these differences in natural inputs of water.
- Sprinkler nozzles in the first span that have been oversized to avoid clogging release excessive flow rates. The resulting over-application of irrigation and chemigation can be corrected with VRI solenoid valves (Sadler et al., 2000).
- Variable rate chemigation may be difficult without VRI equipment. With VRI, chemigation and effluent application can be practiced on fields where the law

prohibits agrochemical and effluent applications onto the water bodies within the field (Sadler et al., 2005). Also, some agrochemical applications may be more cost-effective with variable rate chemigation than with other application methods. To prevent double-counting in the conceptual model, all changes in the costs of the irrigation water for chemigation should be counted towards ΔW, whereas all other cost changes related to variable rate chemigation should be counted towards ΔX.

- Pressure in the center pivot lateral may fluctuate due to topography and operation of corner-watering equipment. VRI solenoid valves can perform pressure regulators' function of maintaining flow rate under different pressures (D. L. Martin, personal communication, 2014; Appendix C).
- When enlarging sprinkler wetted diameters is infeasible or sub-optimal, gross irrigation may have been increased in areas with high potential for irrigation runoff, infiltrating the target amount while generating significant runoff. With VRI, splitting irrigation applications or reducing their intensity over these areas may enable the same amount of infiltration while decreasing gross irrigation and runoff (L. Mateos, personal communication, 2014; Appendix C).
- For a given management allowed depletion (Merriam, 1966), the target amount of soil water depletion is proportional to root zone water holding capacity (R). CI leaves a uniform depletion throughout the field, but VRI can tailor depletion to the R of each management zone (Ritchie and Amato, 1990; Chapter 2).
- Certain areas may be prone to saturation as a result of poor internal drainage, shallow water tables, convergent surface/subsurface lateral flow, or a combination thereof. Besides physiologically impairing yield (Kanwar et al. 1988), soil saturation may

indirectly lower yield by disrupting the operation of farm machinery. Plants may be physically damaged when center pivot towers have to be pulled out after getting stuck in a saturated area (W. L. Kranz, personal communication, 2015). Saturated cropped areas may be abandoned because they cannot be traversed by mechanical harvesters (Sadler et al., 2005) or other field equipment. With VRI, special management of these areas—as well as their contributing areas (see the eighth bullet point)—may reduce the extent and severity of saturation (Sadler et al., 2005).

The VRI benefits in each of the three categories were described by a conceptual equation (eqs. 1.1-1.3). The terms in the three equations may be positive, negative, or zero. Many of the ΔW and ΔX terms are related to the application of irrigation and chemigation at amounts closer to what is necessary and the concurrent decrease in the fraction of irrigation and agrochemicals that exits the field without benefiting the crop. Therefore, VRI can be described as a technology that improves the efficiency of irrigation and agrochemicals (D. L. Martin, personal communication, 2015).

$$\Delta W = \Delta W_a + \Delta W_e + \Delta W_f + \Delta W_h + \Delta W_k + \Delta W_m + \Delta W_p + \Delta W_q + \Delta W_r + \Delta W_s \qquad (1.1)$$

where

ΔW_a = irrigation cost reductions from withholding irrigation from avoidance areas

ΔW_e = irrigation cost reductions from adapting irrigation to spatial heterogeneity of ET

ΔW_f = irrigation cost reductions from adapting irrigation to spatial heterogeneity of crop water production function

ΔW_h = irrigation cost reductions from adapting irrigation to spatial heterogeneity of natural hydrological inputs

ΔW_k = irrigation cost reductions from eliminating over-irrigation under the first span

ΔW_m = irrigation cost reductions from practicing variable rate chemigation

ΔW_p = irrigation cost reductions from using VRI solenoid valves as flow control devices

ΔW_q = irrigation cost reductions from adapting irrigation to spatial heterogeneity of irrigation runoff potential

ΔW_r = irrigation cost reductions from adapting irrigation to spatial heterogeneity of R

ΔW_s = irrigation cost reductions from decreasing irrigation over (formerly) saturated areas.

$$\Delta X = \Delta X_a + \Delta X_e + \Delta X_f + \Delta X_h + \Delta X_k + \Delta X_m + \Delta X_p + \Delta X_q + \Delta X_r + \Delta X_s \qquad (1.2)$$

where

ΔX_a = agrochemical cost reductions from withholding agrochemicals from avoidance areas

ΔX_e = agrochemical cost reductions from reduced leaching of agrochemicals when irrigation is adapted to spatial heterogeneity of ET

ΔX_f = agrochemical cost reductions from reduced leaching of agrochemicals when irrigation is adapted to spatial heterogeneity of crop water production function

ΔX_h = agrochemical cost reductions from reduced leaching of agrochemicals when irrigation is adapted to spatial heterogeneity of natural hydrological inputs

ΔX_k = agrochemical cost reductions from eliminating over-chemigation under the first span

ΔX_m = agrochemical cost reductions from reduced application and leaching of agrochemicals when practicing variable rate chemigation

ΔX_p = agrochemical cost reductions from using VRI solenoid valves as flow control devices

ΔX_q = agrochemical cost reductions from reduced leaching of agrochemicals when irrigation is adapted to spatial heterogeneity of irrigation runoff potential

ΔX_r = agrochemical cost reductions from reduced leaching of agrochemicals when irrigation is adapted to spatial heterogeneity of R

ΔX_s = agrochemical cost reductions from reduced leaching and volatilization of agrochemicals in (formerly) saturated areas.

$$\Delta Y = \Delta Y_f + \Delta Y_m + \Delta Y_s \tag{1.3}$$

where

ΔY_f = yield benefit increase from adapting irrigation to spatial heterogeneity of crop water production function

ΔY_m = yield benefit increase from practicing variable rate chemigation

ΔY_s = yield benefit increase from reducing extent and/or severity of prolonged saturation.

This conceptual model of VRI benefits was summarized by a triple Venn diagram (fig. 1.1).

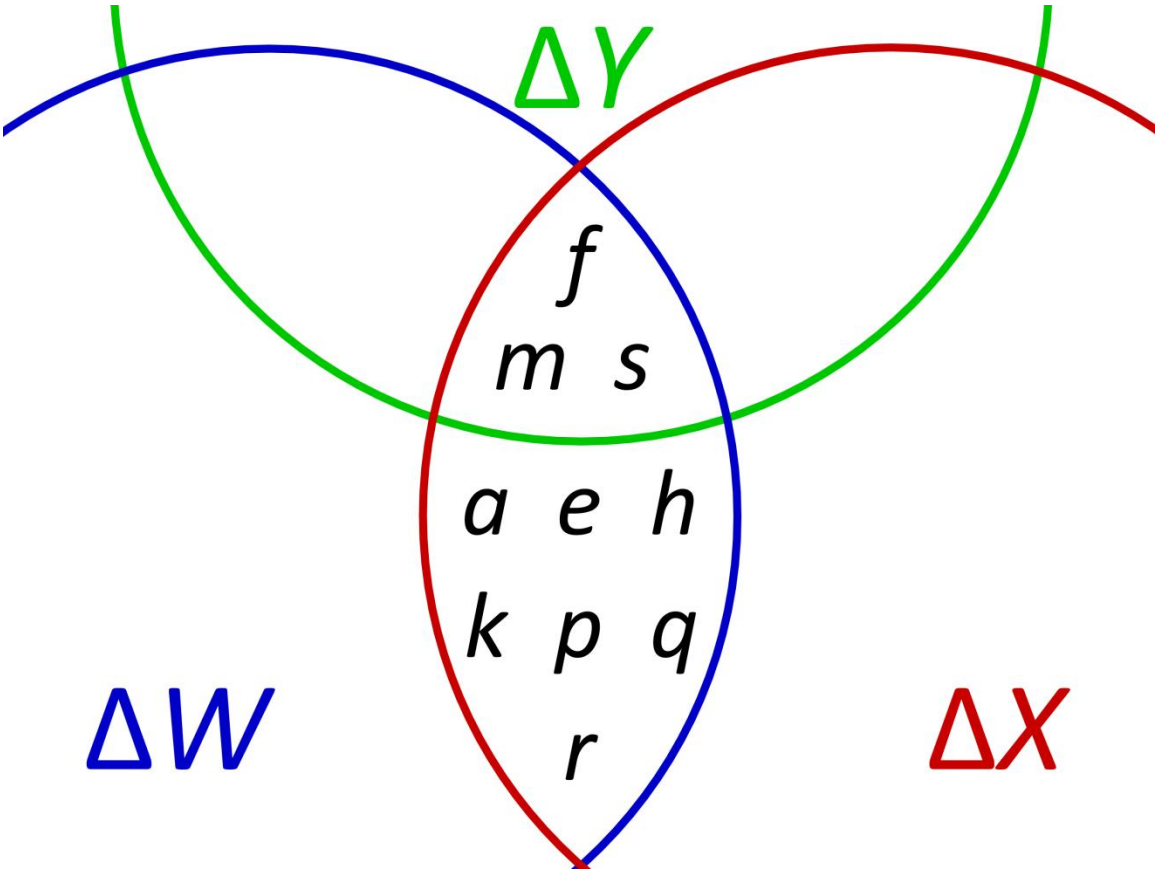

Figure 1.1. Conceptual diagram of VRI benefits where irrigation water supply is non-restrictive; the lowercase letters inside each circle are the reasons for benefits that contribute to each category of benefits (see table 1.1 for the definitions of the letters).

The VRI benefits ΔW, ΔX, and ΔY were simplified as an annual uniform series. Assuming real (vs. nominal) prices and the real discount rate (i; also known as "interest rate") were constant over an amortization period of n years (i.e., equal inflation rates), the present value of this series (PV) were calculated with equation 1.4.

$$PV = \sum_{t=1}^{n} \frac{(\Delta W + \Delta X + \Delta Y)}{(1+i)^t} = (\Delta W + \Delta X + \Delta Y)\frac{(1+i)^n - 1}{i(1+i)^n} \quad (1.4)$$

where t = years since the VRI system began operation.

In the absence of external incentives and disincentives, VRI investment would be favored if PV exceeded the total cost (C_v) of VRI. Researchers and practitioners alike are

invited to use this conceptual model when considering all VRI potential benefits and when evaluating VRI investments.

1.2.2. Current Affordability of VRI

With the conceptual model in place, the magnitude of benefits required to pay for a VRI investment under current market conditions was illustrated for corn (maize) in parts of the Central Plains where irrigation water supply is non-restrictive. The private component of VRI benefits was exclusively considered because the question at hand was about private financial affordability. The terms ΔW, ΔX, and ΔY were thus assumed to be well-expressed in terms of pumping price, N fertilizer price, and corn price, respectively.

Pumping prices can vary drastically among fields due to differences in energy requirements and energy prices. A low pumping price may be represented by an electric pump providing 0 m of lift (i.e., surface water source) and 100 kPa of pressure while consuming anytime interruptible electricity at \$0.0624/kWh (NPPD, 2014). A high pumping price may be represented by a diesel pump providing 60 m of lift and 400 kPa of pressure while consuming farm diesel at \$0.851/L. This diesel price was the 2011-2015 average of the average farm diesel price in Iowa reported during the first half of each April (AMS, 2015a). Both of these irrigation pumps were assumed to be operating at 100% of the Nebraska Pumping Plant Performance Criteria (NPPPC; Kranz, 2010). Neglecting changes in efficiency and total dynamic head as system flow rates decrease with VRI, the two pumping prices were \$0.0026/m^3 and \$0.0947/m^3 of gross irrigation.

N fertilizer prices can also vary among fields. A low N fertilizer price may be represented by anhydrous ammonia (82% N) at \$856/Mg. A high N fertilizer price may be represented by urea ammonium nitrate (UAN; 28% N) at \$406/Mg. Both of these

prices were the 2011-2015 average of the average price of the respective N fertilizer in Iowa reported during the first half of each April (AMS, 2015a). The two N fertilizer prices can be expressed also as $1.04/kg of N and $1.45/kg of N.

In contrast, corn prices have varied less spatially and more temporally in recent years. The 2010-2014 average corn cash price in Grand Island, Nebraska, on the last weekday of each October, which was $208/Mg (AMS, 2015b), was used in this illustration.

An initial capital cost of $400/ha, which is within the range of $200-500/ha given by Evans et al. (2013), was assumed for a zone control VRI system (defined in Chapter 2) irrigating 50 ha. Neglecting any additional operation and maintenance cost of VRI relative to CI, C_v was $20,000. The annual sum of ΔW, ΔX, and ΔY must be $2,590 at breakeven for i = 5% and n = 10 years (eq. 1.4).

For each category of VRI benefits, the annual field-average change in gross irrigation, N fertilizer rate, or corn yield to break even on the VRI investment was calculated using the example prices as if that category alone was contributing towards C_v (table 1.2). The annual field-average changes at breakeven were each inversely proportional to the corresponding price.

Table 1.2. The annual field-average change in gross irrigation, N fertilizer application, or corn yield necessary to pay for a $400/ha zone control VRI system single-handedly over ten years given the example price; the example prices and the discount rate of 5% are assumed to be constant in real terms (i.e., equal inflation rates).

Category of VRI benefit	Example price	Annual field-average change at breakeven
irrigation cost reduction	\$0.0026/m^3 (\$3/ac-ft) of gross irrigation	-1,975 mm (-78 in.) of gross irrigation
	\$0.0947/m^3 (\$117/ac-ft) of gross irrigation	-55 mm (-2 in.) of gross irrigation
agrochemical cost reduction	\$1.04/kg (\$0.47/lb) of N	-50 kg/ha (-44 lb/ac) of N
	\$1.45/kg (\$0.66/lb) of N	-36 kg/ha (-32 lb/ac) of N
yield benefit increase	\$208/Mg (\$5.30/bu) of corn at 15.5% moisture	+0.25 Mg/ha (+4 bu/ac) of corn at 15.5% moisture

Individually, the required gross irrigation reductions and the required N fertilizer reductions appeared to be large. For example, when the low pumping price was assumed, the annual field-average change in gross irrigation at breakeven was several times larger than the average seasonal gross irrigation requirement for corn even in the western Central Plains (NDNR, 2006). These two categories of VRI benefits, overall, are more likely to pay for VRI investments jointly rather than separately. Yet when the high pumping price was assumed, the present value of ΔW_r alone may exceed C_v on 1.5% of center pivot irrigated fields in Nebraska based on data from Chapter 2.

The required yield increase, in contrast, appeared to be small, as observed by Marek et al. (2001). ΔY_s alone would equal C_v if a mere 1.4 ha (3.4 ac) had zero or unharvestable yield under CI but would have 9 Mg/ha (143 bu/ac) yield under VRI. Nonetheless, alternative ways of managing saturated areas, such as grading and drainage, should be also considered in this situation.

This analysis accomplished two purposes. On one hand, it indicated that demonstrating large benefits from VRI for corn in parts of the Central Plains where irrigation water supply is non-restrictive may be difficult under current market conditions if only irrigation cost reductions (except with high pumping prices) or only agrochemical cost reductions were quantified. This finding is in consensus with the majority of studies reviewed in Evans and King (2012). On the other hand, this analysis suggested that VRI might be financially profitable under current market conditions on some of the more heterogeneous corn fields in parts of the Central Plains where irrigation water supply is non-restrictive, especially when all three categories of benefits are considered in combination.

1.3. On the Estimation of the Magnitude of VRI Benefits

The discussion so far remained theoretical. The practical hurdles encountered in VRI investment analysis had not been addressed. Evans et al. (2013) made an insightful claim that producers need to be educated on the management of VRI and need to be shown the increased profits from VRI implementation in their region. Furthermore, producers and service providers need to know how to assess the potential magnitude of the VRI benefits on a specific field before making a VRI investment decision.

This third research need is very complementary to the other two. Results from field trials at a nearby experimental station or a producer's field may convince producers to be more receptive to the idea of adopting VRI. However, the fields farmed by these producers are not identical to where the field trials are conducted. VRI investment analysis thus necessitates field-specific estimates of the magnitude of VRI benefits. Nevertheless, how to manage VRI to maximize the achieved gain, as well as how the

achievable magnitude of benefits might differ from their potential magnitude, have to be discovered through field trials.

VRI benefits diverge in terms of the need for further research on the estimation of their magnitude. For example, the benefits attributed to reasons *a*, *k*, and *p* (table 1.1) can already be quantified with little uncertainty. Yet, the VRI benefits associated with variable crop water production function are difficult to quantify accurately. Predicting production functions has been challenging because both water production functions and N production functions have been noted to display interdependence and interannual variability (Sadler et al., 2002; Stone et al., 2010; Rudnick and Irmak, 2013). This challenge calls for long-term research relating measured production functions to weather variables. Additionally, future VRI research can further investigate yield losses related to excessive water, which is less understood (S. Irmak, personal communication, 2014) and more difficult to predict (D. M. Heeren, personal communication, 2015) than yield losses related to insufficient water.

Quantifying VRI benefits associated with soil N also demands long-term studies. In soils rich in organic matter content, the history of N fluxes may have an enduring impact because of transformations between inorganic and organic pools of N. Lowering N leaching and fertilizer rate for just one year, therefore, might exhibit a different effect on N losses and crop yield than maintaining the two decreases for several years. In conclusion, the benefits ΔX_e, ΔX_f, ΔX_h, ΔX_m, ΔX_q, ΔX_r, and ΔX_s must be determined after soil N has reached equilibrium under the new irrigation and N fertilization practices.

The following two chapters were focused on estimating the magnitude of the VRI benefits from adapting to spatial heterogeneity of *R*. Chapter 2 accessed public

geospatial data to analyze 49,224 center pivots in Nebraska, whereas Chapter 3 collected field data to analyze one center pivot in south central Nebraska. When a producer begins to consider VRI, the method in Chapter 2 provides an initial estimate of the benefits from adapting VRI to spatial heterogeneity of *R*. When a producer approaches the final VRI investment decision, the method in Chapter 3 refines this estimate and informs management of the pending VRI system.

All the quantitative analyses in these chapters were limited in scope to the private component of VRI benefits. The development and application of simple methods to quantify the public component of VRI benefits would be welcomed. The results generated would inform governmental and civil entities that can influence the policy environment for VRI adoption and sponsor VRI research.

1.4. References

AMS. (2015a). Iowa Production Cost Report (Bi-Weekly). Report No. NW_GR210. Washington, D.C.: United States Department of Agriculture. Retrieved from http://search.ams.usda.gov/mnsearch/mnsearch.aspx

AMS. (2015b). Nebraska Grain Elevator Bids. Report No. WH_GR111. Washington, D.C.: United States Department of Agriculture. Retrieved from http://search.ams.usda.gov/mnsearch/mnsearch.aspx

Evans, R. G., & King, B. A. (2012). Site-Specific Sprinkler Irrigation in a Water-Limited Future. *Trans. ASABE*, 55(2), 493-504. doi: 10.13031/2013.41382

Evans, R. G., LaRue, J., Stone, K. C., & King, B. A. (2013). Adoption of site-specific variable rate sprinkler irrigation systems. *Irrig. Sci.*, 31(4), 871-887. doi: 10.1007/s00271-012-0365-x

Grimes, D. W., Yamada, H., & Dickens, W. L. (1969). Functions for Cotton (*Gossypium hirsutum* L.) Production from Irrigation and Nitrogen Fertilization Variables: I. Yield and Evapotranspiration. *Agron. J.*, 61(5), 769-773. doi: 10.2134/agronj1969.00021962006100050035x

Jensen, M. E., & Haise, H. R. (1963). Estimating Evapotranspiration From Solar Radiation. *J. Irrig. Drainage Div. ASCE*, 89(4), 15-44.

Kanwar, R. S., Baker, J. L., & Mukhtar, S. (1998). Excessive Soil Water Effects at Various Stages of Development on the Growth and Yield of Corn. *Trans. ASAE*, 31(1), 133-141. doi: 10.13031/2013.30678

Kranz, W. L. (2010). Updating the Nebraska Pumping Plant Performance Criteria. In *Proc. 22nd Ann. Central Plains Irrig. Conf.* Colby, Kans.: Central Plains Irrigation Association.

Marek, T., Cox, E., Almas, L., & Amosson, S. (2001). The Feasibility of Variable Rate Irrigation with Center Pivot Systems in the Northern Texas High Plains. ASAE Paper No. 011117. St. Joseph, Mich.: ASAE. doi: 10.13031/2013.3443

Matthews, M. A., & Anderson, M. M. (1988). Fruit Ripening in *Vitis vinifera* L.: Responses to Seasonal Water Deficits. *American J. Enology Viticulture*, 39(4), 313-320.

Merriam, J.L. (1966). A Management Control Concept for Determining the Economical Depth and Frequency of Irrigation. *Trans. ASAE*, 9(4), 492-498.

NDNR. (2006). Net Corn Crop Irrigation Requirement. Lincoln, Neb.: Nebraska Department of Natural Resources. Retrieved from http://www.dnr.ne.gov/swr/net-irrigation-requirement-map-may-2006

NPPD. (2014). Electric Service For Irrigation. Columbus, Neb.: Nebraska Public Power District. Retrieved from http://www.nppd.com/assets/irrigationbrochure.pdf

Ritchie, J. T., & Amato, M. (1990). Field Evaluation of Plant Extractable Soil Water for Irrigation Scheduling. *Acta Horticulturae*, 278: 595-616.

Rudnick, D. R., & Irmak, S. (2013). Impact of Water and Nitrogen Management Strategies on Maize Yield and Water Productivity Indices under Linear-Move Sprinkler Irrigation. *Trans. ASABE*, 56(5), 1769-1783. doi: 10.13031/trans.56.10215

Sadler, E. J., Camp, C. R., Evans, D. E., & Millen, J. A. (2002). Spatial Variation of Corn Response to Irrigation. *Trans. ASAE*, 45(6), 1869-1881. doi: 10.13031/2013.11438

Sadler, E. J., Evans, R. G., Buchleiter, G. W., King, B. A., & Camp, C. R. (2000). Design Considerations for Site Specific Irrigation. In *Proc. 4th Decennial Natl. Irrig. Symp.*, pp. 304-315. St. Joseph, Mich.: ASAE

Sadler, E. J., Evans, R., Stone, K. C., & Camp, C. R. (2005). Opportunities for conservation with precision irrigation. *J. Soil Water Cons.*, 60(6), 371-378.

Stone, K. C., Camp, C. R., Sadler, E. J., Evans, D. E., & Millen, J. A. (2010). Corn Yield Response to Nitrogen Fertilizer and Irrigation in the Southeastern Coastal Plain. *Appl. Eng. Agric.*, 26(3), 429-438. doi: 10.13031/2013.29954

CHAPTER 2: POTENTIAL IRRIGATION REDUCTIONS FROM INCREASING PRECIPITATION UTILIZATION WITH VARIABLE RATE IRRIGATION [1]

2.1. Abstract

Methods to quantify the magnitudes of the potential benefits of variable rate irrigation (VRI) on unsampled fields have not been proposed. In this research, the field-average amount of root zone available water capacity (*R*) that is unutilized (*U*) by conventional irrigation (CI) served as an indicator of the potential for irrigation reductions from increasing precipitation utilization with VRI. Based on the values of *U* that were calculated using publicly available data for 49,224 center pivot irrigated fields in Nebraska, this application of VRI may enable significant irrigation reductions on a minority of analyzed fields. Statewide, however, these potential irrigation reductions may be small compared to total seasonal irrigation. At current VRI and pumping energy prices, pumping energy savings alone may fail to justify VRI adoption on most fields in Nebraska. Producers are encouraged to consider all potential benefits during the VRI investment decision process. Although the prevalence of fields with large *U* differed among counties and among soil associations, ruling out the occurrence of either small or large *U* in a county or soil association might be difficult. The research findings should be useful to producers considering VRI and other entities interested in the potential impact of this particular application of VRI.

[1] Previous version submitted as a meeting paper for the 2015 Emerging Technologies for Sustainable Irrigation symposium:
Lo, T., Heeren, D. M., Mateos, L., Luck, J. D., Martin, D. L., & Eisenhauer, D. E. (2015). Potential Irrigation Reductions From Increasing Precipitation Utilization With Variable Rate Irrigation. ASABE Paper No. 152147702. St. Joseph, Mich.: ASABE.

2.2. Introduction

Variable rate irrigation (VRI), in the words of Evans et al. (2013), is "the ability to spatially vary water application depths across a field to address specific soil, crop, and/or other conditions". For center pivots, VRI is currently accomplished by two mechanisms. Speed control varies the fraction of time that the outermost tower is moving, so application depth can be different in each sector of the field (fig. 2.1a). Nozzle control varies the fraction of time that each sprinkler or bank of sprinklers is turned on, so application depth can be different angularly and radially. Both mechanisms may be integrated for zone control VRI (fig. 2.1b).

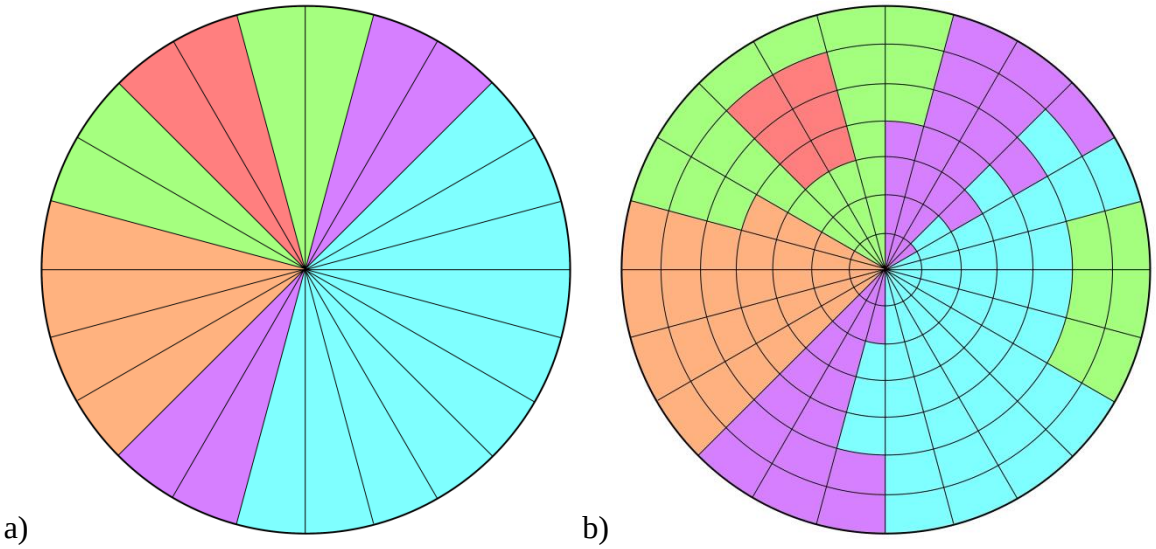

a) b)

Figure 2.1. Example prescription map for a) a speed control and b) a zone control variable rate irrigation (VRI) center pivot; each color indicates a different irrigation application depth.

Like other precision agricultural technologies, VRI facilitates the adaptation of management to known field heterogeneity and offers opportunities for improved profitability and environmental stewardship, such as:

- variable rate chemigation of fertilizers and pesticides;

- irrigation of crops grown concurrently in the same field but with diverse water requirements due to differences in planting dates, maturity lengths, or even species;
- reduction of application intensities over sectors with poor infiltration capacity when switching to sprinklers with larger wetted diameters is impractical or not preferred;
- avoidance of over-irrigation, which can damage yield due to promotion of plant diseases, decrease in nutrient availability, and limited root growth and function (Irmak, 2014); and
- transfer of excess irrigation water from fully irrigated soils to deficit irrigated soils for yield-increasing transpiration when water supply is inadequate for full irrigation throughout the field.

However, an appropriate way to predict the potential magnitude of VRI's proposed benefits on farmers' fields has not been developed. Previous research quantified some of VRI's benefits on several intensely studied fields by conducting simulations (Nijbroek et al., 2003; DeJonge et al., 2007; Hedley and Yule, 2009) or field experiments (King et al., 2006; Khalilian et al., 2008; Hillyer and Higgins, 2014). With the diversity among fields in their levels of spatial variability, it is unclear how those research results can be extrapolated to inform VRI investment decisions on other fields.

This chapter describes a method to estimate on unsampled fields the magnitude of one of VRI's many possible benefits: irrigation reductions enabled by additional utilization of soil water captured from rainfall. This benefit exists for regions where precipitation causes irrigated soils to exceed their field capacities before or early in the

irrigation season. In the Central Plains, average precipitation between April and June ranges from 175 mm (46% of annual average) at Scottsbluff, Nebraska, in the semi-arid west and 320 mm (38% of annual average) at Falls City, Nebraska, in the sub-humid east (Prism Climate Group, 2012). Consequently, the managed root zone is generally refilled in the spring. The idea of scheduling irrigation to deplete the stored water by the end of the growing season and letting it be naturally replenished was put forth by Woodruff et al. (1972), as cited in Lamm et al. (1994). In comparison to keeping the managed root zone full throughout the growing season, "planned soil moisture depletion" (Woodruff et al., 1972) reduces not only pumping expenses but also the leaching of nitrate, carried by water draining out of the root zone after rain infiltrates into an already wet soil. With conventional irrigation (CI; i.e., non-site-specific irrigation), though, this strategy cannot be implemented to its maximum extent on fields with a variety of root zone available water capacity (*R*) values. As CI is typically managed to avoid water stress in most of the field, it treats the entire field as having a small *R*, thus leaving a small, uniform depletion but a variable amount of readily available water (Allen et al., 1998) across the field. In other words, the soils with larger *R* have unutilized *R*. VRI, in contrast, can capitalize on this unutilized *R* by applying less irrigation to these soils and allowing more stored rainwater to be extracted from them. An early study on this concept was conducted by Ritchie and Amato (1990). Therefore, VRI empowers farmers to further increase energy savings and further decrease nitrogen loading into groundwater beyond what can be achieved with CI planned soil water depletion. The reduction of nitrate leaching may be an important public benefit of VRI in communities where high nitrate concentrations in the groundwater have become a significant problem for drinking water supplies. It is

worth noting that once the spatial distribution of *R* within a field is well-characterized, generating prescription maps to increase precipitation utilization with VRI is straightforward. So, this particular application of VRI is ready to be adopted by farmers to benefit themselves and the public.

The method introduced by this study is applied to 49,224 center pivot irrigated fields in Nebraska to:

1. describe the statistical distribution of field-average unutilized *R* under CI for Nebraska's center pivot irrigated fields;
2. analyze the geographical distribution of the fields with large field-average unutilized *R* in relationship to counties and soil associations;
3. assess the potential regional impact of irrigation reductions from increasing precipitation utilization with VRI; and
4. infer about the economics of adopting VRI solely for irrigation reductions from increasing precipitation utilization.

2.3. Methods

A main data source for this study was the gridded Soil Survey Geographic database (gSSURGO; NRCS, 2014). Unlike its vector-formatted counterpart, which was used in Lo et al. (2014), the raster-formatted gSSURGO conveniently packaged the spatial and tabular soil information for the state of Nebraska into one database. In gSSURGO, each contiguous area with similar soils has been delineated as a map unit (fig. 2.2). Each distinct soil within a map unit has been designated as a component that composed a percentage of the map unit. In turn, the soil profile of each component has been divided into horizons, each with a top depth, a bottom depth, and an available water

capacity (AWC). For all soil properties (i.e., percent composition, top depth, bottom depth, AWC), the "representative" value (NRCS, 2014) was exclusively taken in this study.

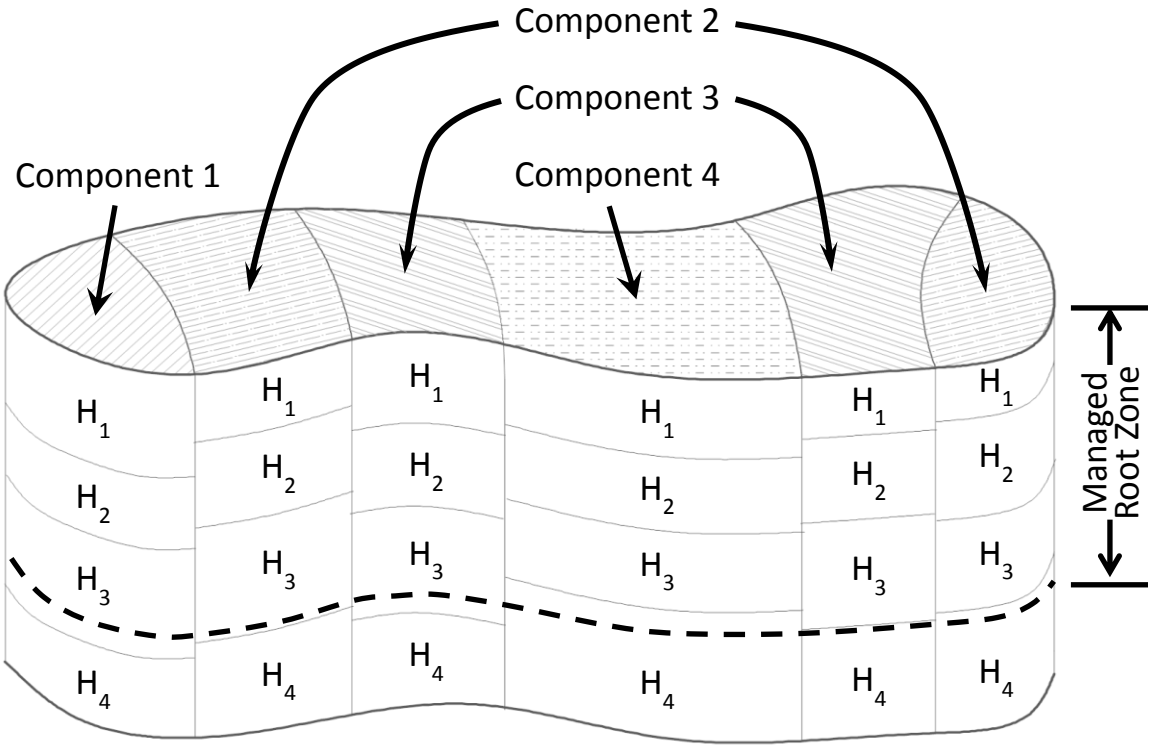

Figure 2.2. Diagram of a soil map unit in the gridded Soil Survey Geographic database (gSSURGO; NRCS, 2014); the *f*th soil horizon from the soil surface is labeled as H_f.

The core calculations were completed by running a Python script (Python, 2012; Appendix A) inside ArcGIS (ArcGIS, 2013). Horizons, components, and map units were excluded from the calculations if they met certain criteria (table 2.1). These criteria stipulated when to reject the data and instead assume that it can be well-represented by what was included.

Table 2.1. Criteria for excluding horizons, components, and map units from the calculations of root zone water holding capacity (*R*) for each component and map unit in Nebraska.

	If AWC or *R* is…		Also excluded if:
	zero:	negative:	
Horizon	–	excluded, except assumed zero for rock horizon	• missing top depth or bottom depth; • missing AWC, except assumed zero for rock horizon; or • horizons depths were discontinuous
component	excluded	excluded	• managed root zone not entirely covered by included horizons; or • percent composition was negative or over 100%
map unit	excluded	excluded	• the sum of the percent compositions of excluded and missing/excess components was at least 10%

To begin, the *R* of every component was determined. Starting at the soil surface, each horizon's AWC was multiplied by the horizon's thickness and then summed (eq. 2.1). This computation ended at the bottom of the managed root zone—assumed to occur at a depth of 120 cm or at the top depth of the first "lithic bedrock" or "paralithic bedrock" restrictive layer (NRCS, 2014), whichever was shallower.

$$R_k = \sum_{f}^{g} \left[\left(\min\left(z_{B,f}, d_k \right) - z_{T,f} \right) \times AWC_f \right] \tag{2.1}$$

where

k = index for the included components within a map unit (-)

R_k = R of component k (mm)

f = index for the included horizons in component k (-)

g = number of included horizons at least partially within the managed root zone of component k (-)

$z_{B,f}$ = bottom depth of horizon f (mm)

d_k = depth of the managed root zone in component k (mm)

$z_{T,f}$ = top depth of horizon f (mm)

AWC_f = AWC of horizon f (cm^3/cm^3).

Subsequently, each component's R was weighted by the component's percent composition and then averaged to obtain an average R for the map unit (eq. 2.2). Whenever the percent compositions of included components did not sum to 100% in an included map unit, they were normalized to 100%.

$$R_j = \frac{\sum_{k}^{s} (q_k R_k)}{\sum_{k}^{s} q_k} \tag{2.2}$$

where

j = index for the included map units within a field (-)

R_j = R of map unit j (mm)

s = number of included components in map unit j (-)

q_k = percent composition of component k, as a decimal (-).

Another main data source of this study was the 2005 Nebraska center pivots data layer (CALMIT, 2007). It outlined the state's "active" center pivots during the 2005 growing season that were identified from satellite and aerial imagery (CALMIT, 2007). The original 52,127 polygons underwent four filtering steps. First, the polygons were clipped by a data layer marking the borders of Nebraska (NRCS, 2009a). The twelve polygons that were entirely outside the state were removed. Second, the polygons were

converted to a center pivot raster matching the datum, grid size, and projection of gSSURGO. This step paired each center pivot cell with a gSSURGO cell. Each center pivot cell was not shared by polygons but was always assigned to the largest polygon that at least partially overlapped the center pivot cell. In the event of a tie between equally large polygons, the polygon with the larger feature identification number (FID) was given priority. Twenty-seven polygons were eliminated because no center pivot cells were assigned to them. Third, the 2728 remaining polygons with less than 2024 cells of 10 m × 10 m (50 ac) were discarded. The intent of this step was to exclude artifacts from the mapping process and fields that were less likely to be considered for VRI due to their small area. Fourth, the 136 remaining polygons were omitted because less than 90% of their cells corresponded to gSSURGO cells that belonged to included map units. The assumption that the area with excluded map units could be well-represented by the area with included map units was deemed to be unsuitable for those polygons. The 49,224 final polygons (94% of the original number) were analyzed in this study to represent all the center pivot irrigated fields in Nebraska. For each of these fields, only the *R* values of the corresponding gSSURGO cells that belonged to included map units were accepted as the *R* values for the field, but the total cell area of the field was preserved as the field area. From this point onward until the limitations subsection, excluded map units and excluded polygons were no longer be discussed.

This study made several assumptions that are common among one-dimensional soil water balance models. All soils were assumed to be at their field capacities at least once before or early in the irrigation season. From when the next irrigation application starts to when the growing season ends, the water fluxes of rainfall infiltration,

evapotranspiration, lateral flow, and capillary rise/deep percolation were assumed to be uniform across the field. As for irrigation, CI was assumed to be uniform across the field, whereas VRI was assumed to be uniform within every soil map unit.

Under CI planned soil moisture depletion, a certain *R* within the field was selected, and a constant fraction of this *R* was depleted throughout the field by the end of the growing season. The depletion fraction could be called the management allowed depletion (*MAD*) (Merriam, 1966), and the selected *R* could be called the CI management *R* (R_p). If an aggressive *MAD* was adopted, then the percentile of all *R* values that were less than R_p, which could be called the CI management percentile (*p*), may be under-irrigated. To strike a balance between deep percolation and the risk of water stress, the target *p* was 10% for all fields. When increasing precipitation utilization with VRI, however, each map unit was depleted to the *MAD* of its *R*, and the amount of *R* that exceeded R_p could be utilized. The end-of-season depletion with CI versus VRI, as well as *R* that was left unutilized by CI but could be utilized by VRI, were shown in figure 2.3.

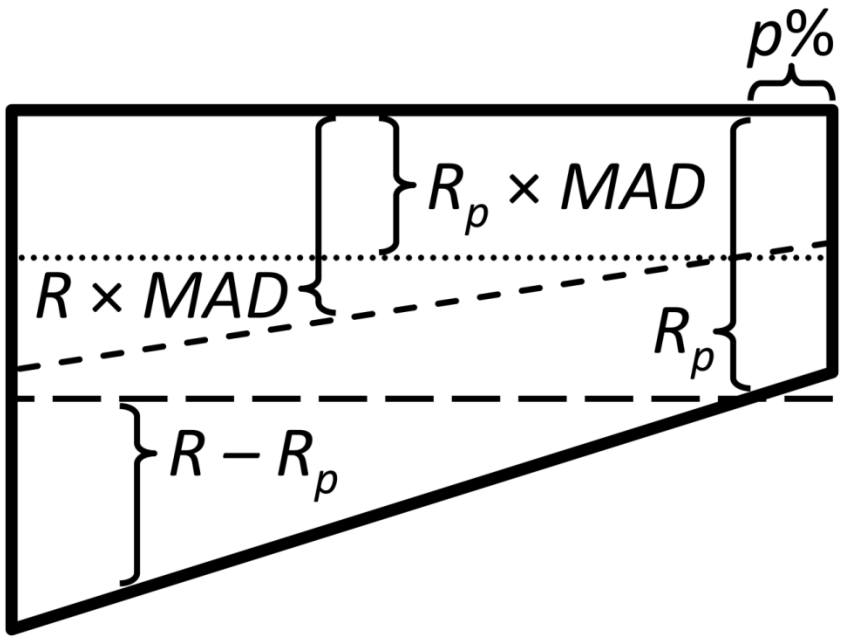

Figure 2.3. Spatial heterogeneity of root zone water holding capacity (*R*) as represented by varying distance between trapezoid legs; end-of-season depletion is *MAD* of *p*th percentile *R* (R_p) with conventional irrigation (CI; dotted line) but can be *MAD* of *R* with VRI (short dashes); $R - R_p$ (distance below long dashes) is *R* unutilized by CI.

The quantity $1 - p$ can be likened to irrigation adequacy. In the framework of irrigation adequacy, *R* is perfectly uniform, but the adequacy fraction of the field receives more water than required because irrigation is nonuniform. In the framework of this study, CI is perfectly uniform, but $1 - p$ of the field end the growing season with depletions smaller than *MAD* of *R* because *R* is nonuniform.

In this study, every field's statistical distribution of *R* was discrete because every field was composed of discrete map units, each with one *R* value. So, whenever the actual *p* could not be equal to 10%, the calculations erred on the side of protecting yield. Hence, R_p was chosen as the largest *R* within the field that was greater than at most 10% of all the field's *R* values.

U, defined as the field-average unutilized *R* under CI planned soil moisture depletion, has the dimension of depth (e.g., mm) and was computed as follows:

$$U = \sum_{j=1}^{m} \left[\left(R_j - R_p \right) \left(\frac{A_j}{A_{inc}} \right) \right] = R_a - R_p \quad (2.3)$$

where

j = index for the map units within the field (-)

m = number of map units within the field (-)

A_j = field area that belonged to map unit j (ha)

A_{inc} = total field area that belonged to included map units (ha)

R_a = area-weighted average R within the field (mm).

As U increased, the potential for irrigation reductions from increasing precipitation utilization with VRI also increased. To discover how the prevalence of large U values might differ between sub-regions of Nebraska, the fields were grouped by counties (NRCS, 2009b) and soil associations (Conservation and Survey Division, 2009) based on the centroids of the center pivot polygons. The number and fraction of fields within various ranges of U were then calculated for each county and soil association.

To increase precipitation utilization beyond CI planned soil moisture depletion, the seasonal net irrigation onto every map unit could be reduced by $(R_j - R_p) \times MAD$. Consequently, Δd_r, the field-average potential depth of seasonal gross irrigation reductions from increasing precipitation utilization with VRI, was estimated as follows:

$$\Delta d_r = \sum_{j=1}^{m} \left[\frac{\left(R_j - R_p \right) MAD}{E_a} \left(\frac{A_j}{A_{inc}} \right) \right] = \frac{U \times MAD}{E_a} \quad (2.4)$$

where E_a = application efficiency, as a decimal (-).

MAD and E_a were assumed to be 0.5 (Kranz et al., 2008a) and 0.85 (Kranz et al., 2008b), respectively, for both CI and VRI. The 15% inefficiency accounted for irrigation

water that was pumped but was never stored in the managed root zone (e.g., droplet evaporation, surface runoff, irrigation season deep percolation triggered by systematic irrigation nonuniformity). It did not include off-season deep percolation or in-season deep percolation triggered by rainfall. If a higher E_a could be achieved with VRI, then VRI would provide greater gross irrigation reductions than Δd_r as estimated by equation 2.4. ΔV_r, a field's potential volume of seasonal gross irrigation reductions from increasing precipitation utilization with VRI, was Δd_r multiplied by the field's total cell area.

Yet where water supply is inadequate for full irrigation, producers will not be interested in reducing irrigation with VRI. On the contrary, current economics will drive them to apply as much irrigation as they can to maximize yield, whether with CI or VRI. Without knowledge of each field's water supply situation, irrigation reductions were not calculated for any fields whose center pivot polygon centroid fell within the four Natural Resources Districts (NRDs; Nebraska Department of Natural Resources, 2011) that enforce NRD-wide groundwater quantity allocations. As opposed to some of the sub-area allocations elsewhere in the state, the NRD-wide multi-year allocations in the South Platte, Upper Republican, Middle Republican, and Lower Republican NRDs are more severe and less likely to be sufficient for full irrigation throughout the allocation period.

Although the potential irrigation reductions from increasing precipitation utilization with VRI is only one of VRI's many possible benefits, estimates of its magnitude can still contribute to informing farmers' VRI purchasing decisions. To break even on a VRI investment solely for this benefit, the total installed cost of VRI (C_v) has to equal the financial present worth of the irrigation reductions (simplified here as a uniform annual series) accumulated over an amortization period of n years (eq. 2.5). Both

the marginal savings from gross irrigation reductions per unit of ΔV_r (C_w) and the annual discount rate (i; also called "interest rate") were assumed to be fixed in real terms (i.e., equal inflation rates) during the amortization period.

$$C_v = \sum_{t=1}^{n}\left[\frac{C_w \times \Delta V_r}{(1+i)^t}\right] = C_w \times \Delta V_r \times \frac{(1+i)^n - 1}{i(1+i)^n} \tag{2.5}$$

where t = years since the VRI system began operation (-).

Estimating the breakeven C_v for every field with confidence would be difficult because of uncertainty in C_w. For instance, pumping cost, which contributes to C_w, can differ drastically between fields depending on energy source and energy requirement. Nevertheless, by manipulating equation 2.5, C_v and C_w could be combined into a cost ratio, defined as C_v divided by the marginal savings from 1,233 m^3 (1 ac-ft) of gross irrigation reductions. The attractiveness of a VRI investment solely for irrigation reductions from increasing precipitation utilization could thus be expressed in terms of the breakeven cost ratio B (eq. 2.6).

$$B = \frac{C_v}{C_w(1{,}233\,\mathrm{m}^3)} = \frac{\Delta V_r}{(1{,}233\,\mathrm{m}^3)} \times \frac{(1+i)^n - 1}{i(1+i)^n} \tag{2.6}$$

2.4. Results and Discussion

2.4.1. Statistical Distribution of U

The distributions of the two variables from which U (eq. 2.3) was calculated, R_a and R_p, are first presented (fig. 2.4). The distribution of R_a was left-skewed, and 61% of fields had an R_a value between 203 mm and 254 mm. Slightly bimodal but also left-skewed, the distribution of R_p loosely followed the shape of the R_a distribution with two

noticeable exceptions. More R_p values than R_a values fell in the 76-102 mm range, whereas more R_a values than R_p values fell in the 229-254 mm range.

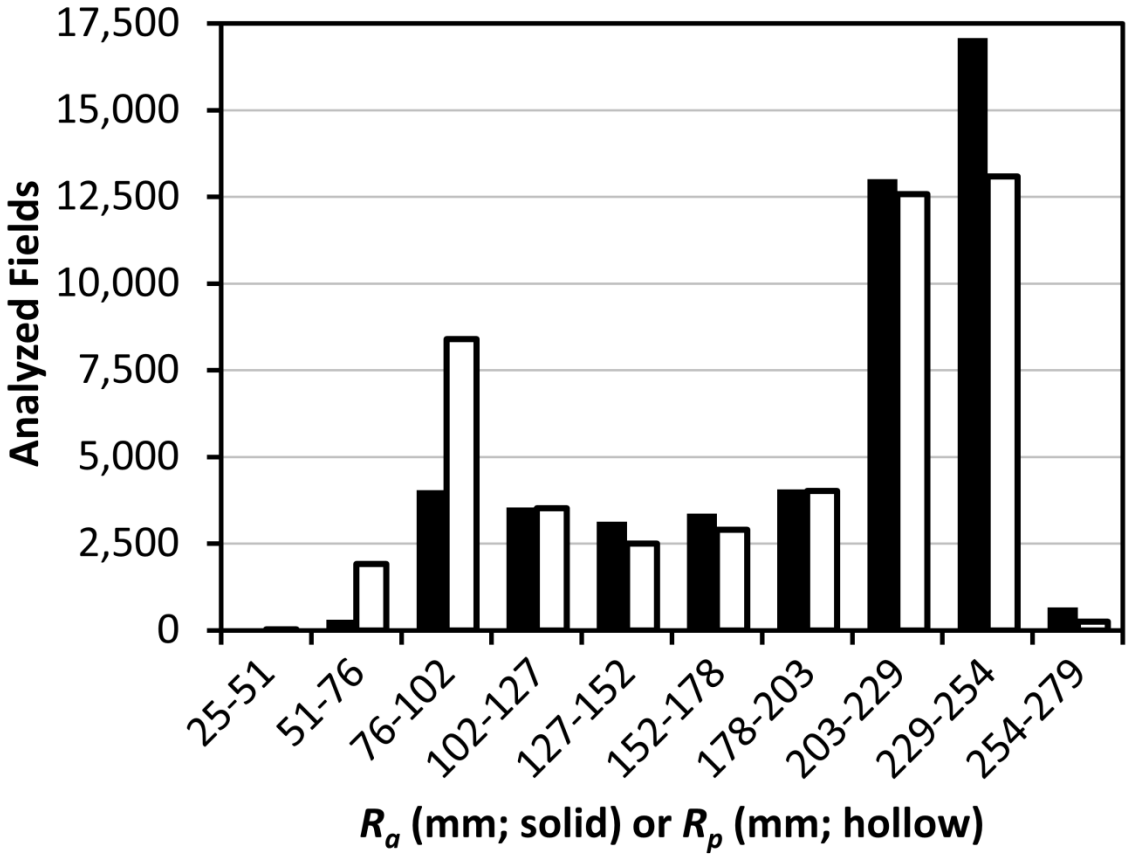

Figure 2.4. The distributions of field-average root zone water holding capacity (R_a; solid bars) and the root zone water holding capacity value that determines the target end-of-season depletion under conventional irrigation (R_p; hollow bars) for the analyzed fields.

In contrast, the distribution of U was right-skewed (fig. 2.5), with an observed range from -16 mm to 164 mm. Among the U values, 6% were negative, 83% were 0-51 mm, 10% were 51-102 mm, and 1% was greater than 102 mm. These results suggested that, in the majority of analyzed fields, CI planned soil water depletion only left a small total amount of unutilized R for VRI to exploit additionally.

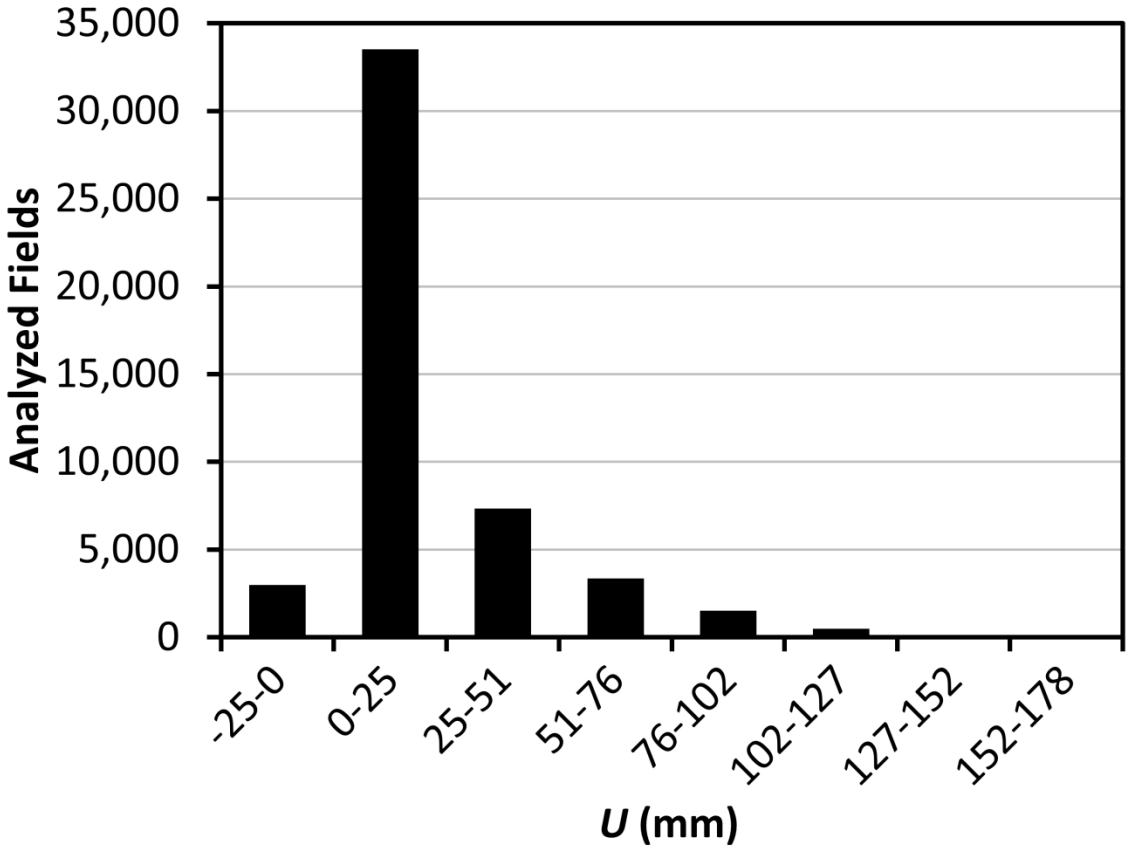

Figure 2.5. The distribution of unutilized root zone water holding capacity under conventional irrigation (*U*) for the analyzed fields.

The end-of-season depletion under CI, which was $R_p \times MAD$, would exceed *MAD* in a soil whose *R* was less than R_p. Such a soil could be said to have over-utilized *R* or negative unutilized *R*. In equation 2.3, such a soil subtracted from the value of *U*. If a field's total amount of over-utilized *R* exceeded its total amount of unutilized *R*, *U* became negative. Practically, a negative *U* indicated that switching from CI to VRI while maintaining *MAD* would call for an irrigation increase—rather than an irrigation reduction—to shrink the depletion fraction in the soils with over-utilized *R* to the specified *MAD*.

The value of *U* can be sensitive to the choice of the target *p*, which was the percentile of the field whose *R* was less than R_p. Because the statistical distribution of *R*

within each field was discrete in this study, a small change in target *p* could trigger a large change in R_p. To examine this sensitivity, R_p and *U* in every analyzed field were calculated using a target *p* of 5% and 15% as well. The distributions of R_p and *U*, shown in table 2.2, were generally similar for the three values of target *p*. Furthermore, 80% of *U* values remained the same after using a target *p* of 5%, and 83% of *U* values remained the same after using a target *p* of 15%. Yet among the *U* values that changed, a target *p* of 5% led to a 20 mm average increase in *U*, whereas a target *p* of 15% led to a 19 mm average decrease in *U*. In one field, *U* was changed by as much as 220 mm. The number of fields with a negative *U*, in particularly, was clearly affected when target *p* was altered. Overall, although many fields had a *U* value that was insensitive to target *p* between 5% and 15%, some fields had a *U* value that was very sensitive. The choice of target *p*, therefore, is important for appropriate comparisons between CI and VRI because *U* could be overestimated if target *p* is too low and underestimated if target *p* is too high.

Table 2.2. The distributions of the root zone water holding capacity (R) value that determines the target end-of-season depletion under conventional irrigation (R_p; left) and unutilized R under conventional irrigation (U; right) if R_p was chosen as the largest R within the field that is greater than R in at most p = 5%, 10%, or 15% of the field.

	# of fields with R_p in range			# of fields with U in range		
Range (mm)	Target p = 5%	Target p = 10%	Target p = 15%	Target p = 5%	Target p = 10%	Target p = 15%
-25-0	0	0	0	1232	2976	5036
0-25	2	0	0	32717	33510	33466
25-51	70	32	23	8135	7350	6608
51-76	2326	1916	1617	3988	3350	2785
76-102	9031	8396	7929	2098	1513	1065
102-127	3465	3523	3422	877	480	248
127-152	2584	2506	2515	156	43	16
152-178	2904	2907	2922	17	2	0
178-203	4272	4022	3950	2	0	0
203-229	12883	12578	12195	2	0	0
229-254	11498	13088	14325	0	0	0
254-279	189	256	325	0	0	0
279-305	0	0	1	0	0	0

2.4.2. Geographical Distribution of Large U Values Among Counties

The locations of the analyzed fields in each of three ranges of U are displayed in figures 2.6a-c. It is evident that the fields were neither randomly nor regularly distributed across Nebraska in any of the three figures. Additionally, whereas in some parts of the state, fields with large U—the sparser dots on figures 2.6b and 2.6c—seemed scattered throughout fields with small U—the denser dots on figure 2.6a, some other parts of the state appeared to be densely covered in figure 2.6a but almost blank in figures 2.6b and 2.6c. These observations pointed to differences in the prevalence of large U values among subregions of Nebraska.

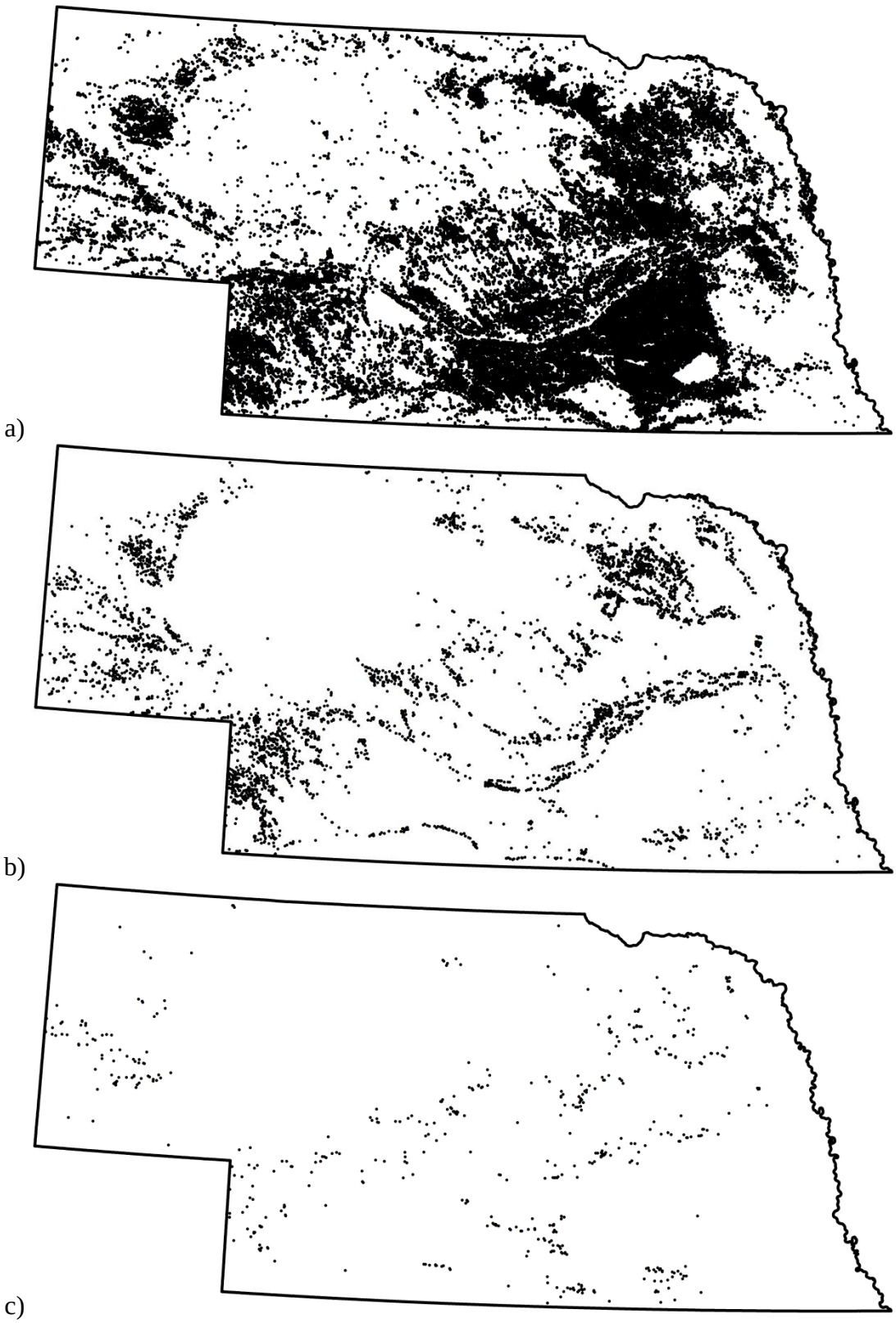

a)

b)

c)

Figure 2.6. The centroids of the analyzed fields with unutilized root zone water holding capacity under conventional irrigation (*U*) a) less than 51 mm, b) at least 51 mm but less than 102 mm, and c) at least 102 mm.

To further explore and to quantify these differences, the number of *U* values that were at least 51 mm and that were at least 102 mm, respectively, were counted in each of Nebraska's 93 counties. The counties with the most *U* values in these ranges were listed in tables 2.3 and 2.4.

Table 2.3. The 36 Nebraska counties with at least 40 values of unutilized root zone water holding capacity under conventional irrigation (*U*) that are at least 51 mm, ranked in descending order by their number of *U* values in this range.

Rank	County	Number	Percent	Rank	County	Number	Percent	Rank	County	Number	Percent
1	Antelope	472	24%	13	Cedar	122	20%	25	Knox	69	18%
2	Chase	313	23%	14	Dundy	108	12%	25	Phelps	69	6%
3	Perkins	277	27%	15	Greeley	103	18%	27	Brown	67	24%
4	Morrill	258	36%	16	Scotts Bluff	93	26%	28	Kearney	64	6%
5	Lincoln	255	17%	17	Sheridan	85	18%	29	Butler	57	8%
6	Pierce	240	24%	18	Keith	82	12%	30	Dixon	55	36%
7	Box Butte	230	20%	18	Thayer	82	8%	30	Stanton	55	26%
8	Custer	197	14%	20	Howard	80	17%	32	Logan	51	27%
9	Merrick	193	25%	21	Buffalo	78	6%	33	Dakota	47	43%
10	Holt	149	7%	21	Dodge	78	14%	34	Banner	45	23%
11	Cheyenne	143	31%	23	Hall	70	10%	35	Nance	43	12%
12	Madison	125	16%	23	Kimball	70	26%	35	Webster	43	11%

Table 2.4. The 35 Nebraska counties with at least 4 values of unutilized root zone water holding capacity under conventional irrigation (*U*) that are at least 102 mm, ranked in descending order by their number of *U* values in this range.

Rank	County	Number	Percent	Rank	County	Number	Percent	Rank	County	Number	Percent
1	Morrill	36	5%	13	Adams	15	1%	25	Brown	6	2%
2	Custer	34	2%	14	Dixon	14	9%	25	Dodge	6	1%
3	Lincoln	30	2%	15	Perkins	13	1%	25	Polk	6	0.7%
3	Thayer	30	3%	16	Furnas	10	3%	28	Cedar	5	0.8%
5	Chase	25	2%	16	Pierce	10	1%	28	Dakota	5	5%
5	Scotts Bluff	25	7%	18	Buffalo	9	0.7%	28	Dawson	5	0.6%
7	Greeley	24	4%	18	Stanton	9	4%	31	Franklin	4	0.7%
8	Kearney	23	2%	20	Butler	8	1%	31	Hall	4	0.6%
9	Antelope	22	1%	20	Howard	8	2%	31	Holt	4	0.2%
10	Merrick	20	3%	20	Phelps	8	0.7%	31	Keith	4	0.6%
10	Webster	20	5%	23	Boone	7	0.6%	31	Sheridan	4	0.9%
12	Madison	17	2%	23	Box Butte	7	0.6%				

Part of the clustered nature of large *U* values could be attributed to the clustered nature of the analyzed fields, over 50% of which were in nineteen counties (20%). Given equal spatial variability in *R*, a county with more analyzed fields would have a greater number of large *U* values than a county with fewer analyzed fields. As a result, the 22

counties (24%) with the most analyzed fields contained over 50% of all *U* values that were at least 51 mm, and the 24 counties (26%) with the most analyzed fields contained over 50% of all *U* values that were least 102 mm.

Nonetheless, some counties' number of large *U* values was vastly disproportionate to their number of analyzed fields. On one extreme, York and Fillmore Counties, with the third and the fifth most analyzed center pivots (1609 and 1472), respectively, both had no *U* values of at least 51 mm. On the opposite extreme, Stanton and Dixon Counties, with the 64th and the 70th most analyzed center pivots (215 and 154), both ranked 30th for *U* values of at least 51 mm and were both within the top twenty for *U* values of at least 102 mm.

In fact, large *U* values were more clustered than the analyzed fields. Eleven counties (12%) contained over 50% of all *U* values that were at least 51 mm, and ten counties (11%) contained over 50% of all *U* values that were at least 102 mm. Also, large *U* values were not concentrated in all of the same counties as the analyzed fields. The nine counties that ranked in the top fifteen in tables 2.3 and 2.4 were some of the subregions where the prevalence of fields with large *U* values was the highest (fig. 2.7).

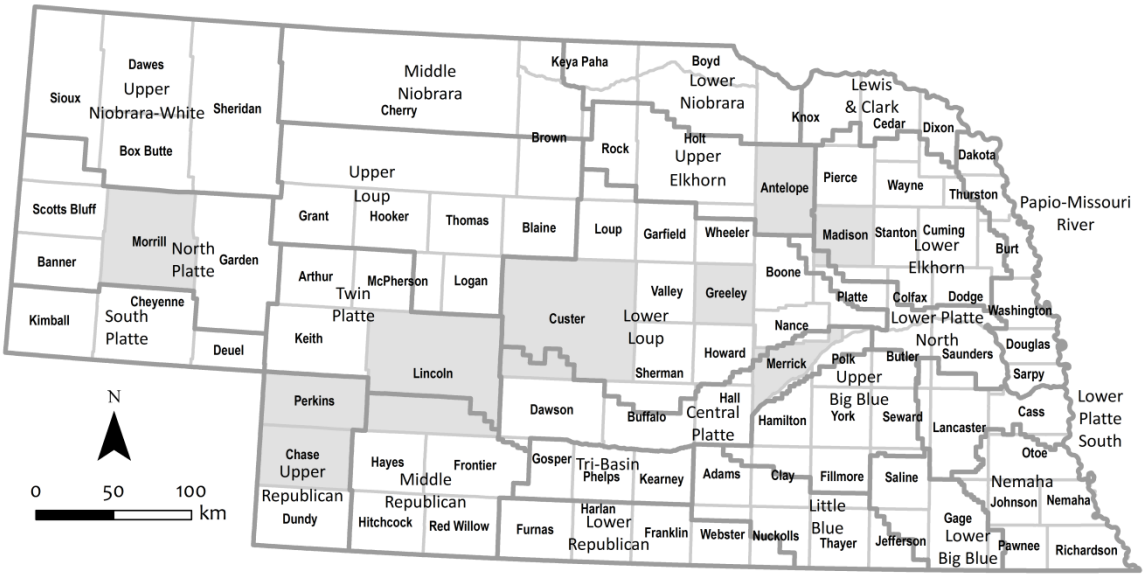

Figure 2.7. The counties (light grey outlines) and Natural Resources Districts (medium grey outlines) of Nebraska; the nine counties that ranked in the top fifteen in tables 2.3 and 2.4 were colored in light grey.

2.4.3. Geographical Distribution of Large U Values Among Soil Associations

Fundamentally, however, the prevalence of large *U* values should be related to soil formation. A classification scheme based on soil formation was approximated by the division of Nebraska's soils into 80 soil associations (Conservation and Survey Division, 2009), each of which was a group of soil series that were generally found in proximity to each other. It was thought that fields with similar soil formation would have similar *U* values. By extension, the prevalence of large *U* values in a soil association should be very high or very low. If this characteristic was true, then the extents of soil associations would be far more effective than county borders for demarcating subregions in which the prevalence of large *U* values was on either extreme.

The analyzed center pivots were even more clustered with respect to soil associations than to counties. Over 50% of all analyzed center pivots were located in just 10 soil associations (13%). Because percentages convey prevalence without being confounded by the number of analyzed fields in each soil association, the percentage of *U*

values that were at least 51 mm and that were at least 102 mm, respectively, were computed in every soil association. The soil associations with some of the highest percentages of *U* values in these ranges were listed in tables 2.5 and 2.6.

Table 2.5. Soil associations ranked in descending order by their percentage of unutilized root zone water holding capacity under conventional irrigation (*U*) values that were at least 51 mm; only the 28 soil associations with a minimum of 20% of *U* values in this range and with a minimum of 30 analyzed fields were listed.

Rank	Code	Soil Association	Percent	Number	Rank	Code	Soil Association	Percent	Number
1	54	Moody-Thurman	44%	102	15	66	Gibbon-Wann	26%	78
2	73	Brunswick-Paka-Simeon	38%	23	16	60	Gothenburg-Platte-Lawet	25%	51
3	69	Nuckolls-Holdrege-Campus	33%	12	17	42	Keith-Alliance-Rosebud	24%	166
4	12	Alliance-Rosebud-Kuma	33%	154	18	15	Hersh-Valentine	23%	407
5	46	Canyon-Alliance-Rosebud	32%	12	19	75	Jayem-Keith	23%	59
6	52	Valent-Sarben-Otero	31%	90	20	36	Jayem-Sarben-Valent	23%	134
7	27	Thurman-Boelus-Nora	30%	634	21	65	Dix-Altvan-Colby	21%	15
8	30	Hord-Cozad-Boel	30%	132	22	50	Gibbon-Zook	21%	93
9	38	Albaton-Haynie-Sarpy	29%	114	23	32	Kuma-Satanta-Rosebud	21%	203
10	61	Kennebec-Nodaway-Zook	28%	17	24	45	Hord-McCook-Inavale	21%	72
11	13	Tripp-Mitchell-Alice	27%	198	25	28	Shell-Muir-Hobbs	20%	109
12	51	Bazile-Thurman-Boelus	27%	155	26	47	Kenesaw-Hersh	20%	188
13	64	Canyon-Rosebud-Rock Outcrop	27%	8	27	49	Lawet-Gothenburg-Platte	20%	53
14	10	Rosebud-Alliance-Canyon	27%	193	28	31	Monona-Ida	20%	7

Table 2.6. Soil associations ranked in descending order by their percentage of unutilized root zone water holding capacity under conventional irrigation (*U*) values that were at least 102 mm; only the 28 soil associations with a minimum of 1% of *U* values in this range and with a minimum of 30 analyzed fields were listed.

Rank	Code	Soil Association	Percent	Number	Rank	Code	Soil Association	Percent	Number
1	13	Tripp-Mitchell-Alice	6%	44	15	27	Thurman-Boelus-Nora	2%	46
2	54	Moody-Thurman	6%	14	16	66	Gibbon-Wann	2%	6
3	47	Kenesaw-Hersh	5%	51	17	20	Hobbs-Hord	2%	18
4	46	Canyon-Alliance-Rosebud	5%	2	18	23	Jansen-O'Neill-Meadin	2%	25
5	60	Gothenburg-Platte-Lawet	5%	10	19	35	Cozad-Hord	2%	16
6	30	Hord-Cozad-Boel	4%	16	20	39	Gibbon-Gothenburg-Platte	2%	7
7	45	Hord-McCook-Inavale	3%	11	21	73	Brunswick-Paka-Simeon	2%	1
8	15	Hersh-Valentine	3%	54	22	28	Shell-Muir-Hobbs	2%	8
9	16	Valentine-Els-Wildhorse	3%	2	23	18	Valent-Woodly-Jayem	1%	21
10	31	Monona-Ida	3%	1	24	37	Crofton-Alcester-Nora	1%	2
11	69	Nuckolls-Holdrege-Campus	3%	1	25	40	Satanta-Jayem-Canyon	1%	3
12	38	Albaton-Haynie-Sarpy	3%	10	26	32	Kuma-Satanta-Rosebud	1%	11
13	52	Valent-Sarben-Otero	2%	7	27	10	Rosebud-Alliance-Canyon	1%	8
14	48	Tassel-McKelvie-Rock Outcrop	2%	1	28	36	Jayem-Sarben-Valent	1%	6

The eight soil associations that ranked in the top fifteen in tables 2.5 and 2.6 are highlighted in figure 2.8. All these soil associations were described as being formed from juxtapositions of coarser parent materials, such as eolian sand or sandstone, with finer parent materials, such as loess (Conservation and Survey Division, 2009). Also, three of these soil associations (codes 13, 30, and 38) appeared to have been affected by alluvial processes during their formation (Conservation and Survey Division, 2009), which may be why stretches of several major rivers in Nebraska can be roughly traced on the maps

of the analyzed center pivots with large *U* values (fig. 2.6b-c). These evidences support the claim that the greater prevalence of large *U* values in these soil associations may indeed be explained by soil formation.

Figure 2.8. The soil associations of Nebraska (black outlines); the eight soil associations that ranked in the top fifteen in tables 2.5 and 2.6 were colored in various shades of grey.

Yet contrary to expectations, the statistical distributions of the prevalence of large *U* values among soil associations were not more bimodal than the statistical distributions of the prevalence of large *U* values among counties (fig. 2.9). For the prevalence of *U* values that were at least 102 mm (dashed lines), the two distributions were similar overall. For the prevalence of *U* values of at least 50.8 mm (solid lines), the soil associations' distribution (grey) had a smaller lower tail and a larger upper tail than the counties' distribution (black), but intermediate prevalence percentages compose a substantial proportion of both distributions.

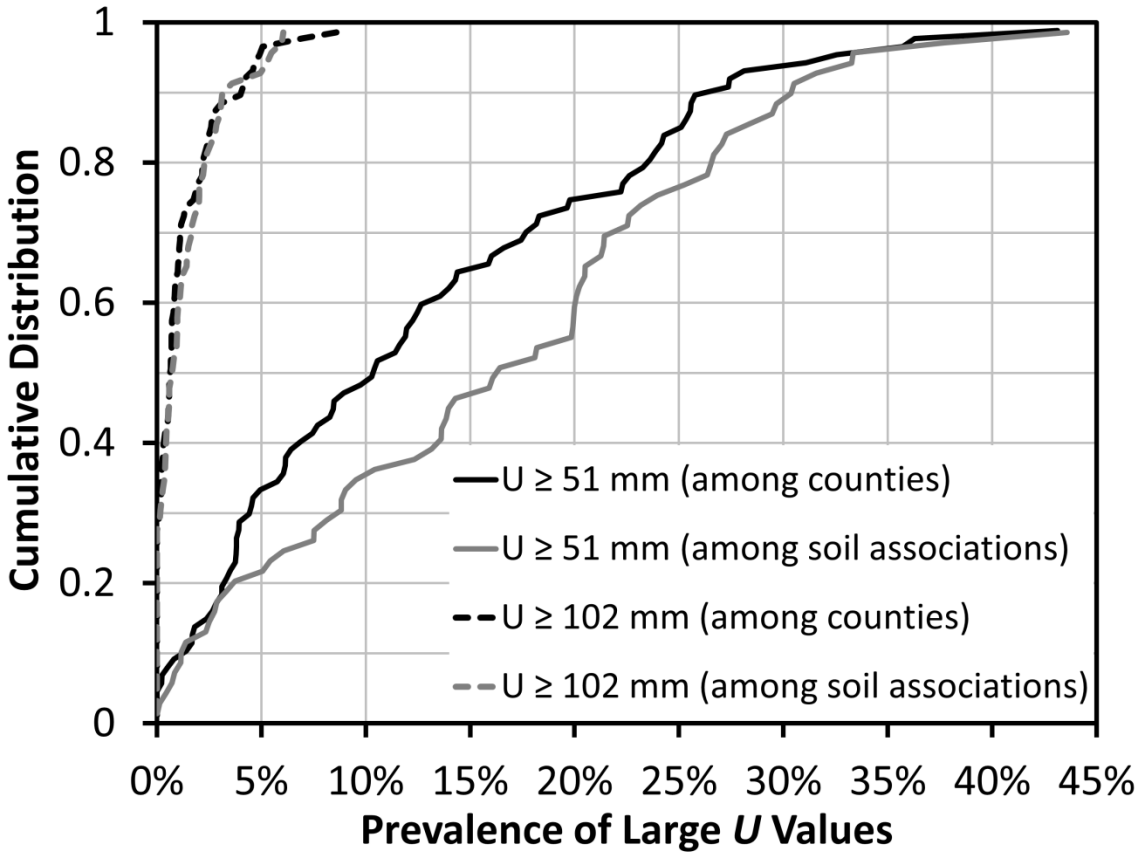

Figure 2.9. The cumulative distribution functions of the prevalence of large values of unutilized root zone water holding capacity under conventional irrigation (*U*) among Nebraska's counties and soil associations.

Most subregions, whether counties or soil associations, contained a majority of small *U* values and a minority of large *U* values. Several subregions lacked large *U* values, but none of the subregions contained large *U* values exclusively. Thus, subregional-scale information is not enough in the Central Plains to identify fields with a large potential for irrigation reductions from increasing precipitation utilization with VRI.

2.4.4. Potential Regional Impact of Irrigation Reductions From Increasing Precipitation Utilization with VRI

The potential regional impact of the irrigation reductions from increasing precipitation utilization with VRI was estimated for two hypothetical extents of

implementation. With the smaller extent, this application of VRI was implemented on every analyzed field with Δd_r (eq. 2.4) greater than 51 mm. With the larger extent, this application of VRI was implemented on every analyzed field with Δd_r greater than 25 mm. For both extents, the percentage of implemented fields, the area-weighted average Δd_r among implemented fields, and the total ΔV_r were calculated in each of the nineteen NRDs without NRD-wide groundwater quantity allocations (table 2.7). Readers should bear in mind that these irrigation reductions would result from a shift in the source of evapotranspired water and not from a change in the quantity of evapotranspiration. Any reduction in groundwater withdrawal due to this application of VRI would be conditional upon a roughly equivalent reduction in groundwater recharge by water percolating past the root zone. Therefore, the water supply for other uses in the watershed is not expected to be augmented by these irrigation reductions.

Table 2.7. Each Natural Resources District's (NRD) percentage of implemented fields, area-weighted average depth of gross irrigation reductions (Δd_r) among implemented fields, and total volume of gross irrigation reductions (ΔV_r) for two VRI implementation extents; four NRDs were omitted due to NRD-wide groundwater quantity allocations.

NRD	Analyzed Fields	Δd_r > 51 mm			Δd_r > 25 mm		
		Implemented Fields	Avg. Δd_r (mm)	Total ΔV_r ($\times 10^6$ m^3)	Implemented Fields	Avg. Δd_r (mm)	Total ΔV_r ($\times 10^6$ m^3)
Central Platte	3666	3%	59	2.62	14%	40	9.81
Lewis & Clark	602	9%	58	1.48	34%	43	4.59
Little Blue	3348	2%	62	2.44	4%	51	3.47
Lower Big Blue	1079	0.09%	51	0.02	10%	30	1.52
Lower Elkhorn	3700	3%	60	3.93	19%	41	13.63
Lower Loup	6087	3%	61	5.25	11%	43	14.06
Lower Niobrara	1443	0.9%	57	0.34	12%	35	3.08
Lower Platte North	1989	1%	61	0.51	11%	37	3.83
Lower Platte South	104	0%	0	0	16%	34	0.27
Middle Niobrara	678	2%	59	0.33	20%	36	2.33
Nemaha	181	2%	65	0.24	25%	40	0.96
North Platte	1652	8%	61	3.76	33%	42	11.24
Papio-Missouri River	436	5%	59	0.64	25%	41	2.62
Tri-Basin	2563	2%	66	1.50	7%	43	3.81
Twin Platte	1826	4%	60	2.16	20%	40	7.76
Upper Big Blue	6841	0.04%	56	0.08	0.2%	34	0.23
Upper Elkhorn	3059	3%	57	2.13	25%	37	14.02
Upper Loup	380	2%	57	0.16	21%	38	1.48
Upper Niobrara-White	1763	3%	58	1.39	28%	37	9.39
Total	41397	2%	60	29.00	13%	40	108.07

A trend pervaded the listed NRDs in table 2.7. As the extent of implementation was expanded, the total ΔV_r increased while the area-weighted average Δd_r decreased. Since implementation was assumed to prioritize the fields with the largest Δd_r, Δd_r of the next field never surpasses Δd_r of any implemented field. At the same time, there were appreciable differences between NRDs. For instance, for both extents of implementation, the Lewis & Clark and North Platte NRDs had much higher percentages of implemented fields than the Upper Big Blue and Little Blue NRDs.

The relative magnitude of the potential irrigation reductions was illustrated by comparing statewide reductions with statewide gross irrigation. The NASS Farm and Ranch Irrigation Survey, which gathered farmers' mandatorily self-reported irrigation data, tallied 2,943,836 ha under center pivot irrigation in Nebraska for the 2013 growing

season (NASS, 2014). If the analyzed fields (2,430,562 ha), which represented Nebraska's center pivots during the 2005 growing season, were also representative of Nebraska's center pivots installed after the 2005 growing season, then total ΔV_r in 2013 would be 35.13 million m^3 and 130.89 million m^3 for the two extents of implementation, respectively. These two volumes would be 0.35% and 1.3% of the 9,953.12 million m^3 of gross irrigation in Nebraska during 2013 (NASS, 2014). Granted, well-managed CI planned soil moisture depletion was used in this study as the baseline for the irrigation reductions from increasing precipitation utilization with VRI. A smaller volume of gross irrigation would probably have been applied during 2013 if well-managed CI planned soil moisture depletion was practiced on every irrigated field in Nebraska. The results, nevertheless, suggested that increasing precipitation utilization with VRI should not be expected to enable momentous reductions in statewide gross irrigation.

For energy utilities, this finding implied that the irrigation reductions from increasing precipitation utilization with VRI might not have a significant impact on the total energy consumption by Nebraska's center pivot irrigation pumps. Yet, this application of VRI may have an appreciable impact on peak power demand. When applying a reduced depth onto soils with larger *R*, the system flow rate would be lowered, or the operation time would be shortened. The instantaneous power demand may decrease with system flow rate depending on the pump performance curve. Also, some low-capacity systems might be enabled to switch from continuous to interruptible electricity service without incurring water stress.

From an environmental perspective, this application of VRI might be a measure to be evaluated for minimizing nitrate leaching in areas where it is a critical concern.

Increasing precipitation utilization with VRI decreases deep percolation from soils with larger *R*. This decrease can be significant relative to the magnitude of annual deep percolation from these soils—even though the associated irrigation reductions may be moderate relative to the magnitude of annual irrigation.

Yet for the farmers of most center pivot irrigated fields in Nebraska, increasing precipitation utilization with VRI may generate relatively small additional savings in pumping energy costs beyond what is gained from practicing well-managed CI planned soil moisture depletion. As a comparison, the Nebraska Agricultural Water Management Network (Irmak et al., 2010), which advocates for the use of the ETgage atmometer (ETgage Company, Loveland, Colo.) and Watermark granular matrix soil moisture sensors (Irrometer Company, Riverside, Cal.) to improve CI scheduling, was estimated to reduce seasonal gross irrigation by 56 mm for corn and 46 mm for soybeans (UNL Extension, 2009). These amounts are quite large considering that they are the average for 105 responding farmers managing over 70,000 ha (UNL Extension, 2009) and are likely to be achievable on many fields without yield-limiting water quantity allocations. Furthermore, the investment required for improving CI scheduling is presently far less than what is required for purchasing and implementing VRI.

In summary, in agreement with Evans et al. (2013), this study supports the view that there are multiple tiers of irrigation technology and management. Producers who are interested in reducing their seasonal irrigation should first improve their CI scheduling because this step is more broadly applicable and generally more cost-effective than increasing precipitation utilization with VRI. Afterwards, producers can take the next

step and implement this application of VRI on their fields with large potential for additional irrigation reductions.

2.4.5. Economics of Adopting VRI Solely for Irrigation Reductions From Increasing Precipitation Utilization

Irrespective of the expected regional impact, irrigation reductions from increasing precipitation utilization with VRI—on their own—may justify VRI investment on the fields with the largest ΔV_r. For an amortization period of ten years and for three different annual discount rates i, the linear relationships between ΔV_r and breakeven cost ratio B (eq. 2.6) were shown in figure 2.10. As ΔV_r increased or as i decreased (i.e., declining profitability of alternate investments), B is increased, which meant a higher C_v relative to C_w could be accepted. Alternatively, if B is decreased as C_v decreased relative to C_w, then irrigation reductions from increasing precipitation utilization with VRI would justify VRI investment on fields with smaller ΔV_r and higher i. In this study, the largest ΔV_r estimated for a field was 138 thousand m^3, which translated into B of 1,122, 866, and 689 for i of 0%, 5%, and 10%, respectively.

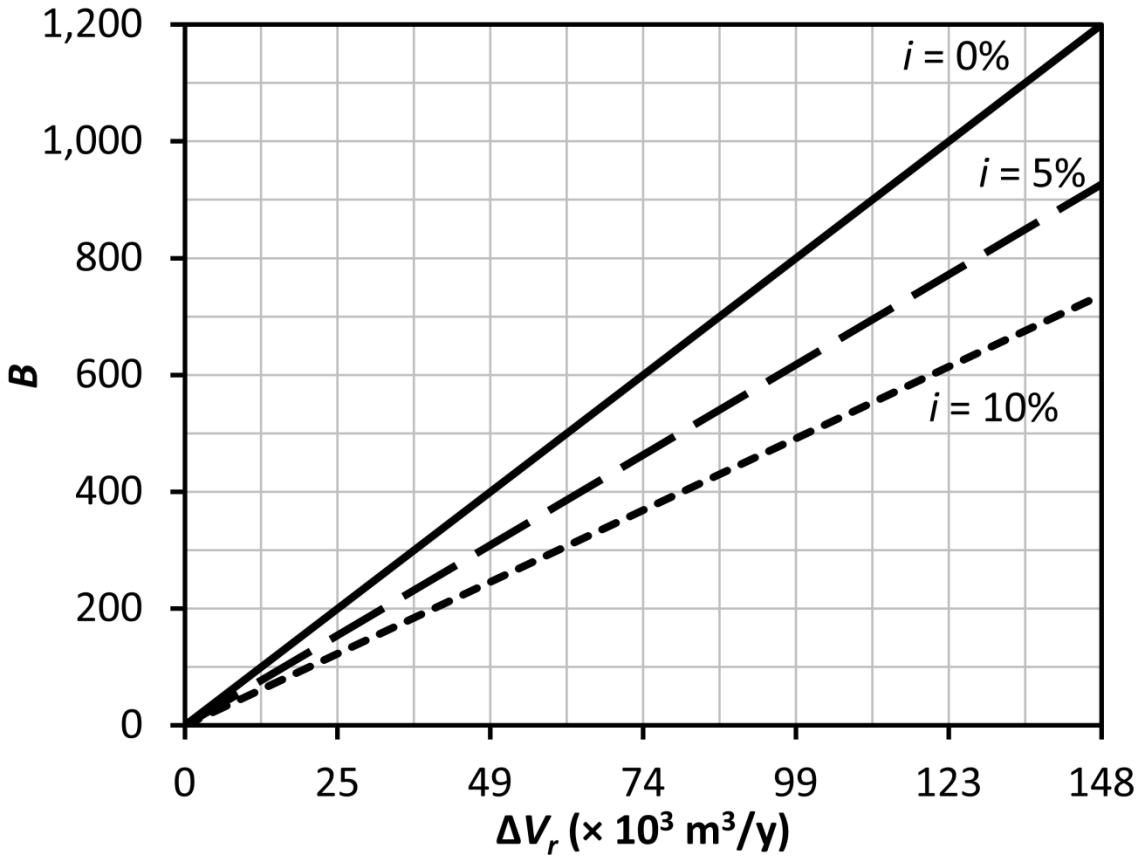

Figure 2.10. Breakeven cost ratio between total installed cost of VRI and marginal savings per 1,233 m^3 of gross irrigation reductions (B) versus volume of gross irrigation reductions (ΔV_r) for an amortization period of ten years and for a discount rate (i) of 0%, 5%, and 10%; i and all prices are assumed to be constant in real terms.

A cumulative distribution function of B for each of the three i values was generated by combining the breakeven relationships in figure 2.10 with the estimates of ΔV_r on the analyzed fields without NRD-wide groundwater quantity allocations. The probabilities of exceedance were calculated using the Weibull formula. If it was temporarily supposed that the market presented the same cost ratio to every field, then the fields whose B was greater than this cost ratio would receive a net benefit from this application of VRI. In other words, the probability of exceeding a given B may be a reasonable estimate of the percentage of all fields without NRD-wide allocations that would adopt VRI solely for increasing precipitation utilization when presented with this

cost ratio. Because ΔV_r had a right-skewed distribution, the adoption percentage generally increased exponentially as B decreased linearly (fig. 2.11).

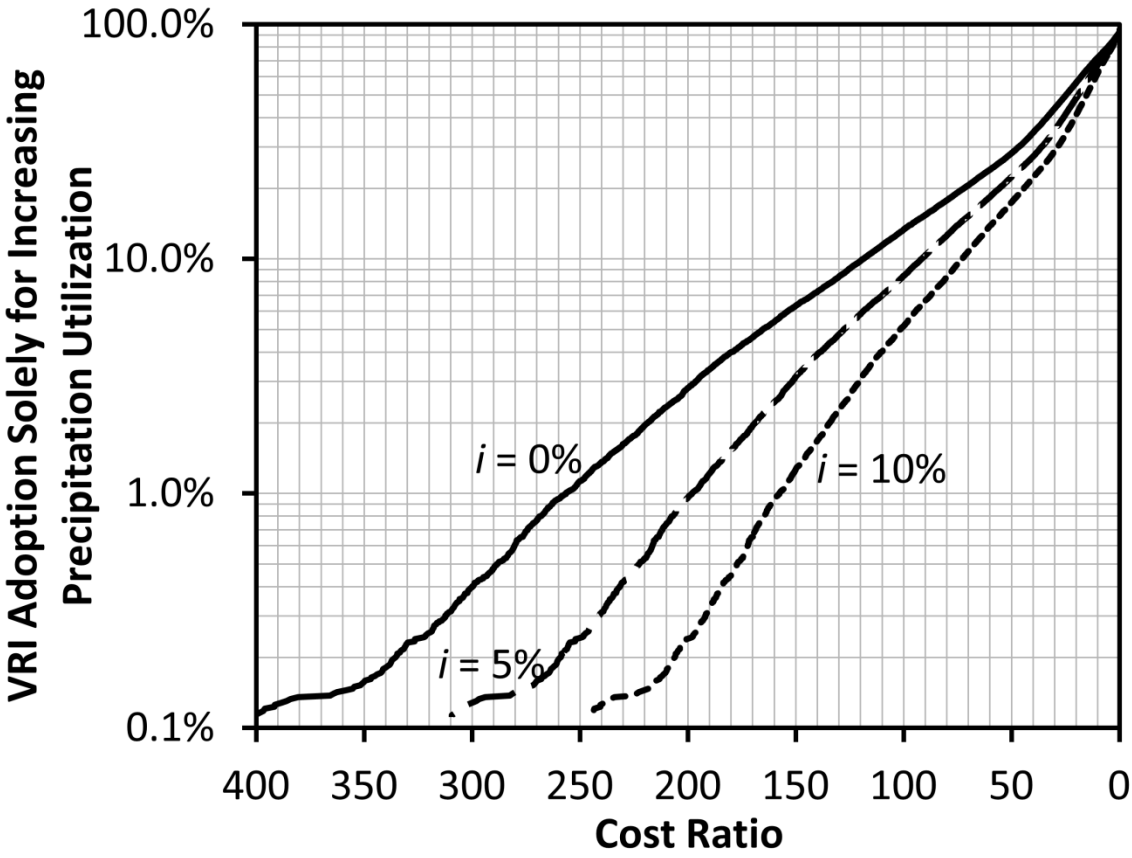

Figure 2.11. Cumulative distribution function of the breakeven cost ratio between total installed cost of VRI and marginal savings per 1,233 m^3 of gross irrigation reductions for an amortization period of ten years and three discount rates (i); the probabilities of exceedances were assumed to be the adoption rates at the corresponding cost ratios.

Because breakeven C_v was positively proportional to C_w (eq. 2.5), VRI adoption solely for irrigation reductions from increasing precipitation utilization was least favored when C_w only includes the cost of pumping energy. Based on the 2013 irrigation survey (NASS, 2014), a typical irrigation well in Nebraska might be connected to an electric pump (55% of all irrigation pumps in Nebraska) supplying 25 m of lift (average depth to water in Nebraska's irrigation wells is 20.7 m "at the start of the irrigation season") and 276 kPa of pressure (Nebraska's average operating pressure of pumped wells). If such a

pump operated at 100% of the Nebraska Pumping Plant Performance Criteria (Kranz, 2010) and purchased additional anytime interruptible electricity service at $0.0624/kWh (NPPD, 2014), the marginal pumping cost would be $16.87 per 1,233 m^3.

A marginal pumping cost that is calculated in this manner may be larger than the marginal pumping savings from reducing irrigation over soil map units with large *R*. If the pump was well-selected and well-maintained, such a marginal pumping cost represented changes in pumping time while operating near the best efficiency point on the pump performance curve. In contrast, whenever irrigation reductions were nonuniform along the center pivot lateral, marginal pumping savings represented changes in pump operation point, which may lower pump efficiency and increase total dynamic head needlessly. The discrepancy between such a marginal pumping cost and marginal pumping savings would be dependent on the pump performance curve and the change in system flow rate. For simplification, the above marginal pumping cost was assumed to be the marginal pumping savings with the understanding that the latter may be overestimated.

With an amortization period of ten years and i = 5%, C_v would have to be $5,349 for 0.1% adoption, $3,341 for 1% adoption, and $1,547 for 10% adoption. According to this example, widespread adoption of VRI in the Central Plains solely to save pumping energy costs by increasing precipitation utilization is not expected unless prices for zone control VRI capability, "about $200-$550 ha^{-1}" (Evans et al., 2013), drop dramatically relative to pumping energy costs. Speed control VRI capability is less expensive, but the effectiveness of management sectors at matching spatial variability in *R* and the consequent magnitude of the achievable irrigation reductions are uncertain.

Nonetheless, increasing precipitation utilization and reducing seasonal irrigation with VRI may also lower the private cost of fertilizer (due to less nitrogen loss through denitrification and nitrate leaching), the public cost of drinking water with safe nitrate concentrations, and/or the environmental cost of pumping energy generation and of fertilizer production and application. The magnitude of these neglected benefits may be difficult to estimate, but their inclusion in the quantification of C_w would improve the attractiveness of this application of VRI as compared to what was portrayed in the example above.

Though this study focused on the quantification of U, the consideration of C_w is equally important for evaluating the field-specific profitability of increasing precipitation utilization with VRI. A wide range in C_w is expected under current market conditions in the Central Plains due to large differences in the prices and requirements (e.g., pumping water level) of pumping energy (Chapter 1). Thus, the financial benefit from this application of VRI may vary greatly among fields with the same U, which was not considered in the example above.

2.4.6. Discussions on the Methodology

Because publicly available geospatial data were used "as is" without any corrections, problems that exist in the data were unavoidably inherited by this study. In the center pivot map, there were inaccuracies in the number and boundaries of Nebraska's center pivot irrigated fields. In addition to containing imperfect delineations of map units as well as uncertainties and measurement errors in the various soil properties values, gSSURGO lacksed detailed information about heterogeneities below the map unit

level because the soil surveys were not conducted with precision agriculture purposes in mind (Brevik et al., 2003). These problems all contributed to the limitations of this study.

In addition, the method used in this study was built on a series of simplifying assumptions. The violation of these assumptions would cause the predicted potential irrigation reductions to deviate from the actual potential irrigation reductions. First, if a period of heavy rainfall occurs after the amounts of R above R_p have begun to be utilized under VRI, soils with larger R may retain more of the infiltrated water than soils with smaller R, which may experience more deep percolation. Second, as soils with larger R are typically located in lower topographic positions, they may capture more water during recession infiltration due to longer opportunity times. In these instances, the potential irrigation reductions from increasing precipitation utilization with VRI would be underestimated by this study because the soil water difference that can be utilized by VRI is not limited to the one-time mining of unutilized R.

In other situations, the potential irrigation reductions from increasing precipitation utilization with VRI would be overestimated by this study. In eastern Nebraska, there may be seasons where the depletion fraction in soils with large R never reaches the specified *MAD* because initial soil moisture and in-season rainfall are abundant. In western Nebraska, on the other hand, if every soil was depleted up to the specified *MAD* at the end of the previous growing season, there may be seasons where only soils with small R are refilled by rainfall infiltration. Also, if an intense rain occurs after the amounts of R above R_p have begun to be utilized under VRI, soils with larger R may capture less water than soils with smaller R because soils with larger R tend to be composed of finer textures and have lower infiltration capacities than soils with smaller R.

A key disadvantage of this study's vast geographical coverage was the impracticality of checking how reality diverges from the simplifying assumptions, especially because the validity of these assumptions could be affected by the management practices on each field. Intending to avoid this set of assumptions and to improve the accuracy of the irrigation reduction estimates, spatiotemporal physical hydrologic modeling, which is far more complex than the current method, could be employed instead. Such an endeavor will undoubtedly demand a substantial investment of time and labor to collect additional data and to calibrate the model. However, the modeling results might be ultimately bundled with a set of assumptions that are equally difficult to verify and a collection of uncertainties that are comparable in magnitude. For example, the model would likely require values for parameters such as surface storage and effective saturated hydraulic conductivity, which not only are challenging to measure accurately and representatively but also depend on management practices. In view of the obvious complications but doubtful improvements associated with modeling, the simplicity of this study was preserved.

This study also assumed a constant E_a for both CI and VRI. Future work can analyze how the fate of applied irrigation differs between CI and VRI. Improvements in E_a from VRI implementation can then be estimated.

2.5. Conclusion

In this study, a minority of Nebraska's center pivot irrigated fields were estimated to have large values of U and Δd_r. Implementing VRI on these fields to reduce irrigation by increasing precipitation utilization may make a valuable contribution to decreasing

nitrate leaching and peak energy demand, but the regional impact on pumping energy consumption through pumpage reduction was expected to be small.

On most of the analyzed fields, pumping energy savings alone may be insufficient to financially justify VRI investment at prevailing prices. The adoption of VRI for reducing irrigation by increasing precipitation utilization would be more favored if nitrogen fertilizer savings were known and if the positive externalities to the public and to the environment were internalized to the producers. Lower VRI prices relative to the cost of pumping energy would also encourage the adoption of VRI for this particular application. In general, though, increasing precipitation utilization with VRI should only be considered after practicing well-managed CI planned soil moisture depletion.

The results of this study also revealed clear differences in the prevalence of large *U* values among Nebraska's counties and soil associations. Notably, some counties and some soil associations had many center pivot irrigated fields but few, if any, large *U* values. In spite of these observations, knowing the county or soil association in which a field was located rarely guaranteed knowledge of the magnitude of *U* in that field. This finding underscored the importance of field-specific analyses for precision agricultural management.

2.6. References

Allen, R. G., Pereira, L. S., Raes, D., & Smith, M. (1998). Crop Evapotranspiration: Guidelines for Computing Crop Water Requirements. FAO Irrigation and Drainage Paper 56. Rome, Italy: Food and Agriculture Organization of the United Nations.

ArcGIS. (2013). *ArcGIS Desktop 10.2*. Redlands, Cal.: ESRI.

Brevik, E. C., Fenton, T. E., & Jaynes, D. B. (2003). Evaluation of the Accuracy of a Central Iowa Soil Survey and Implications for Precision Soil Management. *Precision Agric.*, 4(3), 331-342. doi: 10.1023/A:1024960708561

CALMIT. (2007). 2005 Nebraska Center Pivot Irrigation Systems. Lincoln, Neb.: University of Nebraska–Lincoln. Retrieved from ftp://dnrftp.dnr.ne.gov/pub/data/state/IrrigatedPivots2005.zip

Conservation and Survey Division. (2009). Soils of Nebraska. Lincoln, Neb.: University of Nebraska–Lincoln. Retrieved from http://snr.unl.edu/data/geographygis/NebrGISsoils.asp

DeJonge, K. C., Kaleita, A. L., & Thorp, K. R. (2007). Simulating the effects of spatially variable irrigation on corn yields, costs, and revenue in Iowa. *Agric. Water Mgmt.*, 92(1), 99-109.

Evans, R. G., LaRue, J., Stone, K. C., & King, B. A. (2013). Adoption of site-specific variable rate sprinkler irrigation systems. *Irrig. Sci.*, 31(4), 871-887.

Hedley, C. B., & Yule, I. J. (2009). Soil water status mapping and two variable-rate irrigation scenarios. *Precision Agric.*, 10(4), 342-355.

Hillyer, C. C., & Higgins, C. W. (2014). A Demonstration of Energy & Water Savings Potential of Variable Rate Irrigation. ASABE Paper No. 141914755. St. Joseph, Mich.: ASABE.

Irmak, S. (2014). Plant Growth and Yield as Affected by Wet Soil Conditions Due to Flooding or Over-Irrigation. NebGuide G1904. Lincoln, Neb.: University of Nebraska–Lincoln. Retrieved from http://ianrpubs.unl.edu/live/g1904/build/g1904.pdf

Irmak, S., Rees, J. M., Zoubek, G. L., van DeWalle, B. S., Rathje, W. R., DeBuhr, R., Leininger, D., Siekman, D. D., Schneider, J. W., & Christiansen, A. P. (2010). Nebraska Agricultural Water Management Demonstration Network (NAWMDN): Integrating Research and Extension/Outreach. *Appl. Eng. Agric.*, 26(4), 599-613.

Jiang, P., Anderson, S. H., Kitchen, N. R., Sudduth, K. A., & Sadler, E. J. (2007). Estimating Plant-Available Water Capacity for Claypan Landscapes Using Apparent Electrical Conductivity. *Soil Sci. Soc. America J., 71*(6), 1902-1908. doi: 10.2136/sssaj2007.0011

Khalilian, A., Han, Y., & Farahani, H. (2008). Site-Specific Irrigation Management in Coastal Plain Soils. In *Proc. 2008 South Carolina Water Resources Conf.* Clemson, S.C.: Clemson University.

King, B. A., Stark, J. C., & Wall, R. W. (2006). Comparison of Site-Specific and Conventional Uniform Irrigation Management for Potatoes. *Appl. Eng. Agric.*, 22(5), 677-688.

Kranz, W. L. (2010). Updating the Nebraska Pumping Plant Performance Criteria. In *Proc. 22nd Ann. Central Plains Irrig. Conf.* Colby, Kans.: Central Plains Irrigation Association.

Kranz, W. L., Irmak, S., van Donk, S. J., Yonts, C. D., & Martin, D. L. (2008a). Irrigation Management for Corn. NebGuide G1850. Lincoln, Neb.: University of Nebraska–Lincoln. Retrieved from http://www.ianrpubs.unl.edu/epublic/live/g1850/build/g1850.pdf

Kranz, W. L., Martin, D. L., Irmak, S., van Donk, S. J., & Yonts, C. D. (2008b). Minimum Center Pivot Design Capacities in Nebraska. NebGuide G1851. Lincoln, Neb.: University of Nebraska–Lincoln. Retrieved from http://ianrpubs.unl.edu/live/g1851/build/g1851.pdf

Lamm, F. R., Rogers, D. H., & Manges, H. L. (1994). Irrigation Scheduling with Planned Soil Water Depletion. *Trans. ASAE*, 37(5), 1491-1497.

Lo, T., Mateos, L., Heeren, D. M., & Luck, J. D. (2014). The Applicability of VRI for Managing Variability in Infiltration Capacity and Plant-Available Water: A Preliminary Discussion and GIS Study. ASABE Paper No. 141897710. St. Joseph, Mich.: ASABE.

Merriam, J.L. (1966). A Management Control Concept for Determining the Economical Depth and Frequency of Irrigation. *Trans. ASAE*, 9(4), 492-498.

NASS. (2004). 2003 Farm and Ranch Irrigation Survey. Washington, D.C.: United States Department of Agriculture. Retrieved from http://www.agcensus.usda.gov/Publications/2002/FRIS/

NASS. (2009). 2008 Farm and Ranch Irrigation Survey. Washington, D.C.: United States Department of Agriculture. Retrieved from http://www.agcensus.usda.gov/Publications/2007/Online_Highlights/Farm_and_Ranch_Irrigation_Survey/

NASS. (2014). 2013 Farm and Ranch Irrigation Survey. Washington, D.C.: United States Department of Agriculture. Retrieved from http://www.agcensus.usda.gov/Publications/2012/Online_Resources/Farm_and_Ranch_Irrigation_Survey/

Nebraska Department of Natural Resources. (2011). Nebraska Natural Resources District Boundaries – NRD. Lincoln, Neb.: Nebraska Department of Natural Resources. Retrieved from http://dnr.ne.gov/boundaries-plss

Nijbroek, R., Hoogenboom, G., & Jones, J. W. (2003). Optimizing irrigation management for a spatially variable soybean field. *Agric. Systems*, 76(1), 359-377.

NPPD. (2014). Electric Service For Irrigation. Columbus, Neb.: Nebraska Public Power District. Retrieved from http://www.nppd.com/assets/irrigationbrochure.pdf

NRCS. (2009a). Processed TIGER 2002 Counties + NRCS Additions Dissolve. Washington, D.C.: United States Department of Agriculture. Retrieved from http://datagateway.nrcs.usda.gov

NRCS. (2009b). Processed TIGER 2002 Counties plus NRCS Additions. Washington, D.C.: United States Department of Agriculture. Retrieved from http://datagateway.nrcs.usda.gov

NRCS. (2014). Gridded Soil Survey Geographic (gSSURGO) by State. Washington, D.C.: United States Department of Agriculture. Retrieved from http://datagateway.nrcs.usda.gov

Prism Climate Group. (2012). 1981-2010 Precipitation Normals. Corvallis, Oreg.: Oregon State University. Retrieved from http://www.prism.oregonstate.edu

Python. (2012). *Python 2.7.3*. Beaverton, Oreg.: Python Software Foundation.

Ritchie, J. T., & Amato, M. (1990). Field Evaluation of Plant Extractable Soil Water for Irrigation Scheduling. *Acta Horticulturae*, 278: 595-616.

UNL Extension. (2009). NAWMDN Survey. Lincoln, Neb.: University of Nebraska–Lincoln. Retrieved from http://water.unl.edu/c/document_library/get_file?uuid=7c342db7-0a59-488f-bccf-62120e4c8088&groupId=1882&.pdf

Woodruff, C. M., Peterson, M. R., Schnarre, D. H., & Cromwell, C. F. (1972). Irrigation scheduling with planned soil moisture depletion. ASAE Paper No. 72-222. St. Joseph, Mich.: ASAE.

CHAPTER 3: FIELD CHARACTERIZATION OF ROOT ZONE WATER HOLDING CAPACITY FOR VARIABLE RATE IRRIGATION

3.1. Abstract

One application of variable rate irrigation (VRI) is adapting to spatial heterogeneity of root zone water holding capacity (*R*). If such management is under consideration, an accurate estimate of the potential benefits is valuable for any associated investment decisions, and an accurate map of *R* is valuable for the design of VRI prescription maps. These two needs may be met by the field characterization of *R*. In this method, observational field capacity (FC_{obs}) is determined at chosen locations by measuring volumetric water content in the field after the wet soil has had time to drain following substantial precipitation. Then, the corresponding observational *R* (R_{obs}) is predicted throughout the field by regression with an auxiliary geospatial variable. This method was applied to a center pivot irrigated field in south central Nebraska. At this field site, parameterizing a daily soil water balance model with FC_{obs} values accounted for more of the observed spatial variability in soil moisture over time than with FC estimates determined from the gridded Soil Survey Geographic database (gSSURGO) or a pedotransfer function (PTF).

Other findings at the field site led to recommendations for producers and service providers on the use of this cost-effective method of spatially characterizing R_{obs}. To identify trends in R_{obs} successfully, it is important to sample FC_{obs} in the entire managed root zone, and it may also be important to sample FC_{obs} at close spacings in rapidly transitioning areas. Also, auxiliary variables for predicting *R* should be selected based on

an understanding of the spatial trends in R_{obs}. At this field site, R_{obs} correlated poorly with apparent soil electrical conductivity (EC_a) but correlated well with elevation. Where a VRI system is available regardless of the financial benefit from adapting to spatial heterogeneity of *R*, the field characterization of *R* is advised if the expected magnitude of the benefit exceeds the cost of the method. Where the purchase of a VRI system depends at least partially on the financial benefit from adapting to spatial heterogeneity of *R*, the method should be considered if the expected magnitude of the benefit, subtracting the cost of the method, is favorable for the purchase.

3.2. Introduction

Any soil water remaining at the end of one growing season will not be retained for crop transpiration if it is in the pore spaces that will be filled by precipitation before or early in the next growing season. In response to this phenomenon, the practice of planned soil moisture depletion (Woodruff et al., 1972; as cited by Lamm et al., 1994) reduces irrigation to allow greater consumption of stored soil water. To avoid water stress under conventional irrigation (CI; i.e., non-site-specific irrigate ion), however, the depletion has to be kept at a particular management allowed depletion (*MAD*; Merriam, 1966) of a low root zone water holding capacity (*R*) portion of the field. Consequently, in portions with larger *R*, where the end-of-season depletion under CI is smaller than *MAD*, the additional available soil water is unutilized and may leave through deep percolation after the irrigation season. This drained amount not only represents excessive irrigation but also can leach nitrogen (N) out of the root zone and into the groundwater. By using variable rate irrigation (VRI) to customize irrigation based on *R* in each portion of the field, the entire field can end the growing season at *MAD*, thus maximizing

utilization of stored precipitation and minimizing deep percolation. Therefore, adopting VRI in fields with spatial heterogeneities of *R* can generate benefits for producers by reducing irrigation costs and N fertilizer costs.

Previous research developed and implemented a method to estimate the magnitude of gross irrigation reductions from this particular application of VRI (Chapter 2). The simplicity of this method enabled the analysis of many center pivots. Nevertheless, reliance on the gridded Soil Survey Geographic database (gSSURGO; NRCS, 2015) predisposed this method to uncertainties. These uncertainties might be acceptable in a regional study such as Chapter 2, but they should not be overlooked when they may affect a producer's final VRI investment decision and VRI management for a particular field. Without ever leaving the computer, a producer can take the preliminary field-specific estimates from Chapter 2 and screen for fields where VRI benefits from adapting to spatial heterogeneity of *R* are expected to be large. Yet before the producer purchases a VRI system for this application or begins to manage VRI in this way, a more accurate characterization of *R* and a more accurate quantification of the potential benefits are desirable. These tasks would require visiting and collecting data from the field of interest.

One source of uncertainty in Chapter 2 was the values of *R* in gSSURGO. Water holding capacity values reported in gSSURGO for soil horizons were sometimes determined from laboratory measurements by assuming a certain soil water pressure for field capacity (FC). But according to the Soil and Water Terminology standard (ASAE Standards, 2007), FC is defined as the "amount of water remaining in a soil when the downward water flow due to gravity becomes negligible". In other words, FC is defined

by water flux and not by a fixed pressure, unlike permanent wilting point (PWP). The relationship between FC and the associated soil water pressure head (h_{FC}) has been found to be somewhat related to textural composition but generally difficult to predict (Romano and Santini, 2002). Also, soil layering can increase FC (Romano and Santini, 2002; Martin et al., 1990), an effect for which an isolated soil sample from one horizon cannot account. Furthermore, the tabulated values were rarely derived from samples taken at the exact soil map unit polygon of interest, so any natural or manmade local peculiarities would most likely not be reflected. In short, calculating *R* as the thickness-weighted sum of the gSSURGO water holding capacity values following Chapter 2 is convenient and informative but can be subject to significant error. In view of these problems, it is not surprising that Romano and Santini (2002) recommended field determinations of FC.

Another source of uncertainty in Chapter 2 was the spatial extent of soil map units, which dictated the spatial distribution of *R* in gSSURGO. The original Natural Resources Conservation Service (NRCS) soil survey maps were not conducted at a scale intended for precision agriculture (Brevik et al., 2003) and were not georeferenced with the Global Positioning System (GPS). Therefore, the boundaries of the soil survey map unit polygons should not be assumed to be sufficiently accurate for detailed maps of *R*. Dense geospatial data are sought for predicting field-determined *R* beyond the sampling locations due to the impracticality of dense field determinations of *R*.

Apparent soil electrical conductivity (EC_a) is a variable that can be measured densely by on-the-go sensors. In theory, EC_a is related to volume of the solid phase, volume of the liquid phase in fine pores, electrical conductivity of the solid phase, and electrical conductivity of the liquid phase in large pores (Rhoades et al., 1989). In twelve

fields across the north-central U.S., EC_a widely related well to clay content and cation exchange capacity (Sudduth et al., 2005). EC_a has also been claimed to locate the actual transitions between soil map units (Veris Technologies, 2002).

In the literature, EC_a has been used to predict *R* as well. This technique is attributed to Waine et al. (2000; as cited by Hezarjaribi and Sourell, 2007), and it has been implemented using Geonics (Mississauga, Ontario, Canada) electromagnetic induction (EMI) type sensors or Veris (Salina, Kans.) coulter type sensors (Hezarjaribi and Sourell, 2007). An indirect approach would first delineate the field into management zones based on the dense EC_a data and then assign a uniform *R* to each management zone based on *R* of the sampled locations within that management zone (Hedley and Yule, 2009). A direct approach would be to use regression (Hezarjaribi and Sourell, 2007) or geostatistics to predict *R* throughout the field based on the *R* and EC_a datasets. Regardless of the approach, a strong relationship between *R* and EC_a is critical to the success of this technique of making *R* maps. If such a relationship does not exist on the field of interest, then other dense geospatial datasets would be needed.

The field characterization of *R* can reduce uncertainties in the values of *R* and their spatial distribution. The classical experiment for measuring FC requires saturating the soil profile, covering the soil surface, and monitoring soil water content (Romano and Santini, 2002). A less demanding option for quantifying FC would be to measure "observational field capacity" (FC_{obs}; as in "observational study"), an estimate of FC that is determined under non-experimental conditions in the field. The concept of FC_{obs} is consistent with the suggestion by Martin et al. (1990) that "[a] good indication of the field capacity water content can be determined by sampling field soils one to three days

after a thorough irrigation or rain and when crop water use is small". Expressed as a depth over the managed root zone, the difference between FC_{obs} and permanent wilting point (PWP) is observational R (R_{obs}). Jiang et al. (2007) measured R_{obs} within two fields in a claypan landscape, found EC_a to correlate well with R_{obs} on both fields, and used the correlation to predict R_{obs} spatially. Whereas Jiang et al. (2007) was focused on developing methodology, Miller (2015) measured R_{obs} and evaluated its correlation to several soil and topographic variables specifically in the context of VRI. Miller (2015) found that R_{obs} was most correlated with EC_a in one field but not in the other field. Also, Miller (2015) assumed that actual FC was closer to FC_{obs} than to FC estimates from gSSURGO or from the Saxton and Rawls (2006) pedotransfer function (PTF).

By conducting the field characterization of R at a different field site, the main goal of this research was to generate recommendations on the use of this method for improving the mapping of R and the estimation of VRI benefits from adapting to spatial heterogeneity of R. Four finer objectives were addressed. First, variability in soil moisture and soil composition within the field site was described to provide context for the rest of the chapter and to offer advice on soil moisture measurements for the field characterization of R. Second, the reliability of FC_{obs} values was assessed by comparing them with FC values predicted from gSSURGO and the Saxton and Rawls (2006) PTF in terms of their effectiveness as parameters in a daily soil water balance model to account for observed spatial variability in soil moisture. Third, to derive guidelines on the selection of an auxiliary variable for predicting R in unsampled locations, EC_a and an alternate variable (chosen post-sampling based on understanding of the spatial trends in R) were compared in terms of their suitability as the auxiliary variable in the field site.

Fourth, the estimated magnitude of VRI benefits from adapting to spatial heterogeneity of *R* and its implications for the field characterization of *R* were discussed.

3.3. Methods

3.3.1. Field Site

This study was conducted on a private field in Hamilton County in south central Nebraska. Like most fields in Nebraska's loess plain, it predominantly consisted of upland loess-derived soils. From the point of highest elevation in the north, the field sloped down into two valleys (fig. 3.1a). According to the National Hydrography Dataset (USGS, n.d.), each of these valleys contained an ephemeral stream. The stream in the wider valley intersected the southwest of the field and had carved out a channel. This channel was dry at the beginning of the growing season, but after a large rain, it remained ponded for most of the monitoring period. An area along the banks of this channel was uncropped and inhabited by riparian vegetation. The stream in the narrower valley, on the other hand, intersected the east of the field and did not carve out a channel. Though the soil surface showed signs of overland water movement before the start of the monitoring period, the flow path was never observed to be ponded during the monitoring period. The difference between the maximum and the minimum elevation in this field was 12 m (USGS, 2014).

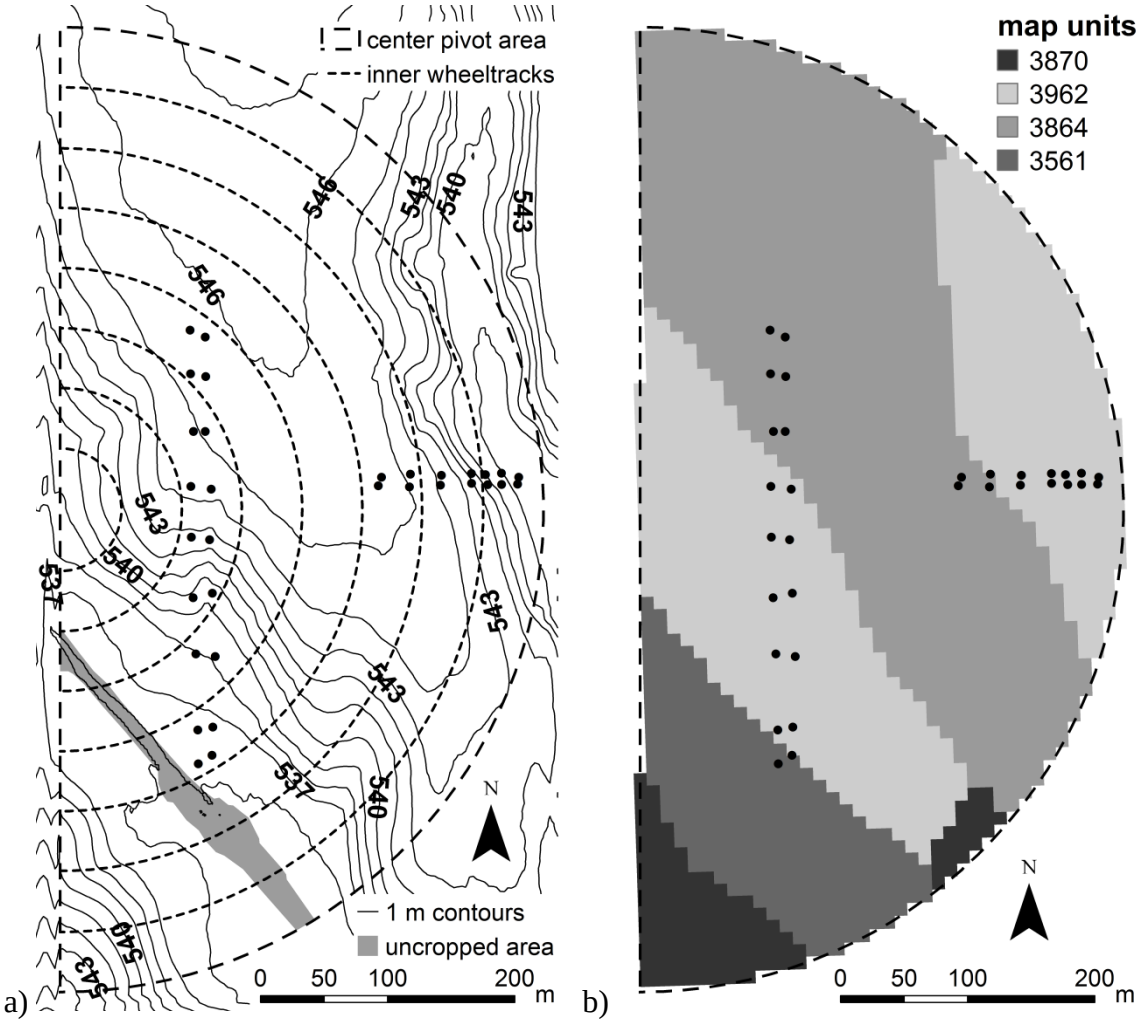

Figure 3.1. a) Topographic map and b) gridded Soil Survey Geographic database (gSSURGO; NRCS, 2015) map of the field site; the measurement locations (closed dots) form a pair of topographic transects parallel to corn rows (north-south) and a pair of topographic transects perpendicular to corn rows (east-west).

To characterize the soil water variability in this field with pronounced relief, soil water measurement locations were selected along topographic transects (fig. 3.1a). Nine slope positions were monitored along a pair of longer transects extending down into the wider valley. These nine slope positions were divided into three topographic groups: #1-3 as top, #4-6 as middle, and #7-9 as bottom. Seven slope positions were monitored along a pair of shorter transects extending into the narrower valley. These seven slope positions were also divided into three topographic groups: #1-2 as top, #3-5 as middle,

and #6-7 as bottom. Because the permanent ridge-tilled crop rows ran in the north-south direction, the longer transects—the parallel transects—were parallel to crop rows whereas the shorter transects—the perpendicular transects—were perpendicular to crop rows. The parallel transects spanned a larger elevation range but contained gentler slopes than the perpendicular transects (fig. 3.2).

a)

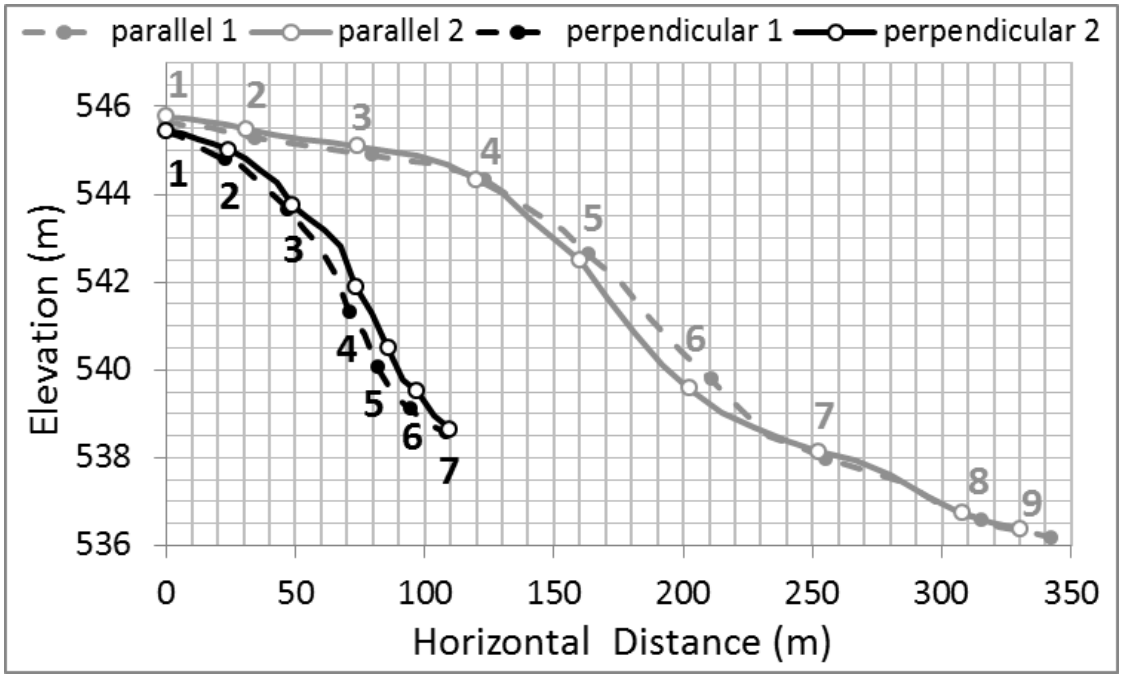

b)

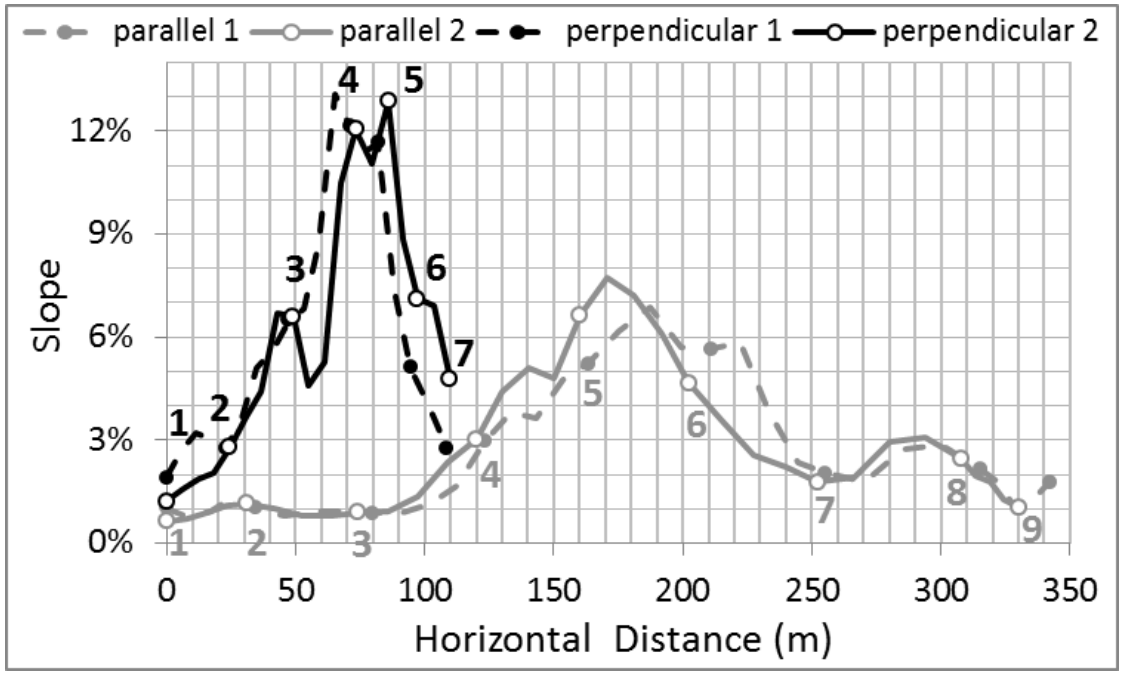

Figure 3.2. a) Elevation and b) slope along the two topographic transects parallel to corn rows and the two topographic transects perpendicular to corn rows, plotted against horizontal distance from the top of each transect; the 32 measurement locations are marked by dots and labeled with their respective slope position number.

The surface features of this field tended to channelize overland flow. The peak of the ridges could be 15 cm higher than the trough of the furrows as a consequence of the annual ridge tillage operation, which occurred after installations (see next subsection) but

before the monitoring period in 2014. Overland flow was thus expected to move predominantly along the furrows. Throughout the chapter, however, all depths were relative to the soil surface before the ridge tillage operation in 2014. The wheeltracks of the center pivot (fig. 3.1a), facilitated by steep inclines in this field, were expected to intercept and concentrate overland flow from intersecting furrows. These wheeltracks were filled between the 2013 and 2014 growing seasons as well as between the 2014 and the 2015 growing seasons. During the 2014 growing season, the wheeltracks were re-created as the center pivot made its first pass between 9 and 18 July 2014. The center pivot was frequently shut off partway through a pass due to rain.

As on many fields in the region, a corn-soybean rotation was generally practiced on this field. However, the 2014 growing season was a consecutive corn crop. The head rows were planted on 2 May 2014 whereas the rest of the field was planted on 3 May 2014. A center pivot irrigation system provided supplementary water between 9 July and 10 September 2014.

3.3.2. Soil Sampling and Neutron Gauge

On 3 June and 9 June 2014, a hydraulic direct-push soil sampling probe (Giddings Machine Company, Windsor, Colo.) was used to make holes and to insert aluminum access tubes at the measurement locations. The extracted soil cores were the source of soil samples centered at target depths of 15 cm, 46 cm, 76 cm, 107 cm, 137 cm, and 168 cm. Each sample was trimmed to a target length of 10 cm and placed in a metal soil can that was then sealed with electrical tape. After the soil samples were oven-dried, bulk density and volumetric water content (θ_v) were calculated.

The textural composition and organic matter content of the oven-dried samples were analyzed by Ward Laboratories, Inc. (Kearney, Neb.). A soil sample centered at the 15 cm depth was not collected at two measurement locations, so each of these two missing samples was assumed to have the same textural composition and organic matter content as the corresponding sample at the same slope position on the paired transect. Two-sample t-tests and Mann-Whitney tests were conducted in the statistical software R (R Core Team, 2015) for statistical comparisons of soil composition between the top and bottom topographic groups of each pair of transects. The t-test compared the means of two groups and assumed normality and equal group variance. The Mann-Whitney test avoided these assumptions by comparing the sums of the ranks of the group members. Because of small sample sizes (six measurement locations in the parallel top and bottom groups; four measurement locations in the perpendicular top and bottom groups), conformity with the two assumptions was not assessed formally to select the more appropriate statistical test. Instead, both tests were employed to identify any potentially noteworthy differences in soil composition between top and bottom topographic groups.

In this study, soil moisture measurements were obtained from 30 s readings by a CPN (Concord, Cal.) 503 Elite Hydroprobe neutron gauge. Target measurement depths were 15 cm, 46 cm, 76 cm, 107 cm, 137 cm, and 168 cm relative to the soil surface on installation day. Each measurement was assumed to represent the 30 cm layer that was centered at the target depth. On both installation dates, neutron gauge readings were taken later on the same day and then were divided by a standard count to compute count ratios. These count ratios were compared with the lab-determined θ_v of the corresponding soil samples (fig. 3.3). Soil samples that were questionable according to

field notes were omitted. The linear regression equation between count ratio and θ_v was applied as the gauge-specific, field-specific neutron gauge calibration. A different calibration was used for the 15 cm depth than for the deeper measurement depths.

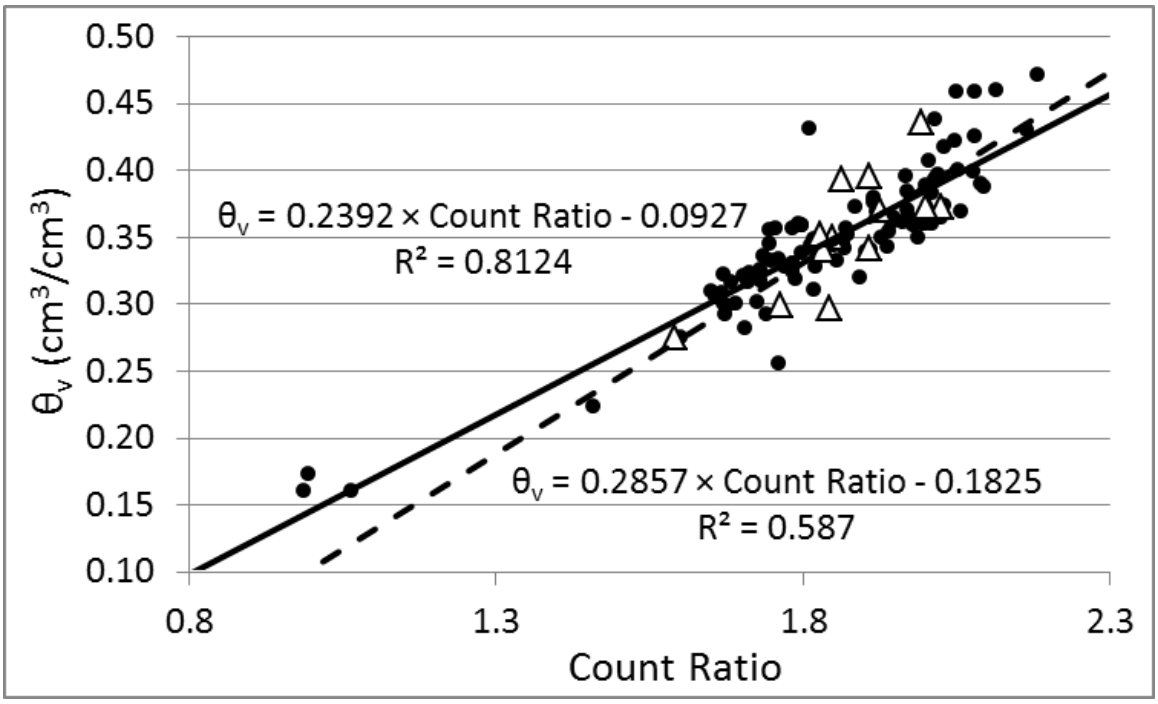

Figure 3.3. Gauge-specific, field-specific neutron gauge calibration, with volumetric water content (θ_v) determined by oven-drying intact soil cores, for the 15 cm measurement depth (triangles and dashed line) and for the deeper measurement depths (46 cm, 76 cm, 107 cm, 137 cm, and 168 cm; circles and solid line).

The neutron gauge product manual stated that a linear calibration is expected for θ_v between 0 and 0.4 cm^3/cm^3 (CPN International, 2013). The several points in figure 3.3 that were above 0.4 cm^3/cm^3 appeared to be generally underestimated by the calibration equations. If the relationship between count ratio and θ_v above 0.4 cm^3/cm^3 was truly steeper than the current calibrations, then θ_v differences between soil moisture measurements above 0.4 cm^3/cm^3 and those below 0.4 cm^3/cm^3 would be systematically underestimated.

Dry bentonite pellets were buried just beneath the soil surface around the access tubes. They were expected to swell upon absorbing moisture. Thus, a seal would be

created to hinder the entrance of water into the holes through the gap between the access tube and the surrounding soil. However, because bentonite has different water retention characteristics than topsoil, the sensitivity of the 15 cm neutron gauge readings to soil water changes in the top 30 cm may have been affected.

Neutron gauge standard counts were taken at least once per installation day or measurement day in the fully retracted position for 256 s. On 3 June 2014, standard counts were conducted on the tailgate of a pickup truck at the northwest corner of the field. On 9 June 2014 and onward, standard counts were conducted 1.5 m above the ground at the southeast corner of the field.

The monitoring period started on 18 June 2014 and ended on 19 March 2015. This chapter used only the seven dates when all 32 access tubes were read by the neutron gauge. Total soil water in the managed root zone of 122 cm (TW; relative to $\theta_v = 0$) was calculated as the product of 122 cm and the average of the measured θ_v at 15 cm, 46 cm, 76 cm, and 107 cm. Statistical analyses on the temporal rank stability of soil water (Vachaud et al., 1985) and on the soil water differences between top and bottom topographic groups were conducted with the neutron gauge data and were presented in Appendix C.

3.3.3. Estimation of FC and R

Following Miller (2015), FC and *R* were estimated from gSSURGO, from a PTF, and from soil moisture measurements (i.e., the observational method). The gSSURGO soil property values designated as "representative" (NRCS, 2015) were used exclusively. For every soil horizon up to a depth of 200 cm in the four soil map units found in this field (i.e., map unit symbols 3561, 3864, 3870, and 3962), gSSURGO reported its

volumetric water content at 15,000 cm of tension (θ_{15000}; i.e., PWP) and its available water capacity (i.e., water holding capacity). The FC of a horizon was calculated as the sum of its θ_{15000} and its water holding capacity. Total soil water in the managed root zone at FC (TW_{FC}; relative to $\theta_v = 0$) was then calculated as the horizon thickness weighted sum of FC between the depths of 0 and 120 cm. Likewise, *R* was calculated as the horizon thickness weighted sum of water holding capacity in the top 120 cm. When a soil map unit comprised more than one component soil, the components' values of TW_{FC} and *R* were each weighted by that component's percent composition and then averaged. All the gSSURGO computations were conducted according to Chapter 2.

The Saxton and Rawls (2006) PTF has been commonly used for Nebraska soils (Deck, 2010; Mortensen, 2011; Rudnick and Irmak, 2014). This PTF relies on multiple regression to predict the soil water retention function and the unsaturated conductivity function (Saxton and Rawls, 2006). The PTF was applied to all soil samples from the access tube holes. In addition to sand, clay, and organic matter, bulk density is also one of the necessary inputs for the PTF (Saxton and Rawls, 2006). Confident bulk density measurements were not obtained for many of the soil samples. For consistency of comparison, the average of all the bulk density measurements that were included in the neutron gauge calibration, which was 1.37 g/cm^3, was used in every PTF prediction. Noticeable trends in bulk density along the topographic transects at a given sampling depth were not observed within the managed root zone of 122 cm. However, higher bulk densities at 137 cm and 168 cm in the bottom topographic groups than in the top topographic groups were suspected from the limited data.

θ_{15000} was calculated by entering a tension of 15,000 cm into the predicted soil water retention function. Without extra information, the predicted soil water content at a tension of 333 cm (θ_{333}) was estimated as FC (Rudnick and Irmak, 2014). Water holding capacity was thus the difference between θ_{333} and θ_{15000}. The values for each soil sample were assumed to represent the 30 cm layer centered at that soil sample's target sampling depth. At each of the measurement locations, the PTF TW_{FC} and *R* were the layer thickness weighted sum of θ_{333} and water holding capacity, respectively, predicted for the 15 cm, 46 cm, 76 cm, and 107 cm soil samples.

As stated earlier, FC is preferably determined in the field rather than in the laboratory. Proper field measurement of FC is performed by saturating the soil beyond the depth of interest and then monitoring the water content decline in the absence of evapotranspiration (ET) (Romano and Santini, 2002). Reaching the state of negligible drainage in this test can take a long time even with a homogeneous soil profile (Romano and Santini, 2002). Yet in a center pivot irrigated field with adequate internal drainage, the managed root zone is unlikely to be completely saturated by rain or irrigation. In addition, ET is rarely avoidable while a crop is developing. Both characteristics cause FC to be approached more quickly after wetting during the growing season than during the proper field experiment. Operationally, drainage could become negligible as compared to other water fluxes after one to three days (Martin et al., 1990).

In this study, FC was not measured. However, the values of TW on 18 June 2014 were chosen as in-situ observational estimates of TW_{FC}. 18 June 2014 was the first day of the monitoring period and three days after a large rain near the end of a wet period. For 20 out of the 32 measurement locations, TW on this date was the largest among the

seven measurement dates. Because drainage rates were not confirmed to be negligible, TW on 18 June 2014 may differ from TW_{FC} as measured in the classical field capacity experiment. Also, the influence of other hydrological fluxes, namely capillary rise and subsurface lateral flow, could have been present in the TW measurements on 18 June 2014. FC_{obs}, in summary, should be treated as an operational quantity rather than a scientific constant.

Within fully irrigated fields in humid or sub-humid climates, the managed root zone may never reach PWP under normal conditions. Estimating PWP with soil moisture measurements might be impossible in this setting without interfering with water inputs. However, the pressure plate is the standard technique for measuring PWP because PWP is operationally defined at -1.5 MPa and is also relatively insensitive to deviations around this fixed pressure (Romano and Santini, 2002). In the absence of pressure plate measurements, the PTF were used to obtain layer-specific, location-specific estimates of PWP, from which R_{obs} was calculated for each measurement location. Saxton and Rawls (2006) had calibrated the PTF to laboratory-determined soil water retention data, and it was generally more accurate at estimating θ_{15000} than θ_{333} (Saxton and Rawls, 2006).

3.3.4. Daily Soil Water Balance

The estimates of TW_{FC} from gSSURGO, the PTF, and the observational method were compared by their effectiveness in accounting for observed spatial variability in TW when used to parameterize a simple daily soil water balance model. This soil water balance model treated the managed root zone at each measurement location as a bucket whose size was equal to the *R* assigned to that measurement location. To initialize the model, the bucket at each measurement location started with TW of that location on 18

June 2014. Each day between 19 June 2014 and 14 August 2014, effective precipitation and net irrigation could add water to the bucket, whereas crop ET and deep percolation could remove water from the bucket. To match how a producer might use a simple irrigation scheduling tool, the parameters for these fluxes were not calibrated.

Precipitation was assumed to be spatially uniform throughout the field. When available and reliable, hourly precipitation data from the tipping bucket rain gauge of a Pessl (Weiz, Austria) weather station in the northeast corner of the field were obtained. Otherwise, daily precipitation data from two nearby Global Historical Climatology Network (GHCN) weather stations (Aurora 4 N and Hampton 0.8 ENE; NOAA, 2014) were downloaded and averaged. Then, daily effective precipitation was determined by subtracting from daily precipitation the amount of runoff predicted by a curve number of 80 (fig. 3.4).

a)

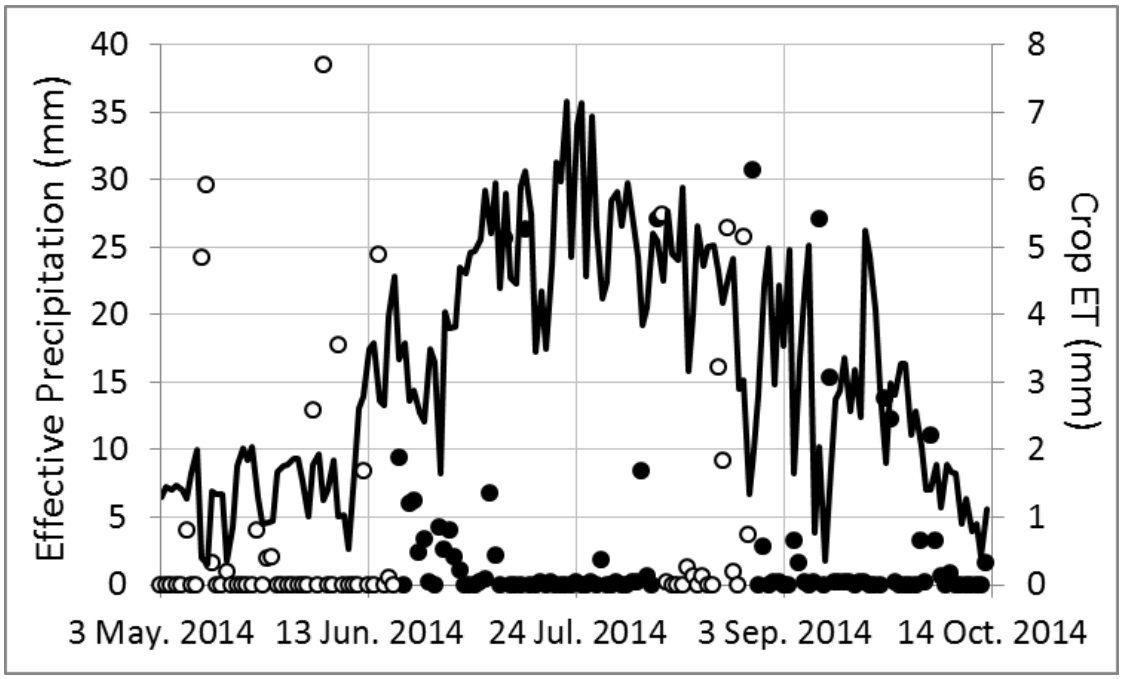

b)

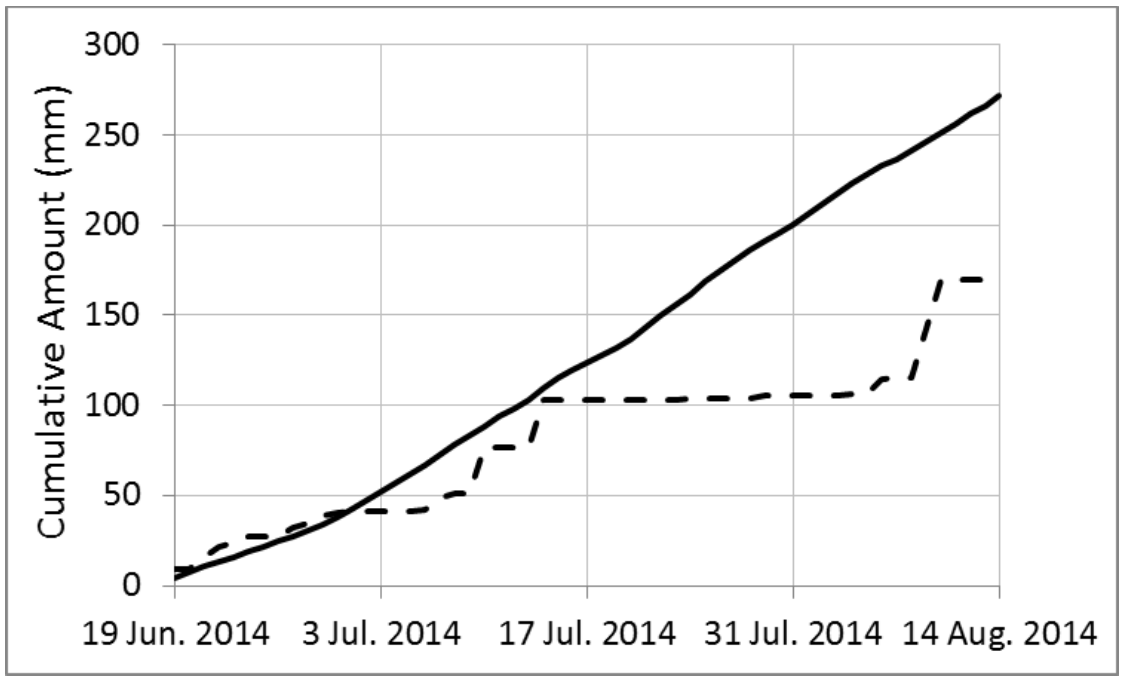

Figure 3.4. a) Daily crop ET calculated from data of an AWDN weather station (black line) and daily effective precipitation calculated from data of two GHCN weather stations (open dots) or an on-site Pessl weather station (closed dots); b) cumulative crop ET (solid line) and cumulative effective precipitation (dashed line) during simulation period.

Target gross irrigation depths were kindly provided by the farmer-cooperators. Pump flow rate readings from a McCrometer (Hemet, Cal.) propeller meter were recorded by a Campbell Scientific (Logan, Utah) CR10X datalogger. This propeller

meter compared well to a Fuji Electric (Tokyo, Japan) PORTAFLOW X ultrasonic flow meter, so it was used to adjust the expected gross irrigation depths to reflect the observed flow rates. Due to insufficient system pressure, the expected gross irrigation depths were further adjusted for each measurement location to account for reduced sprinkler discharges. The design specifications for the center pivot at the field site were provided by the farmer-cooperators, and the elevation of the center pivot towers was obtained from the 1/9 arc-second National Elevation Dataset (NED) tile that included the field (USGS, 2014). Applying the Hazen-Williams pipe friction equation, flow rate and pressure were simulated from sprinkler to sprinkler between the pivot point and the end of the lateral. Reductions in sprinkler discharge along the lateral at various angles of revolution were then estimated by matching simulated system flow rates to observed system flow rates. A constant and uniform application efficiency (E_a) of 0.85 was assumed (Kranz et al., 2008b).

Crop ET was estimated using the two-step approach (fig. 3.4). Daily reference ET was downloaded for the High Plains Regional Climate Center's (HPRCC) Automated Weather Data Network (AWDN) weather station at Grand Island, Nebraska (HPRCC, 2014). HPRCC calculates reference ET using the Penman equation in conjunction with an alfalfa wind function calibrated by Kincaid and Heermann (1974). Wright's tabular mean crop coefficients for field corn (Allen and Wright, 2002) were interpolated with piecewise regression equations to obtain daily single crop coefficients (eqs. 3.1-3.5). 3 May 2014 and 15 July 2014 were used as the planting date and effective cover date inputs to Wright's crop coefficients. Before effective cover, the crop coefficient was a function of f_{ec}, the fraction of time until effective cover (eqs. 3.1-3.2). After effective cover, the

crop coefficient was a function of t_{ec}, the number of days after effective cover (eqs. 3.3-3.5).

$$K_{cr} = 0.2, 0 \leq f_{ec} < 0.3 \tag{3.1}$$

$$K_{cr} = -2.273 f_{ec}^{\ 3} + 5.158 f_{ec}^{\ 2} - 2.4693 f_{ec} + 0.5393, 0.3 \leq f_{ec} < 1 \tag{3.2}$$

$$K_{cr} = -0.00006 t_{ec}^{\ 2} + 0.0011 t_{ec} + 0.9533, 0 \leq t_{ec} < 70 \tag{3.3}$$

$$K_{cr} = 0.74 + (0.35 - 0.74)\left(\frac{t_{ec} - 70}{80 - 70}\right), 70 \leq t_{ec} < 80 \tag{3.4}$$

$$K_{cr} = 0.35 + (0.25 - 0.35)\left(\frac{t_{ec} - 80}{90 - 80}\right), 80 \leq t_{ec} \leq 90 \tag{3.5}$$

Wright's crop coefficients were originally calibrated for use with the 1982 Kimberly Penman reference ET equation (Allen and Wright, 2002). Because HPRCC's method of computing reference ET was more similar to the 1982 Kimberly Penman Reference ET Equation than to the ASCE Standardized Reference ET Equation (J. B. Barker, personal communication, 2015), this study used the original crop coefficient values instead of those modified for compatibility with the ASCE Standardized Reference ET Equation.

Two contrasting simplifying assumptions about deep percolation were tested. The managed root zone returned to TW_{FC} either at the end of the day if TW_{FC} was still exceeded, or at the end of three continuous days above TW_{FC}. End-of-day deep percolation is common among simple daily soil water balance models, whereas three-day delay deep percolation is consistent with measuring FC_{obs} on 18 June 2014, which was three days after a large rain.

Optimally, the simulations would be compared with continuous soil moisture sensors. In the absence of reliable data from such devices, the modeled TW within the managed root zone were compared against measured TW on five later dates during the same growing season. Mean bias (MB) and root mean squared error (RMSE) were calculated within each of the six topographic groups on each comparison date. Positive MB indicated overestimation, whereas negative MB indicated underestimation. The method of estimating TW_{FC} that was most effective in accounting for spatial variability in TW would have the smallest spread in MB among topographic groups.

3.3.5. Geospatial Data and Their Prediction of R

The gSSURGO 10 m soil map unit raster for Nebraska (NRCS, 2015) and the 1/9 arc-second National Elevation Dataset (NED) tile that included the field site (USGS, 2014) were downloaded. The NED digital elevation model (DEM) was in the North American Datum of 1983 (NAD 1983) Universal Transverse Mercator (UTM) Zone 14N projection.

Apparent soil electrical conductivity (EC_a) was collected on 26 April 2015 using a Veris (Salina, Kans.) MSP unit. Readers are referred to Rudnick and Irmak (2014) for the theoretical depth-weighting functions for the shallow and deep EC_a readings. In this study, any sampling point where the shallow or the deep EC_a reading was beyond three interquartile ranges from the field median was filtered out. This step eliminated 360 out of 4,518 total sampling points. Ordinary kriging, as implemented in Geostatistical Wizard of ArcGIS 10.2 (ArcGIS, 2013), was selected as the method for interpolating between EC_a sampling points. Anisotropy was observed and incorporated into the semivariogram model. For shallow EC_a, the nugget, major range, minor range, major

range direction (clockwise from north), and partial sill of the fitted exponential semivariogram were 27 $(mS/m)^2$, 200 m, 102 m, 157°, and 122 $(mS/m)^2$. For deep EC_a, the nugget, major range, minor range, major range direction (clockwise from north), and partial sill of the fitted exponential semivariogram were 42 $(mS/m)^2$, 340 m, 169 m, 149°, and 177 $(mS/m)^2$. Predictions were conducted using two to five closest neighbors in each of four sectors, which were arranged with a 45° offset relative to the direction of maximum range. Comparing the predictions with the measured values at the EC_a sampling points, RMSE was 6.4 mS/m for shallow EC_a and 7.6 mS/m for deep EC_a. Finally, the kriging predictions were exported as a raster with the same cell size and projection as the 1/9 arc-second NED DEM. The EC_a ratio (Kitchen et al., 2005) raster was computed using Raster Calculator in ArcGIS by dividing the value of each shallow EC_a raster cell by the value of the corresponding deep EC_a raster cell.

The latitudes and longitudes of the measurement locations in the World Geodetic System 1984 geographic coordinate system were obtained using a Garmin (Olathe, Kans.) GPSMAP 64s handheld GPS device. The positions were then projected to the NAD 1983 UTM Zone 14N projection. Each of the measurement locations was assigned the value of elevation, shallow EC_a, deep EC_a, and EC_a ratio of the grid cell in which that measurement location fell.

A regression equation between elevation and R_{obs} was obtained for the measurement locations. To avoid the extrapolation of the regression equation beyond the elevation range of the measurement locations, a piecewise approach was adopted. Specifically, any point in the field with an elevation higher than the highest measurement location was assigned the value of R that the regression equation predicted for the highest

measurement location. Likewise, any point in the field with an elevation lower than the lowest measurement location was assigned the value of R that the regression equation predicted for the lowest measurement location. The piecewise prediction function for R_{obs} was applied to the NED DEM in ArcGIS to obtain an R_{obs} map of the field.

In contrast to Miller (2015), this study did not begin with a group of geospatial variables and subsequently select by trial and error elevation as the auxiliary variable for predicting R_{obs}. Rather, in view of the observed spatial trend in R_{obs}, elevation was designated as a natural proxy for the underlying attributes and processes that are causing the variability. This variable choice based on understanding gained from determining R_{obs} was intentional to juxtapose with the use of EC_a variables because it is easy to become overly dependent on EC_a variables.

3.3.6. Quantification of Benefits

In this study, the quantification of VRI benefits from adapting to spatial heterogeneity of R is based on the unutilized R (U) concept developed in Chapter 2. CI is assumed to leave an end-of-season depletion equal to MAD of a particular R within the field. This R is called R_p because it is greater than R in pth percentile of the field, whereas the field-average amount of R in excess of R_p is defined as U. If the managed root zone is always refilled by effective precipitation before or early in the irrigation season, VRI can reduce irrigation over management zones with R larger than R_p and increase utilization of the stored precipitation. The differential irrigation management can continue until the entire field reaches the specified MAD. Because the reduction in net irrigation becomes the reduction in deep percolation, nutrient leaching is decreased as

well. Therefore, adapting to spatial heterogeneity of R with VRI produces a reduction in the public and private costs of irrigation (ΔW_r) and agrochemicals (ΔX_r; Chapter 1).

For simplicity, the values of R and their spatial distribution are assumed to be known perfectly, and irrigation is assumed to be applied exactly as prescribed at all points within the field. In reality, the achievable level of VRI benefits from adapting to spatial heterogeneity of R is not only limited by uncertainties about R but also by the fixed fineness of irrigation zones due to a finite number of sprinklers with overlapping wetting patterns. The performance of VRI systems at the boundaries of irrigation zones has been examined by Hillyer et al. (2013) and Daccache et al. (2015). For a consideration of VRI fineness of control in estimating an achievable level of VRI benefits, readers are referred to Feinerman and Voet (2000) and Miller (2015).

The volume of gross irrigation reductions from adapting to spatial heterogeneity of R was calculated first. Each grid cell in the R_{obs} map was converted to a point, and a table with R_{obs} of every cell was exported. After ranking the R_{obs} values and assigning probabilities of exceedance according to the Weibull formula, the cumulative distribution function of R_{obs} was generated to calculate R_p and U. Repeating these step for the gSSURGO R map enabled comparisons between the Chapter 2 gSSURGO method and from the field characterization of R in terms of the magnitude of U and the sensitivity of U to the choice of p. The rest of the computations to find the volume of gross irrigation reductions followed Chapter 2. A *MAD* of 0.5 (Kranz et al., 2008a) and an E_a of 85% (Kranz et al., 2008b) were assumed. The field site area under the eight-span center pivot (A) was found to be 22.7 ha using the Calculate Geometry command in ArcGIS.

As a comparison, the volume of gross irrigation reductions from enforcing an avoidance zone over the uncropped area (Sadler et al., 2005) was calculated. The uncropped area (fig. 3.1a) was drawn as a polygon in ArcGIS based on aerial imagery from the 2014 National Agricultural Imagery Program (FSA, 2014). The size of this uncropped area was also obtained using the Calculate Geometry command in ArcGIS.

In this study, the amount of agrochemical reductions from adapting to spatial heterogeneity of *R* included only the decrease in leached N due to less deep percolation. All deep percolate was assumed to contain 0.24 kg/ha-mm of N. This concentration was the average nitrate-N concentration measured from lysimeter leachate between 1993 and 1998 under continuous corn—managed according to contemporary best management practices—in North Platte, Nebraska (Klocke et al., 1999). The decrease in N fertilizer application, assumed to be by the same magnitude as the decrease in leached N, results in a private benefit.

The contribution of the private components of ΔW_r and ΔX_r to paying for a potential VRI investment (Chapter 1) at the field site was investigated next. The private component of ΔW_r is the volume of gross irrigation reductions multiplied by the private variable cost of gross irrigation (C_w). At this field site, the pumping water level was measured to be 33.5 m (D. Brar, personal communication, 2014), and the design pressure of the electric irrigation pump is 414 kPa. The pump was assumed to be operating at 100% of the Nebraska Pumping Plant Performance Criteria for electrically powered irrigation pumps (Kranz, 2010), which means 75% pump efficiency and 88% electric motor efficiency. This field subscribes anytime interruptible electricity service, which is estimated to have a variable cost of $0.0624/kWh (NPPD, 2014). Based on the

information above and neglecting non-energy costs, C_w was estimated at \$0.195/ha-mm for the field site.

The private component of ΔX_r is the amount of N fertilizer reductions multiplied by the private variable cost of N fertilizer (C_x). Average fertilizer prices in the neighboring state of Iowa were obtained from Agricultural Marketing Service (AMS, 2015). The anhydrous ammonia (82% N) prices reported in the first half of April in 2011-2015 were averaged without any adjustments for inflation, resulting in a value of \$855.59/Mg. Neglecting non-material costs, C_x was estimated at the equivalent cost per unit of N of \$1.04/kg.

A discount rate (i; also known as "interest rate") of 5% and an amortization period n of 10 years were assumed for the potential VRI system. The present value of the private components of the VRI benefits from adapting to spatial heterogeneity of R, assumed as a uniform annual series, can be calculated using equation 3.6, which is adapted from Chapter 1 and expanded. The discount rate and all prices were assumed to be constant in real terms (i.e., equal inflation rate) during the amortization period.

$$PV_r = \sum_{t=1}^{n} \frac{(\Delta W_r + \Delta X_r)}{(1+i)^t} = \left\{ MAD\left(\frac{C_w}{E_a} + c_x C_x \right) A\left[\frac{(1+i)^n - 1}{i(1+i)^n} \right] \right\} U = q_r U \tag{3.6}$$

where

t = years since the VRI system began operation (-), and

q_r = field-specific coefficient (\$/mm).

Finally, the economic value of the field characterization of R was evaluated. For simplicity, the field characterization of R was assumed to result in perfect information about R and enable the actualization of the estimated VRI benefits from adapting to

spatial heterogeneity of *R*. On some fields, the VRI system is available irrespective of the magnitude of the private benefit from this application of VRI. The value of the field characterization of *R* in this scenario is PV_r, the magnitude of that benefit.

On other fields, the purchase of the VRI system depends at least partly on the magnitude of the private benefit from this application of VRI. The profitability of this potential VRI investment would be $PV_r + PV_o - C_v$, where PV_o is the present value of the private components of the other VRI benefits and where C_v is the total cost of VRI. In this scenario, the value of the field characterization of *R* would equal to the difference in financial outcome when the VRI investment decision is made based on the actual magnitude of PV_r as opposed to the magnitude estimated from gSSURGO.

The breakeven *U* (U_b) was defined as $(C_v - PV_o) / q_r$. If both gSSURGO *U* and actual *U* are less than U_b, then the value of the field characterization of *R* is zero because the VRI investment would not be made. If gSSURGO *U* is greater than or equal to U_b but actual *U* is less than U_b, then the value is $C_v - PV_o$ – actual PV_r because the loss from the VRI investment would have been prevented by the field characterization of *R*. If actual *U* is greater than U_b, then the value is actual $PV_r + PV_o - C_v$ because the profit from the VRI investment is made possible by the field characterization of *R*.

The analysis on the economic value of the field characterization of *R* was applied to both the field site and a typical Nebraska center pivot irrigated field of 50 ha. The bottom of the range of VRI initial capital costs in Evans et al. (2013) was $200/ha. Assuming that this cost per area applies to full-circle center pivots, it was doubled to $400/ha for the field site, which is irrigated by a half-circle center pivot. C_v was thus estimated to be $9,088 for the field site and $10,000 for the typical field. For the typical

field, C_w was assumed to be \$0.137/ha-mm, a typical irrigation pumping energy cost calculated in Chapter 2. The typical field was assumed to have the same C_x of \$1.04/kg N as the field site.

3.4. Results and Discussion

3.4.1. Spatial Variability in Soil Moisture and Soil Composition

Data on the variability in soil moisture and soil composition along the topographic transects at the study site were presented. These descriptions of the field site provided context for the analyses in the later subsections and insights for field data collection as well as VRI management.

Average Deviations from Transect Average θ_v

At different measurement depths, how soil water content at various slope positions generally deviates from the transect average was shown in figures 3.5a-d. Along the parallel and the perpendicular transects, how average soil water content in the 0-122 cm managed root zone generally deviates from the field average was shown in figure 3.5e. Positive values indicated above-average θ_v, whereas negative values indicated below-average θ_v.

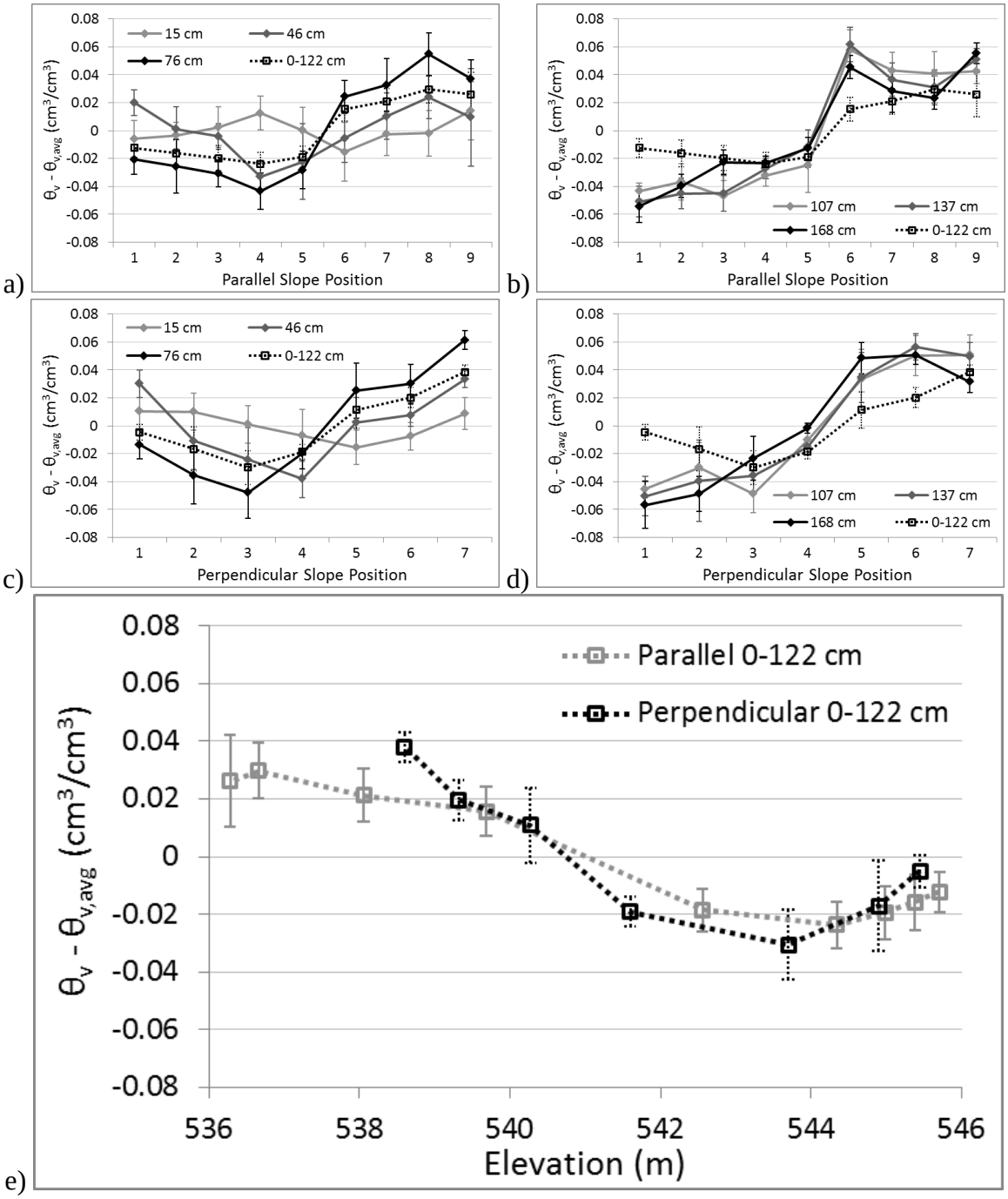

Figure 3.5. The differences, averaged over seven dates, between volumetric water content (θ_v) measured at a slope position and either a-d) transect average θ_v at the same measurement depth on the same day or e) field average θ_v in managed root zone on the same day; error bars indicate standard deviation among 14 replicate-time combinations.

In these graphs, θ_v was most spatially uniform at 15 cm among the six measurement depths. In fact, 0-122 cm averages could not be predicted from 15 cm

measurements because the two spatial trends did not match. It is acknowledged that more neutrons could escape when the neutron gauge was measuring near the soil surface. Also, the neutron gauge calibration used in this study did not account for the water absorbed by the bentonite clay pellets after installation. Despite these limitations, this dataset suggested that characterizing soil water patterns in only the top 30 cm may be insufficient when the managed root zone extended much deeper.

The literature supports the claim that soil water patterns in the topsoil may not match soil water patterns in the subsoil. Hanna et al. (1982) monitored soil moisture with a neutron gauge almost weekly for over two years at four topographic positions within a rainfed field under corn-soybean rotation in Lancaster County, Nebraska. Averaging over time as well as among replicates and hillslopes, the summits had 8 mm more available water than the footslopes at 0-30 cm but 7 mm less available water than the footslopes at 30-60 cm. Yet at 60-90 cm, 90-120 cm, and 120-150 cm, the footslopes had more available water than the summits by 14 mm, 16 mm, and 12 mm, respectively. Hupet and Vanclooster (2002) monitored soil moisture with a neutron gauge 45 times during one growing season in a 15 m grid within a rainfed maize field in Belgium with moderate terrain. At shallow depths, spatial variability in soil water was temporally dynamic, and it was attributed to differences in crop growth and in root water uptake. The spatial variability in soil water at 100 cm and 125 cm, however, was “high” and “very temporally stable”, and it was attributed to differences in subsoil composition. Thus, for VRI research and implementation, soil moisture measurements should be taken at least to the depth of the managed root zone.

At 30-183 cm, θ_v appeared to be related to profile curvature, which is the curvature of the terrain parallel to the slope direction. Curvature has been associated with soil moisture variability in the literature (Sinai et al., 1981; Western et al., 1999). Readers can refer to figure 3.2 for the shape of the two hillslopes and for the slope positions of the measurement locations. On one hand, the 46 cm and 76 cm measurements decreased where the slope was increasingly convex and increased where the slope was increasingly concave. The 107 cm, 137 cm, and 168 cm measurements, on the other hand, exhibited a marked jump where slope was the steepest and profile curvature switched from convex to concave. Along the parallel transect, the pattern was like a stairstep. Similarly low θ_v values were measured from slope positions 1 to 5, and similarly high values were measured from slope positions 6 to 9. Along the perpendicular transects, the largest increase generally occurred between slope positions 4 and 5, but the transition was more gradual overall. Natural features are often expected to lie on a continuum. However, drastic differences in soil water may be found along short, steep hillslope stretches where profile curvature switches from convex to concave. If the soil water distribution along one such hillslope stretch is to be characterized well, closely spaced measurement locations may be warranted.

θ_v Profiles During the Monitoring Period

Whether along the parallel or the perpendicular transects, the middle stretch behaved as a zone of rapid transition rather than a distinct homogeneous area. Average soil water profiles for the top and bottom topographic groups at seven times during the monitoring period were shown in figures 3.6a-g.

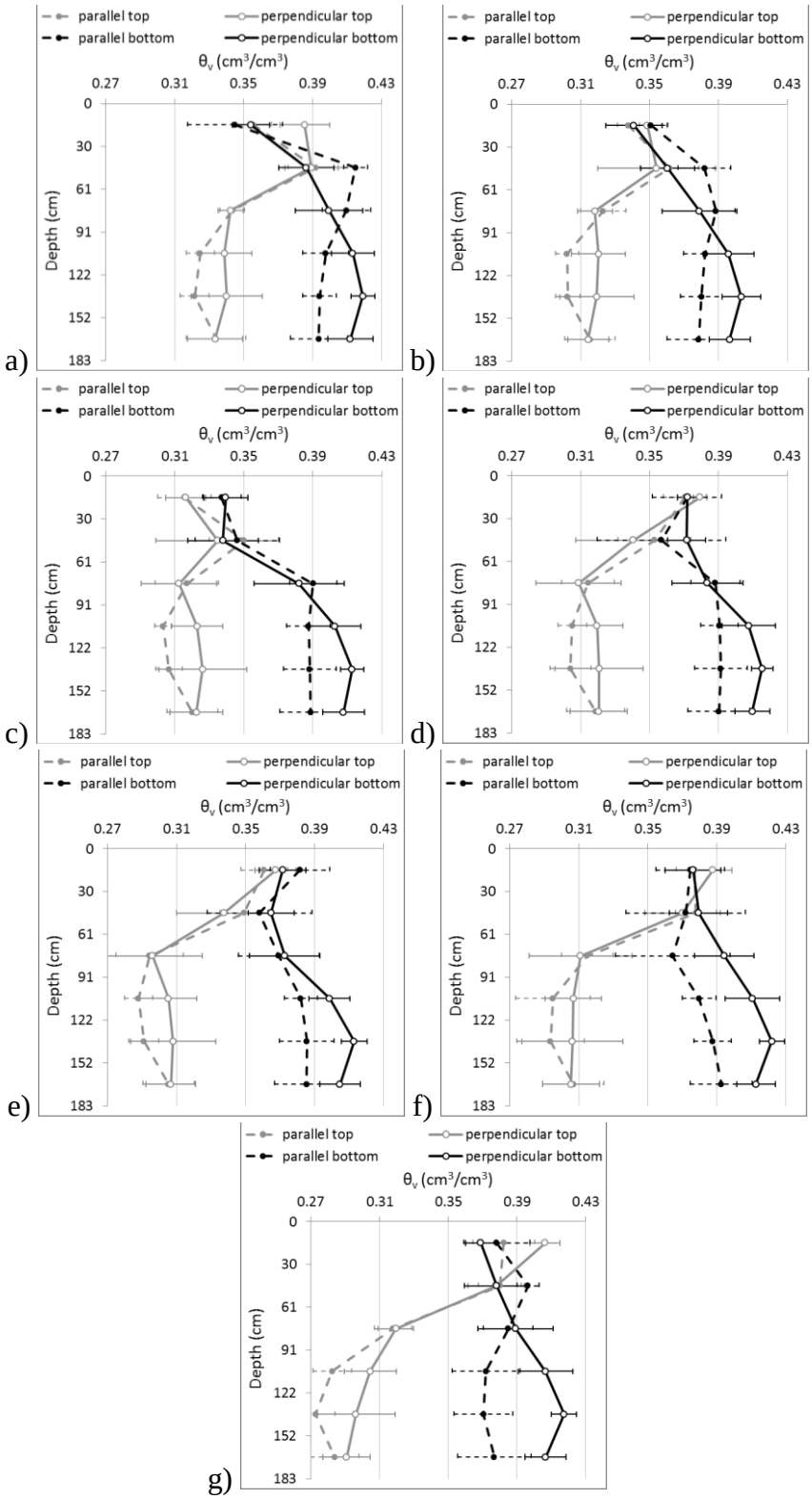

Figure 3.6. Volumetric water content (θ_v), averaged within topographic groups, on a) 18 June 2014, b) 2 July 2014, c) 9 July 2014, d) 17 July 2014, e) 30 July 2014, f) 14 August 2014, and g) 19 March 2015; error bars indicate standard deviation among the four or six measurement locations of the specified topographic group on the specified date.

In agreement with previous observations, the 15 cm measurements and, to a lesser extent, the 46 cm measurements, were similar among topographic groups. The inter-group soil water differences at 61-183 cm, in contrast, were clearer and more persistent. They ranged between 0.057 and 0.079 cm^3/cm^3 on the first measurement date. Subsequently, the inter-group differences at the 107 cm, 137 cm, and 168 cm measurement depths had upward trends. Along the parallel transects, the increase in the differences at those three depths was 0.017, 0.025, and 0.033 cm^3/cm^3, respectively. Along the perpendicular transects, the increase in the differences at those three depths was 0.028, 0.042, and 0.038 cm^3/cm^3, respectively. These findings were similar to the slightly increasing spatial variability in subsoil water content during the growing season as reported by Hupet and Vanclooster (2002).

Just as high temporal stability of the subsoil water content pattern was observed in this study, high temporal stability of the soil moisture pattern has been observed in other VRI-related studies (Starr, 2005; Hedley and Yule, 2009). High temporal stability of soil water patterns has been attributed to the influence of stable properties such as textural composition (Vachaud et al., 1985). This phenomenon allows the selection of sensor locations that routinely represent, for example, the driest or the wettest areas of a field (Vachaud et al., 1985). If the same magnitude of soil water differences recurs every growing season, VRI can be managed to take advantage of these differences with a static prescription map (Starr, 2005) even without sensor input.

Soil Composition

Unlike soil water, soil composition trends along the topographic transects were difficult to discern (fig. 3.7). Most of the soils were distributed along the boundary of silt

loam and silty clay loam on the textural triangle, which is typical of the Loess Plain. From statistical comparisons (table 3.1), the most confident differences between the top and bottom groups on the parallel transects were almost all at the 137 cm and 168 cm depths. There was less silt and more clay at these depths in the bottom group than in the top group. Also, for all sampled depths except 15 cm, there was more organic matter in the bottom group than in the top group. On the perpendicular transects, the bottom group had less clay at 46 cm as well as less silt and more clay at 107 cm and 168 cm as compared to the top group. Like the parallel transect, more organic matter was found at the 76 cm and 168 cm depths in the bottom group than in the top group. Yet, these differences were smaller and statistically less significant than the corresponding differences on the parallel transects. It is certainly possible that the soil composition differences at 168 cm could play a role in the subsoil water content trend along the hillslopes, but evaluating this potential cause-and-effect relationship was beyond the scope of this chapter.

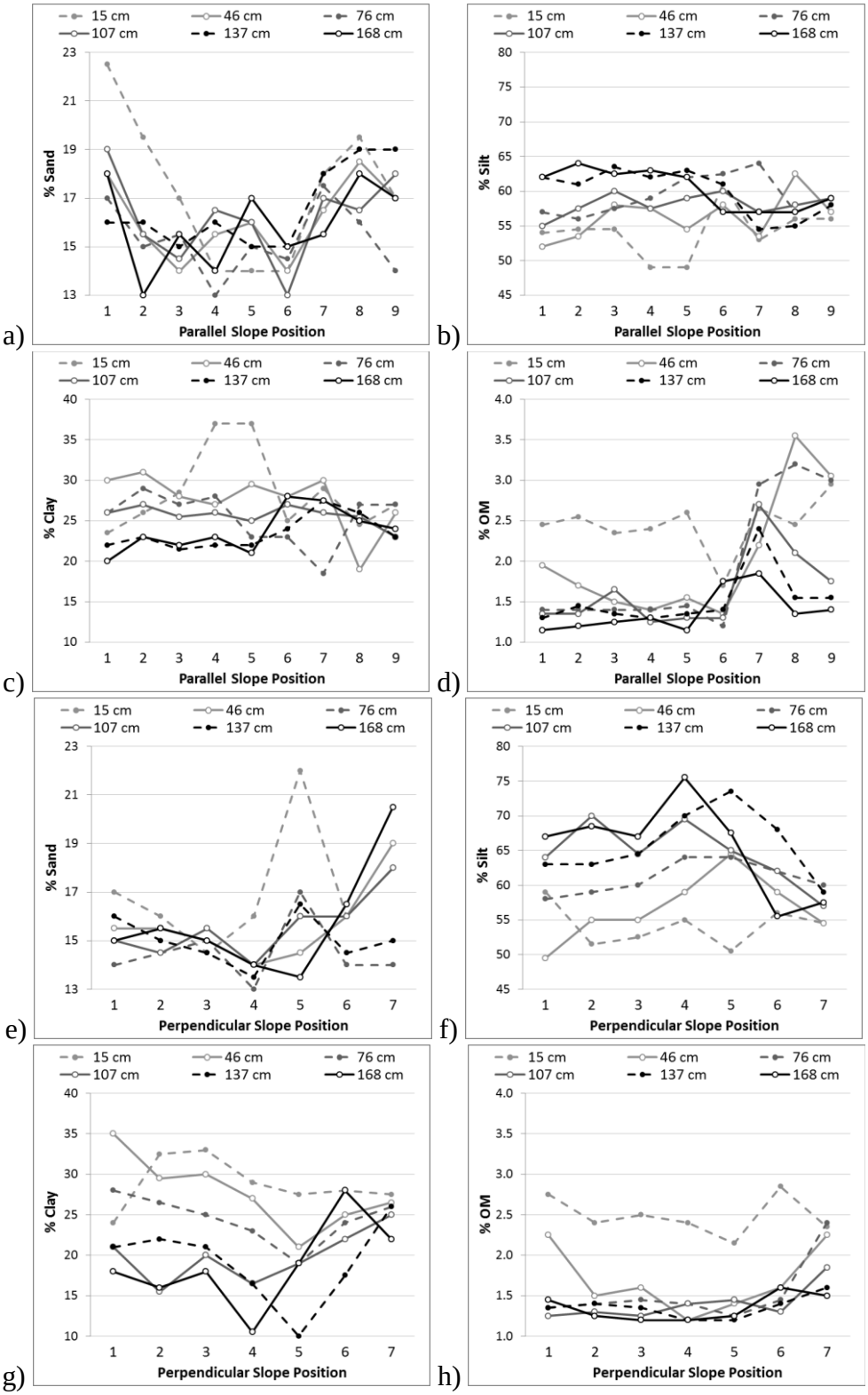

Figure 3.7. The mass percent of sand, silt, clay, and organic matter at the six sampling depths along the topographic transects a-d) parallel or e-h) perpendicular to corn rows (slope position number increases with decreasing elevation), averaged between two replicates except for the 15 cm depth at slope positions 5 and 6 on the parallel transects.

Table 3.1. Results from two-sample t-tests and Mann-Whitney tests comparing soil composition at the locations at the top of the topographic transects parallel or perpendicular to corn rows and at the locations at the bottom of the same transects; only comparisons with one of the p-values < 0.1 was included.

Soil Property	Top group mean (%)	Bottom group mean (%)	t-test p-value (H_a: $\mu_{top} \neq \mu_{bottom}$)	Mann-Whitney test p-value (H_a: top ≠ bottom)
parallel transects				
Sand at 137 cm	16	19	9E-02	3E-01
Silt at 137 cm	62	56	3E-04	5E-03
Silt at 168 cm	63	58	5E-03	6E-03
Clay at 137 cm	22	26	5E-02	4E-02
Clay at 168 cm	22	26	2E-02	2E-02
OM at 46 cm	1.7	2.9	5E-03	5E-03
OM at 76 cm	1.4	3.1	3E-04	5E-03
OM at 107 cm	1.5	2.2	4E-02	1E-02
OM at 137 cm	1.4	1.8	1E-01	4E-02
OM at 168 cm	1.2	1.5	6E-02	7E-03
perpendicular transects				
Sand at 46 cm	15	18	8E-02	5E-02
Silt at 107 cm	66	60	3E-02	3E-02
Silt at 168 cm	68	57	1E-01	9E-02
Clay at 46 cm	32	26	4E-02	4E-02
Clay at 107 cm	19	24	8E-02	2E-01
Clay at 168 cm	17	25	1E-01	9E-02
OM at 76 cm	1.4	1.9	2E-01	7E-02
OM at 168 cm	1.3	1.6	8E-02	7E-02

Subsection Summary

On both the parallel and the perpendicular transects during the monitoring period, the bottom measurement locations had consistently and appreciably more soil water within the managed root zone than the top measurement locations. The predominant differences were found deeper than 51 cm below the ground surface. The transition from drier to wetter subsoils occurred over the steepest stretch of the hillslopes as profile curvature was changing from convex to concave. When conducting soil moisture measurements for determining FC_{obs}, these findings suggested that the entire managed

root zone should be measured and that measurement locations may need to be closely spaced in areas of rapid transition. It remains unclear whether statistically significant soil composition differences at the 168 cm depth contribute to the observed subsoil water content pattern along the hillslopes.

3.4.2. Evaluation of FC Estimation Methods in a Soil Water Balance Model

Adapting VRI to spatial heterogeneity of *R* generally requires an accurate knowledge of TW_{FC}, which can be difficult to obtain. Three methods of estimating TW_{FC} were evaluated: gSSURGO, the Saxton and Rawls (2006) PTF, and the observational method, which determines FC by measuring soil moisture in the field under non-experimental conditions. Ideally, the three sets of TW_{FC} estimates would be compared to TW_{FC} values measured from the classical field capacity experiment in the field, but this experimental procedure was prohibitive for this study. Alternatively, the three sets of TW_{FC} estimates were set as parameters in a daily soil water balance model, and the simulated TW values were compared with neutron gauge TW measurements.

gSSURGO FC

The parallel transects extended across three gSSURGO map units, whereas the perpendicular transects extended across two gSSURGO soil map units (fig. 3.1b). Map units 3864, 3962, and 3561 are, respectively, Hastings silt loam, 0-1% slopes; Hastings silty clay loam, 7-11% slopes, eroded; and Hobbs silt loam, occasionally flooded. The map unit weighted average θ_{15000}, θ_{333}, and FC were reported for every 30 cm layer to a depth of 183 cm in figures 3.8a-c, respectively. The relevant properties of map unit 3870, in which none of the measurement locations were located, were identical to those of map unit 3962.

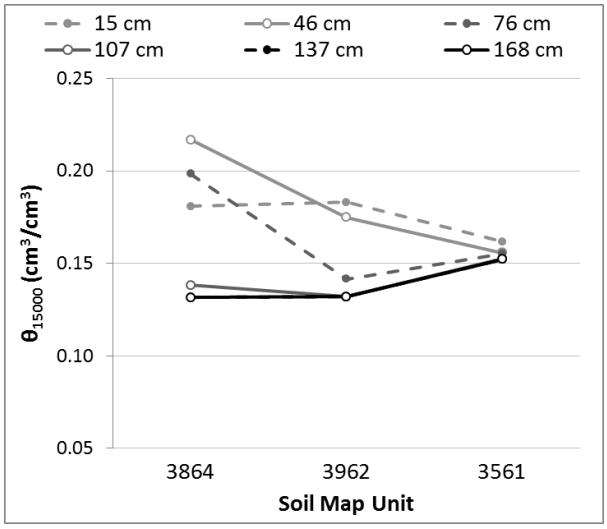

a)

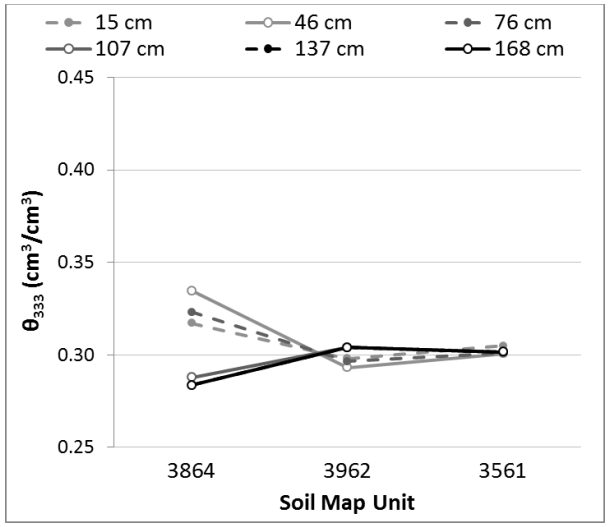

b)

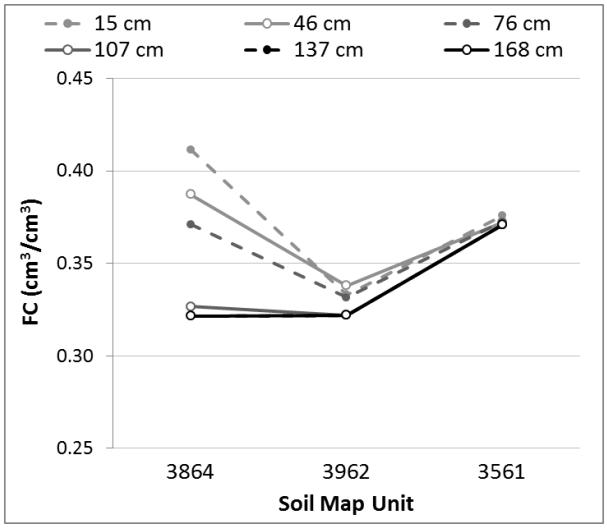

c)

Figure 3.8. Soil map unit weighted average volumetric water content at a) 15,000 cm (θ_{15000}) and b) 333 cm of tension (θ_{333}) and c) weighted average field capacity (FC) calculated for every 30 cm layer to a depth of 183 cm in the three gridded Soil Survey Geographic database soil map units mapped along the topographic transects.

For the six 30 cm layers in these four gSSURGO map units, FC was 0.018-0.094 cm^3/cm^3 larger than θ_{333}, with an average difference of 0.045 cm^3/cm^3. This observation suggested that h_{FC} may be less negative than -333 cm for all soils in this field. Concurringly, field measurements of FC in a Hastings silt loam soil at Clay Center, Nebraska, have corresponded to h_{FC} of around -200 cm (D. E. Eisenhauer, personal communication, 2015). Furthermore, θ_{333} rankings appeared to be different from FC rankings. This limited analysis of the gSSURGO data, in short, suggested that a uniform assumption of -333 cm as h_{FC} might be inappropriate for determining spatial heterogeneity of FC at the field site.

PTF FC

The Saxton and Rawls (2006) PTF received the location-specific soil composition data but a uniform bulk density as inputs. The trends in estimated θ_{15000} and θ_{333} (fig. 3.9) showed remarkable semblance to the trends in clay content (fig. 3.7c and fig. 3.7g). At least when assuming a uniform bulk density, clay content appeared to be an influential parameter in the PTF for both θ_{15000} and θ_{333} estimates.

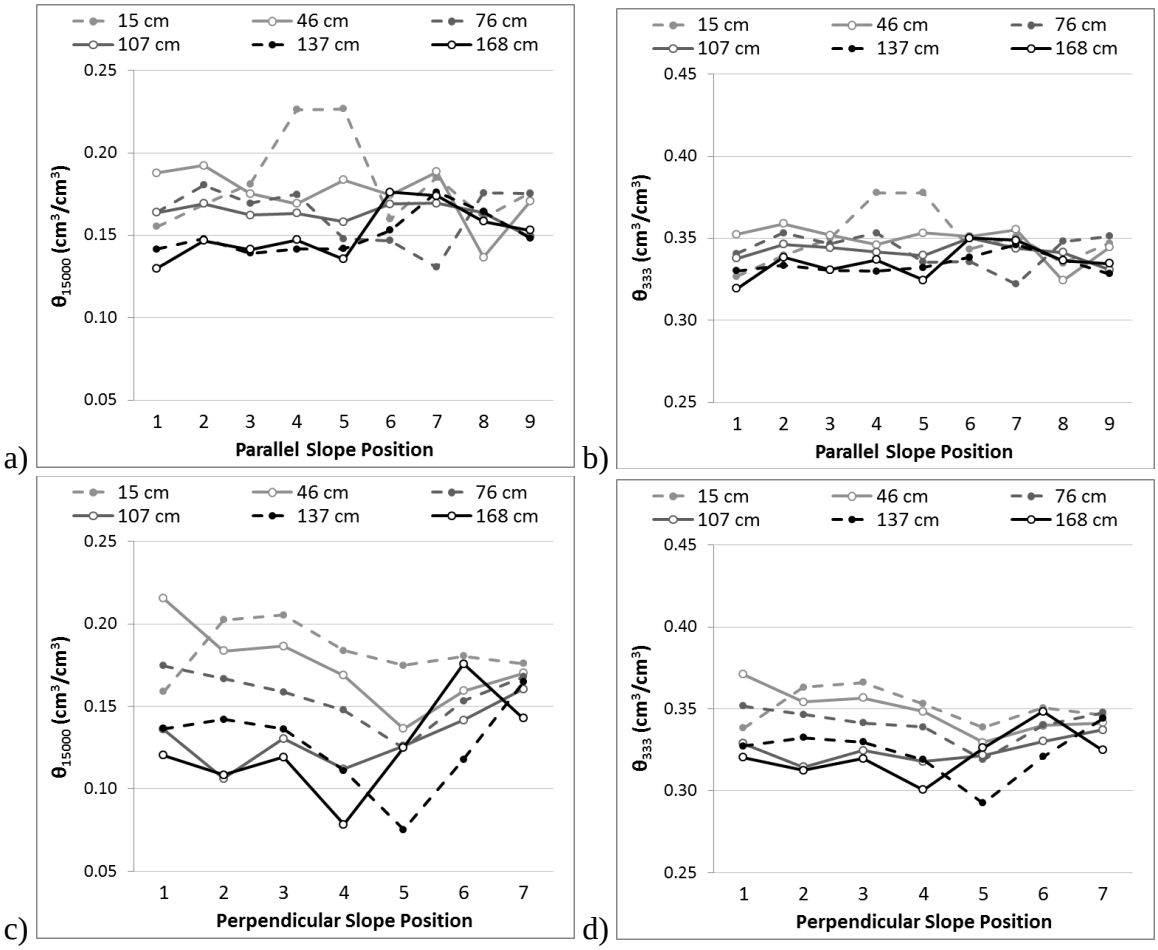

Figure 3.9. Volumetric water content at 15,000 cm (θ_{15000}) and 333 cm of tension (θ_{333}) estimated by a pedotransfer function at six sampling depths along the topographic transects a-b) parallel or c-d) perpendicular to corn rows, averaged between two replicates except for the 15 cm depth at slope positions 5 and 6 on the parallel transects.

$\underline{FC_{obs}}$

The measured water contents on 18 June 2014, three days after a large rain near the end of a wet period, were chosen to be the values of FC_{obs}. These estimates of FC (fig. 3.10) were paired with the corresponding θ_{15000} estimates from the PTF to calculate R_{obs}.

a)

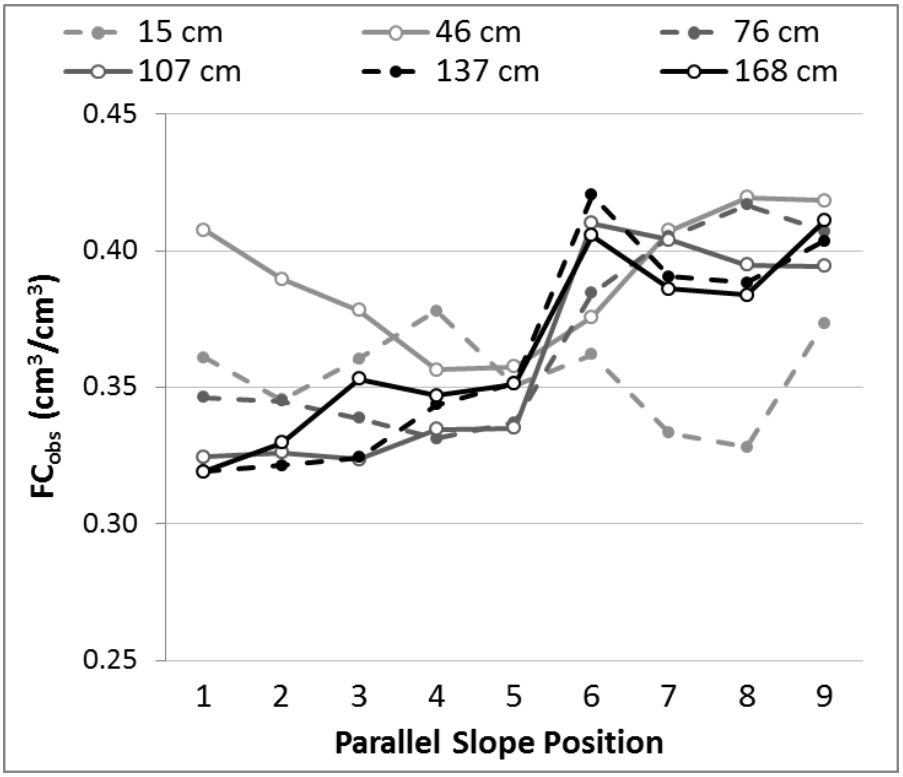

b)

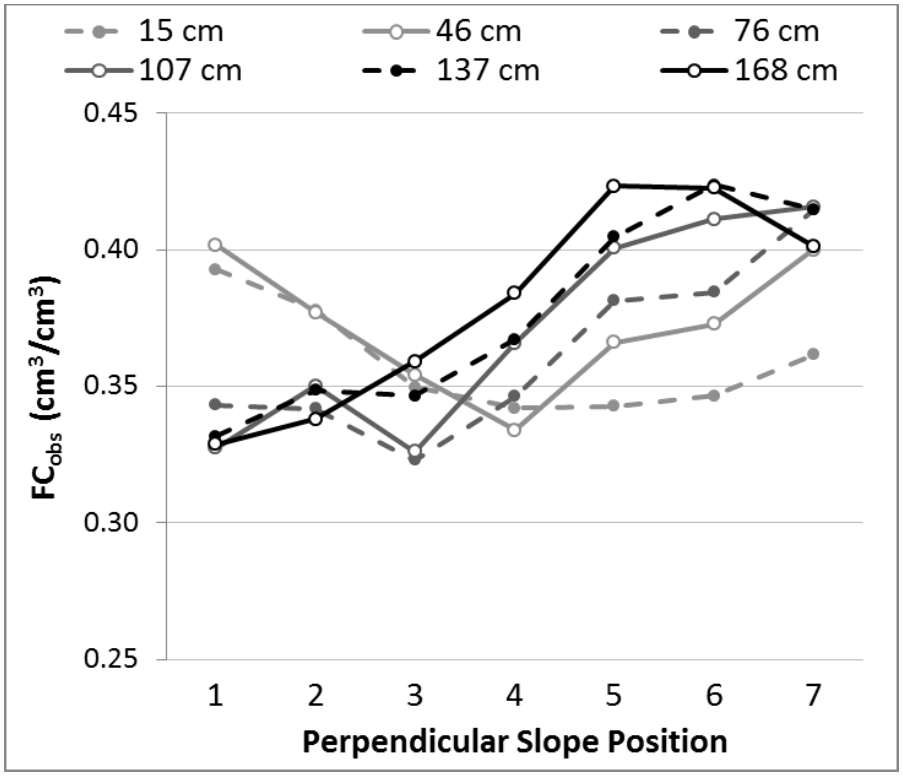

Figure 3.10. Observational field capacity (FC_{obs}) as determined by 18 June 2014 soil moisture measurements at the six measurement depths along the topographic transects a) parallel or b) perpendicular to corn rows (slope position number increases with decreasing elevations.

Performance Statistics

Regardless of the source of the TW_{FC} parameter, the soil water balance model at each measurement location started with the measured TW on 18 June 2014 and then simulated TW daily until 14 August 2014. Assuming that all soil water in the managed root zone in excess of TW_{FC} drains after TW is above TW_{FC} for three consecutive days, all simulated deep percolation occurred during the first 7 days of the simulation period. With gSSURGO estimates of TW_{FC}, 25 of the 32 locations experienced deep percolation, ranging from 0.1 to 98 mm. With PTF estimates of TW_{FC}, 29 of the 32 locations experienced deep percolation, ranging between 4 and 92 mm. With observational TW_{FC}, all locations experienced 8 mm of deep percolation. If all soil water in the managed root zone in excess of TW_{FC} was assumed instead to drain at the end of any day when TW is above TW_{FC}, simulated deep percolation would increase slightly, and slightly lower TW would be inherited throughout the simulation period (not shown). Only the three-day delay deep percolation assumption was considered below.

TW_{FC} ceased to be a controlling parameter as simulated TW fell below TW_{FC} after the first week. Subsequent to the termination of all deep percolation, the daily change in simulated TW at a given location became the same regardless of the source of the TW_{FC} parameter (fig. 3.11). This phenomenon also explained why changes in MB after 2 July 2014 for a given topographic group were identical in tables 3.2a-c.

a)

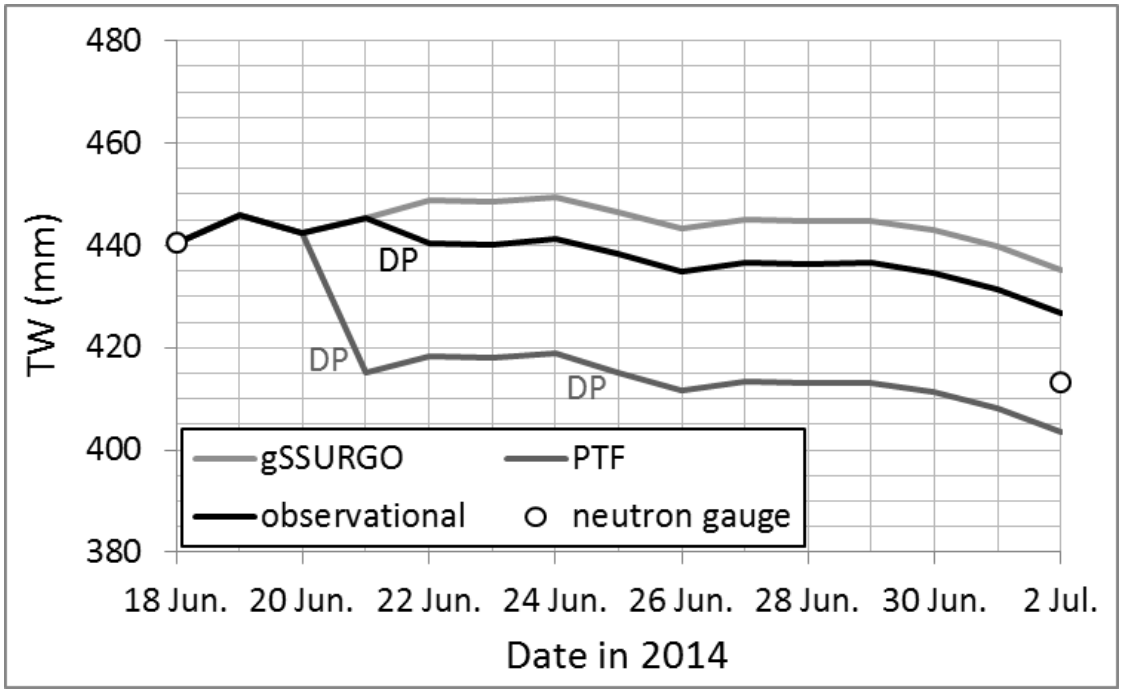

b)

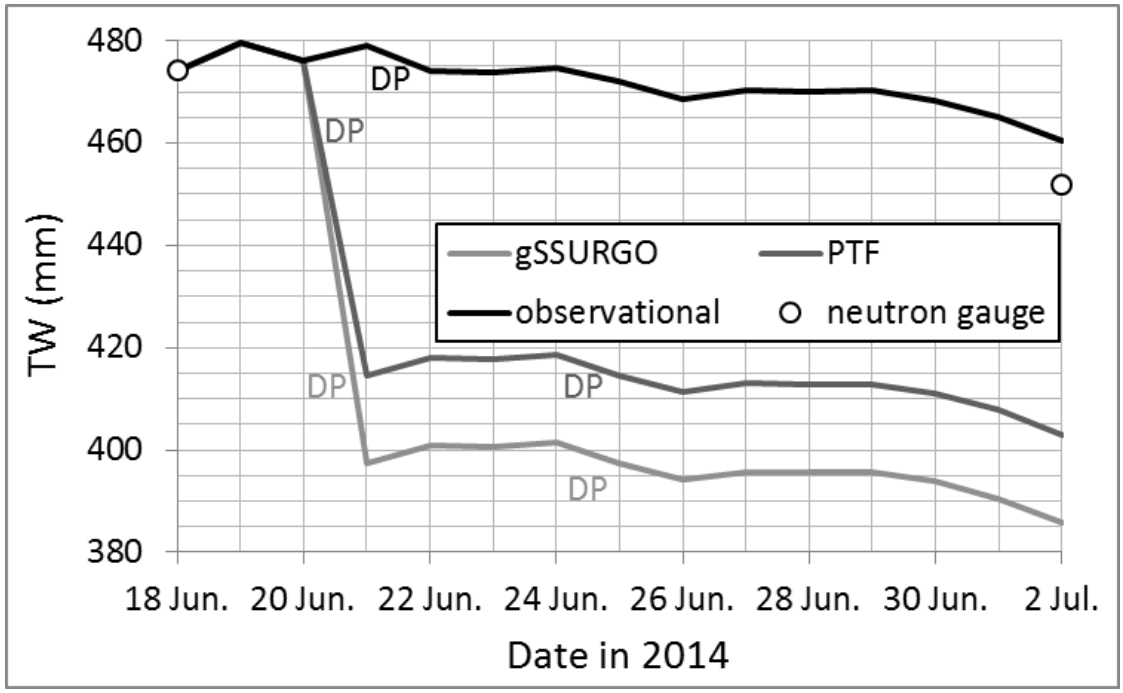

Figure 3.11. At a location in the a) parallel top and b) parallel bottom topographic group, the total water in the managed root zone as measured by a neutron gauge and as modeled based on a daily soil water balance with three sources of field capacity data during the first 14 days of the simulation period; deep percolation events are labeled DP.

Table 3.2. Mean bias (MB) and root mean squared error (RMSE), within topographic groups, of simulated total soil water in the managed root zone as compared with neutron gauge measurements for three sets of field capacity (FC) data; the smaller the MB range, the more effective a set of FC data is in accounting for spatial variability in soil water.

a) Gridded Soil Survey Geographic database soil map unit weighted average FC

Date	2 Jul. 2014		9 Jul. 2014		17 Jul. 2014		30 Jul. 2014		14 Aug. 2014	
Group	MB (mm)	RMSE (mm)	MB (mm)	RMSE (mm)	MB (mm)	RMSE (mm)	MB (mm)	RMSE (mm)	MB (mm)	RMSE (mm)
parallel top	22	23	7	11	15	17	3	10	3	11
parallel middle	-25	34	-39	46	-42	52	-46	55	-47	52
parallel bottom	-64	68	-78	82	-80	87	-86	91	-76	84
perpendicular top	25	27	15	18	23	25	12	15	1	14
perpendicular middle	-12	25	-28	40	-36	44	-39	47	-51	58
perpendicular bottom	-64	65	-87	88	-81	82	-94	95	-98	99
Field-Average MB (mm)	-20		-35		-34		-42		-44	
MB Range in Field (mm)	127		135		144		136		134	

b) Location-specific FC as estimated by Saxton and Rawls (2006) pedotransfer function

Date	2 Jul. 2014		9 Jul. 2014		17 Jul. 2014		30 Jul. 2014		14 Aug. 2014	
Group	MB (mm)	RMSE (mm)	MB (mm)	RMSE (mm)	MB (mm)	RMSE (mm)	MB (mm)	RMSE (mm)	MB (mm)	RMSE (mm)
parallel top	6	13	-9	16	-1	13	-14	17	-14	16
parallel middle	2	24	-11	29	-15	37	-18	39	-19	34
parallel bottom	-54	54	-68	69	-70	73	-75	77	-65	70
perpendicular top	1	12	-9	14	-1	12	-12	17	-23	28
perpendicular middle	0	32	-16	41	-24	42	-28	45	-39	54
perpendicular bottom	-45	47	-68	71	-62	64	-75	77	-79	81
Field-Average MB (mm)	-14		-29		-29		-36		-39	
MB Range in Field (mm)	96		113		124		121		116	

c) Location-specific observational FC as determined by 18 June 2014 soil moisture measurements

Date	2 Jul. 2014		9 Jul. 2014		17 Jul. 2014		30 Jul. 2014		14 Aug. 2014	
Group	MB (mm)	RMSE (mm)	MB (mm)	RMSE (mm)	MB (mm)	RMSE (mm)	MB (mm)	RMSE (mm)	MB (mm)	RMSE (mm)
parallel top	14	15	-1	9	7	10	-6	11	-6	12
parallel middle	14	14	0	7	-4	15	-7	16	-8	15
parallel bottom	6	8	-8	12	-10	22	-16	24	-6	23
perpendicular top	21	22	11	12	19	21	8	11	-3	13
perpendicular middle	18	19	2	10	-6	12	-9	15	-21	24
perpendicular bottom	10	10	-13	15	-7	9	-20	21	-24	25
Field-Average MB (mm)	14		-2		-1		-9		-11	
MB Range in Field (mm)	32		41		63		59		71	

Because the water fluxes of effective precipitation, net irrigation, and crop ET were not calibrated in the soil water balance model, simulated TW for any of the three FC estimation methods were not expected to match measured TW very closely. Instead of comparing MB and RMSE to zero, the range in MB was used as a metric to compare the effectiveness of the three methods in accounting for spatial variability in TW. With no additional deep percolation after 2 July 2014, the range in MB was expected to be stable. It was no longer affected by any spatially uniform overestimates and underestimates of water inputs and outputs in the model.

Across the five measurement dates in table 3.2, the range in MB among the measurement locations averaged 135 mm with gSSURGO TW_{FC}, 114 mm with PTF TW_{FC}, and 53 mm for observational TW_{FC}. As a comparison, an average range in MB of 102 mm would be obtained if the average of all PTF estimated TW_{FC} values had been assigned to every measurement location. According to this metric, the observational method performed the best, whereas both PTF and gSSURGO performed worse than a spatially uniform assumption of average PTF estimated TW_{FC}. The overall RMSE of 16 mm in the 122 cm managed root zone for the soil water balance model with observational TW_{FC} was excellent considering the lack of calibration.

This soil water balance analysis did not verify the absolute accuracy of the observational TW_{FC} values. Yet, whereas methods that were less effective in capturing the spatial trend in TW_{FC} created large TW underestimations in the bottom topographic groups, the observational method eliminated much of the MB differences between topographic groups—particularly along the parallel transects. By naturally integrating the effects of in-situ phenomena such as layering, which can be lost in laboratory (e.g.,

pressure plate) and laboratory-based (e.g., PTF) methods, the observational method may be the best site-specific method for determining FC short of the classical field experiment.

Over the simulation period, MB of the measurement locations was observed to drift relative to field-average MB on the same date. If not the results of neutron gauge error, drifts in MB that occurred when little or no deep percolation was simulated were evidences of spatially nonuniform fluxes for which a simple soil water balance model could not account. Where effective precipitation, application efficiency, and crop ET are relatively uniform as compared with TW_{FC}, this type of model with an improved estimation of TW_{FC} would be effective in accounting for spatial heterogeneity of TW. Where the opposite is true, this type of model would be ineffective even with perfectly measured TW_{FC}, and an improved understanding and parameterization of the nonuniform fluxes would be critical. Based on observational TW_{FC}, the range in group-average TW_{FC} was 48 mm, whereas the maximum group-average drift in MB over the simulation period was 20 mm. This observation was consistent with the previous finding that parameterizing the soil water balance model with observational TW_{FC} was effective in accounting for much of the spatial variability in TW among the measurement locations.

Further Discussions on the FC Estimation Methods

Although both gSSURGO and PTF performed poorly as sources of TW_{FC} in the soil water balance model, figures 3.11b suggested that the reasons are different. Notably, gSSURGO TW_{FC} followed the same spatial trend as observational TW_{FC} along the parallel transects. TW_{FC} first decreased and then increased as the hillslope are descended. Additionally, gSSURGO TW_{FC} compared acceptably to observational TW_{FC} especially at the top and the shoulder of the hillslopes and somewhat at the very bottom of the parallel

transects. If soil map unit 3561, currently mapped at the very bottom of the parallel transects (fig. 3.1b), had included the bottom of the perpendicular transects and more of the parallel transects, the MB ranges with gSSURGO TW_{FC} would be smaller than what were reported in table 3.2a. Therefore, the primary problem of gSSURGO as a source of FC estimates in this field site seemed to be the low spatial precision of the original soil survey, which affected the lower parts of the hillslopes most.

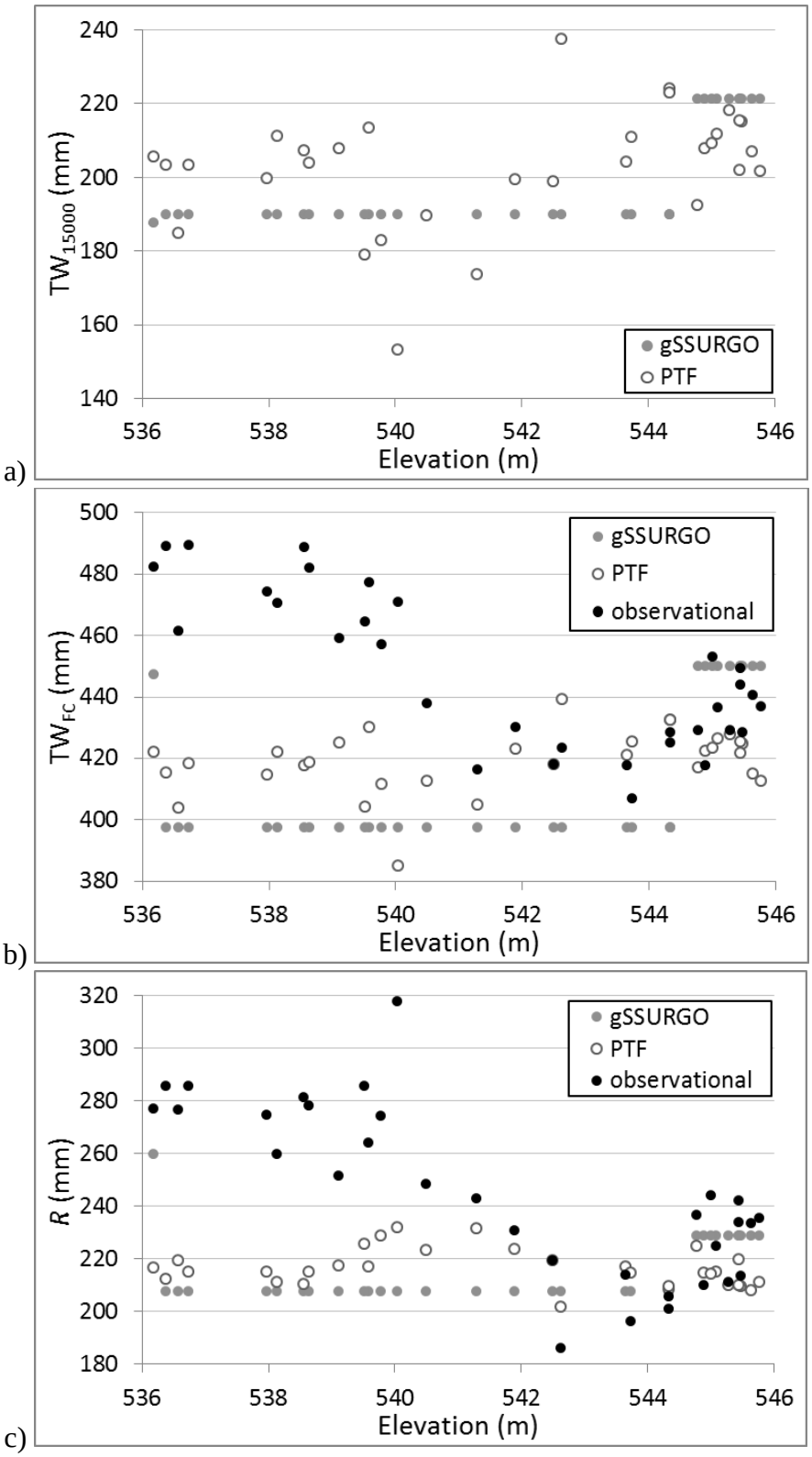

Figure 3.12. Total soil water in the managed root zone a) at 15,000 cm of tension (TW_{15000}) and b) at field capacity (TW_{FC}), and c) root zone water holding capacity (R), as estimated for the 32 measurement locations by gSSURGO, Saxton and Rawls (2006) pedotransfer function (PTF), and the observational method.

The similarities between gSSURGO R and R_{obs} at certain parts of the topographic transects (fig. 3.12c) were encouraging for Chapter 2, which relied completely on R data from gSSURGO. At the same time, the spatial uncertainties were apparent in the gSSURGO R data for this field site. The possible impact of such uncertainties is expected to depend on the application of the gSSURGO R data. Chapter 2 estimation of potential irrigation reductions from adapting VRI to spatial heterogeneity in R may be less sensitive to these uncertainties because the method analyzes only the statistical distribution of R within each field. The management of VRI to adapt to spatial heterogeneity in R may be more sensitive to these uncertainties because the geographic layout of the R values is also crucial to this application. In conclusion, gSSURGO can be a very useful data source, but its limitations for precision agriculture purposes should be considered.

PTF TW_{FC} compared very well to observational TW_{FC} along the convex halves of the hillslopes but not along the concave halves. In a Hastings silt loam soil at Clay Center, Nebraska, Rudnick and Irmak (2014) developed a correction for Saxton and Rawls (2006) PTF-estimated θ_{333} and θ_{15000} based on disturbed soil samples subjected to a pressure plate apparatus. Applying the θ_{333} correction to the data from this study did improve mean difference and root mean squared difference (RMSD) of PTF TW_{FC} relative to observational TW_{FC} (not shown). However, the correction, which was linear, could not cause PTF TW_{FC} to better match observational TW_{FC} trends along the concave halves of the hillslopes.

The PTF was used to estimate θ_{333} and θ_{15000} based on gSSURGO soil composition data for the 46 soil horizons that could be part of the four soil map units

found in this field site. When compared with θ_{333} as reported in gSSURGO, the PTF θ_{333} estimates had an R^2 of 0.18 and an RMSD of 0.066 cm^3/cm^3. The Rudnick and Irmak (2014) θ_{333} correction, on the other hand, had an R^2 of 0.45 and an RMSD of 0.041 cm^3/cm^3. It is unclear why the prediction of θ_{333} by the PTF was worse in this study than in Rudnick and Irmak (2014). When the PTF θ_{333} estimates were instead compared with FC as reported in gSSURGO, R^2 decreases to 0.02. In contrast, when the PTF θ_{15000} estimates were compared with θ_{15000} as reported in gSSURGO, the resulting R^2 of 0.69 and RMSD of 0.028 cm^3/cm^3 were similar to the R^2 of 0.66 and the RMSD of 0.031 cm^3/cm^3 for the θ_{15000} correction presented in Rudnick and Irmak (2014).

Overall, the limited comparisons to gSSURGO and the observational method did not support the use of the Saxton and Rawls (2006) PTF for estimating the spatial variability in FC along the hillslopes of this field site. Most probably, the observed discrepancies between the PTF estimates and those from the other two methods were caused by a combination of both the spatially uniform assumption of -333 cm as h_{FC} and the inherent uncertainty of the PTF θ_{333} estimates. Since the PTF appeared to be heavily influenced by the clay content input, the PTF—with appropriate h_{FC} inputs—may be more useful for estimating spatial variability in FC on fields where FC is strongly positively correlated with clay content.

As for the observational method, the principal limitation was the arbitrary timing of one-time soil moisture measurements without knowing the drainage rate. Yet where irrigation water supply is non-restrictive, opportunities to observe FC are expected to be plentiful. The oven-drying of intact soil cores from mechanical sampling equipment such as a Giddings probe (Windsor, Colo.) may be the simplest and most cost-effective

volumetric water content measurement method for determining FC_{obs}. Cheaper alternatives such as a hand probe may be investigated as a way to collect a disturbed sample from a known in-situ volume, which is critical for accurate calculations of FC_{obs}. If soil samples are already going to be sent to a soil lab for composition and/or nutrient analyses, the added cost for soil moisture determination would be reduced.

When determining FC_{obs}, the measured water contents could have been differentially affected by hillslope hydrology. This unique feature may be a strength rather than a weakness of the observational method for simple characterizations of in-season soil moisture dynamics. Future research can further evaluate the FC_{obs} concept and its applications.

Subsection Summary

Parameterizing a simple daily soil water balance model with FC_{obs} values was demonstrated to be effective in accounting for a substantial portion of the observed soil moisture variability among the measurement locations over a two-month period during the growing season. Using spatially variable TW_{FC} estimates from either gSSURGO or the Saxton and Rawls (2006) PTF was less effective than assuming the average PTF-estimated TW_{FC} for all measurement locations. Among the three FC estimation methods, the observational method is recommended for estimating spatial heterogeneous FC where irrigation water supply is non-restrictive.

3.4.3. Prediction of R_{obs} at Unsampled Locations

To adapt VRI to spatial heterogeneity of *R*, *R* needed to be known throughout the field rather than at several points only. Having sufficient measurement locations for spatial interpolation is generally infeasible where *R* is highly variable in space. Therefore,

auxiliary variables that can be measured more densely were introduced to produce *R* maps with limited *R* point data.

Two auxiliary variables of drastically different natures were compared by the strength of their regression relationships to R_{obs}. On one hand, EC_a is commonly used and highly regarded in precision agriculture for a variety of applications including VRI research and implementation. Producers pay a co-op or a consultant for the on-the-go EC_a sensor measurements on their field and some subsequent computer work. On the other hand, elevation (fig. 3.1a) is merely a natural proxy for the underlying factors driving the observed differences along the hillslopes. High resolution elevation data of the contiguous United States are freely available to the public.

EC_a as the Auxiliary Variable

Maps of shallow EC_a, deep EC_a, and EC_a ratio from a Veris unit were shown in figures 3.12a-c, whereas R_{obs} was plotted against these EC_a variables in figures 3.13a-c.

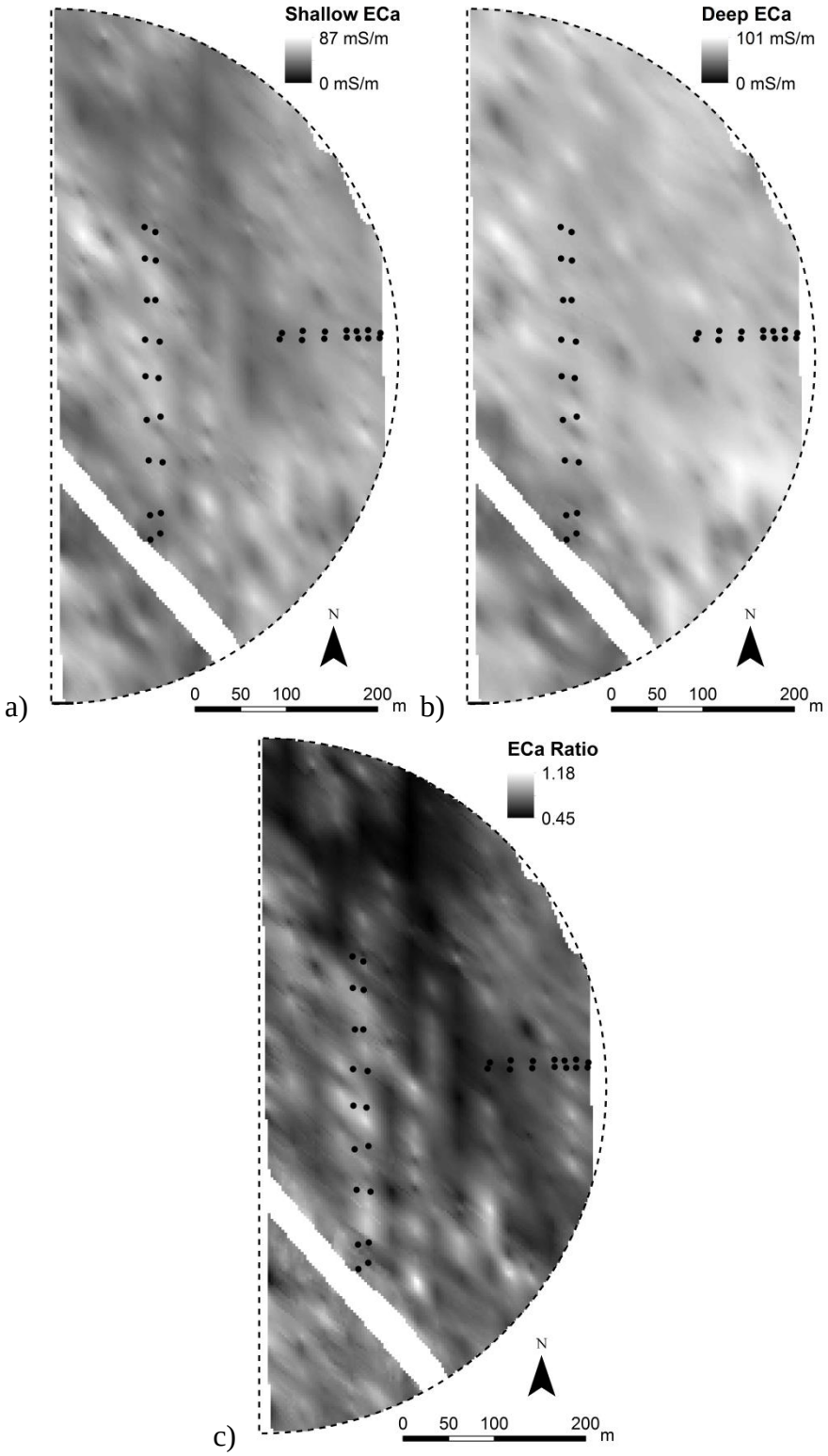

Figure 3.13. Kriged maps of a) shallow apparent soil electrical conductivity (EC_a), b) deep EC_a, and c) EC_a ratio (shallow EC_a divided by deep EC_a) as measured by a Veris (Salina, Kans.) unit.

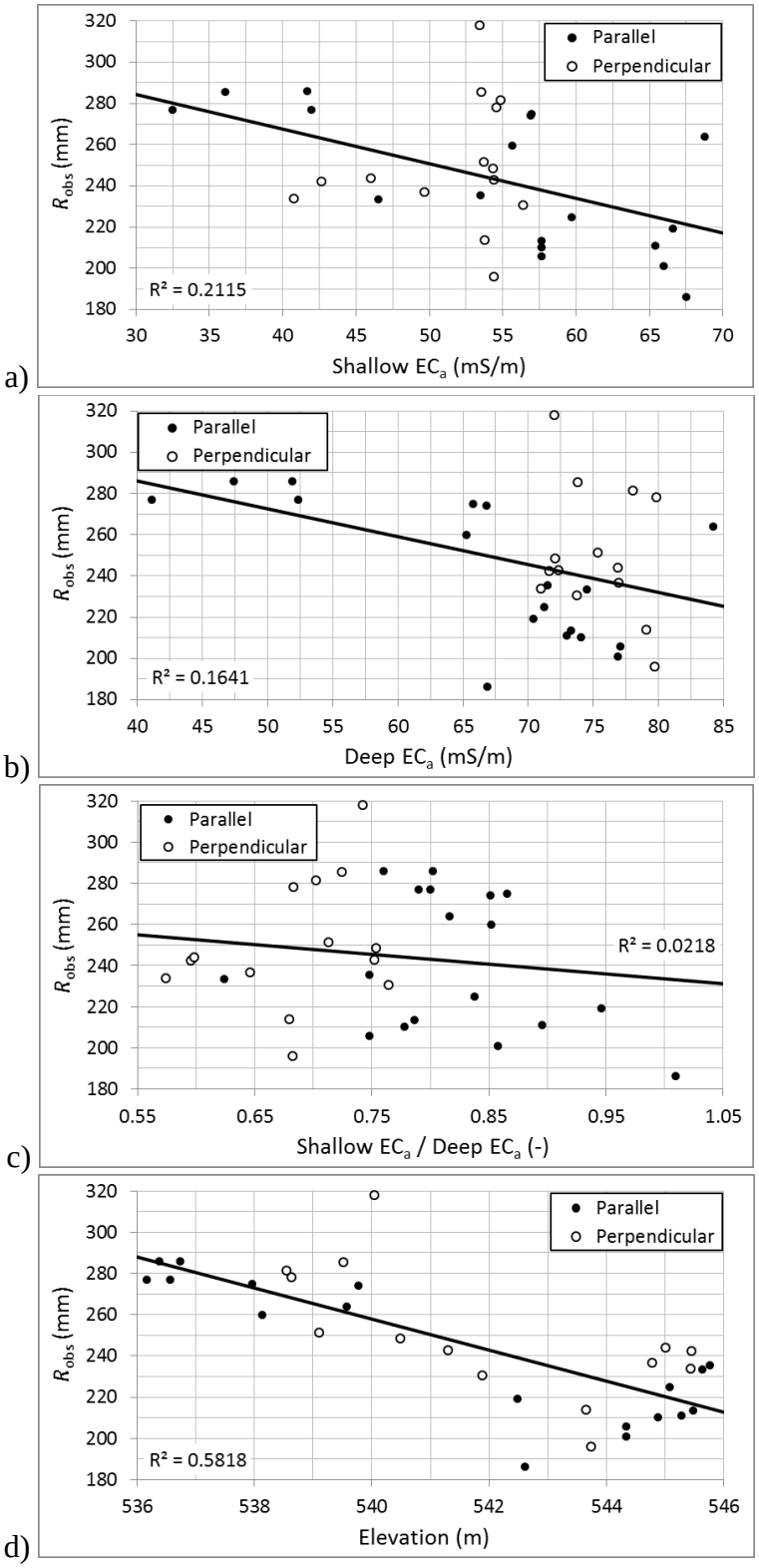

Figure 3.14. Observational root zone water holding capacity (R_{obs}) along the topographic transects parallel or perpendicular to corn rows, plotted against a) shallow apparent soil electrical conductivity (EC_a), b) deep EC_a, c) EC_a ratio, or d) elevation.

The EC_a maps bore much semblance to the gSSURGO map (fig. 3.1b). Shallow EC_a was high in the 3962 and 3870 map units and low in the 3864 and 3561 map units. Deep EC_a was low in the 3561 map unit and high elsewhere. The EC_a ratio was low in the 3864 map unit and high elsewhere. Good matching between EC_a zones and NRCS soil survey map units has been observed in the literature (Veris Technologies, 2002; Grisso et al., 2009).

In this study, shallow EC_a and deep EC_a related somewhat to R_{obs} along the parallel transects but not along the perpendicular transects, where a vast range of R_{obs} corresponded to a small range of EC_a. For all topographic transects, the EC_a ratio related poorly to R_{obs}. These relatively weak relationships between R and EC_a variables caused this study to stand out among much of the existing VRI research and implementation, which have found or assumed a strong relationship between these two variables.

EC_a is known to relate well to clay content (Williams and Hoey, 1987; Sudduth et al., 2005). Since the θ_{333} and θ_{15000} estimates from Saxton and Rawls (2006) were observed to be sensitive to clay content (fig. 3.7c, fig. 3.7g, and fig. 3.9), the EC_a variables were plotted against PTF-estimated R in this study. However, the EC_a variables did not relate any better to PTF-estimated R along the topographic transects (fig. 3.14). Readers are referred to Miller (2015) for further analysis on relating soil and topographic variables with PTF-estimated R and R_{obs}.

a)

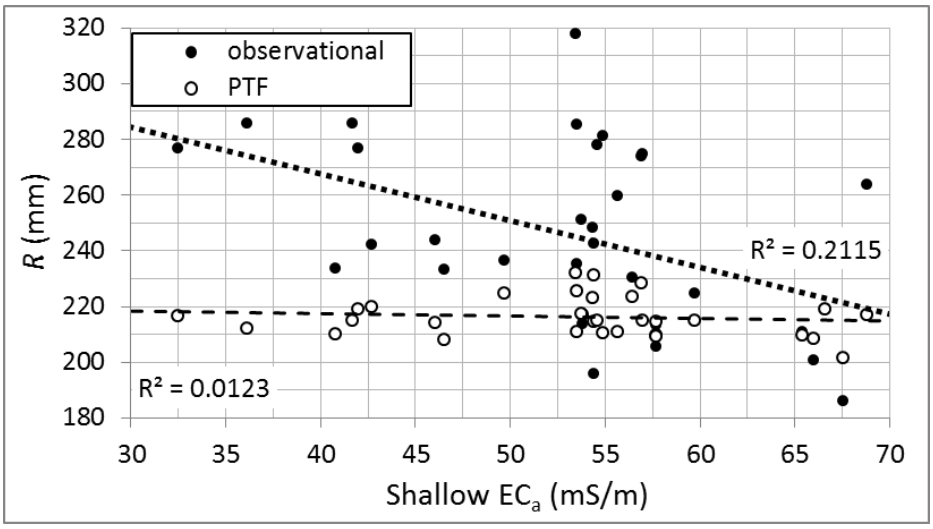

b)

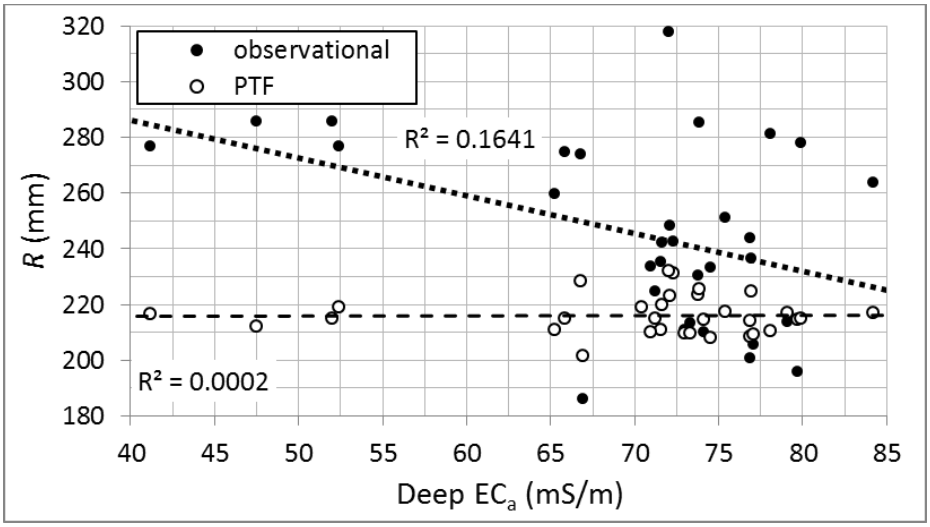

c)

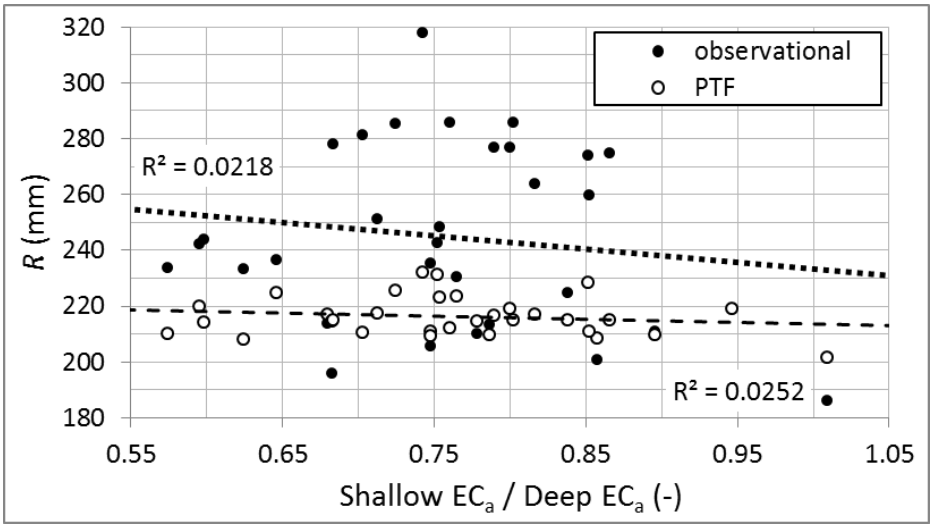

Figure 3.15. Root zone water holding capacity (*R*) as estimated by the Saxton and Rawls (2006) pedotransfer function (PTF) and by the observational method, plotted against a) shallow apparent soil electrical conductivity EC_a, b) deep EC_a, and c) EC_a ratio.

It might be possible to improve the prediction of R_{obs} by using more than one EC_a variable. However, the main problem was that where EC_a variables transitioned from low to high did not correspond with where soil water transitioned from low to high. The limited textural variability and the deep occurrence of much of the observed differences in soil composition and in soil water content may explain the reason for the poor performance of Veris EC_a variables as predictors of R_{obs} in this field. An EC_a sensor that obtains more of its signal at deeper depths might give more success on this field.

Elevation as the Auxiliary Variable

Elevation had a moderately strong correlation to R_{obs} among the measurement locations (fig. 3.13d). No direct, physical causal relationship exists between elevation and R_{obs}, but topography does affect soil formation (Jenny, 1941) and hydrological processes whose influences are incorporated into FC_{obs}. Elevation was thus used as the auxiliary variable while acknowledging that elevation does not relate well to R_{obs} on every field and that the regression equation for this field site cannot be applied elsewhere.

A fourth-order polynomial fitted the data well. Though high-order polynomials may be rarely appropriate for describing a physical relationship, they may be satisfactory for describing an empirical relationship such as the one between R_{obs} and elevation in this field site. For instance, Djaman and Irmak (2013) used fourth-order polynomials to model crop coefficients as a function of days after emergence and growing degree days. Overfitting did not appear to be a concern for the R_{obs} versus elevation fourth-order polynomial because the measurement locations were many relative to the number of fitted parameters (degrees of freedom = 27) and were moderately spread out over their elevation range. The R^2 value of 0.76 is comparable to those obtained between EC_a and

available water holding capacity (Hedley and Yule, 2009) or total available water content (Hezarjaribi and Sourell, 2007) in the literature.

Beyond the range of elevation across the measurement locations, R_{obs} was predicted not to increase or decrease further. The minimum and maximum elevation in this field site were 535 m and 547 m. With the gentle (~1%) slopes within the cropped area at the extreme elevations, the capping of the fourth-order polynomial was thought to be more reasonable than its extrapolation. The piecewise prediction function was shown in figure 3.15.

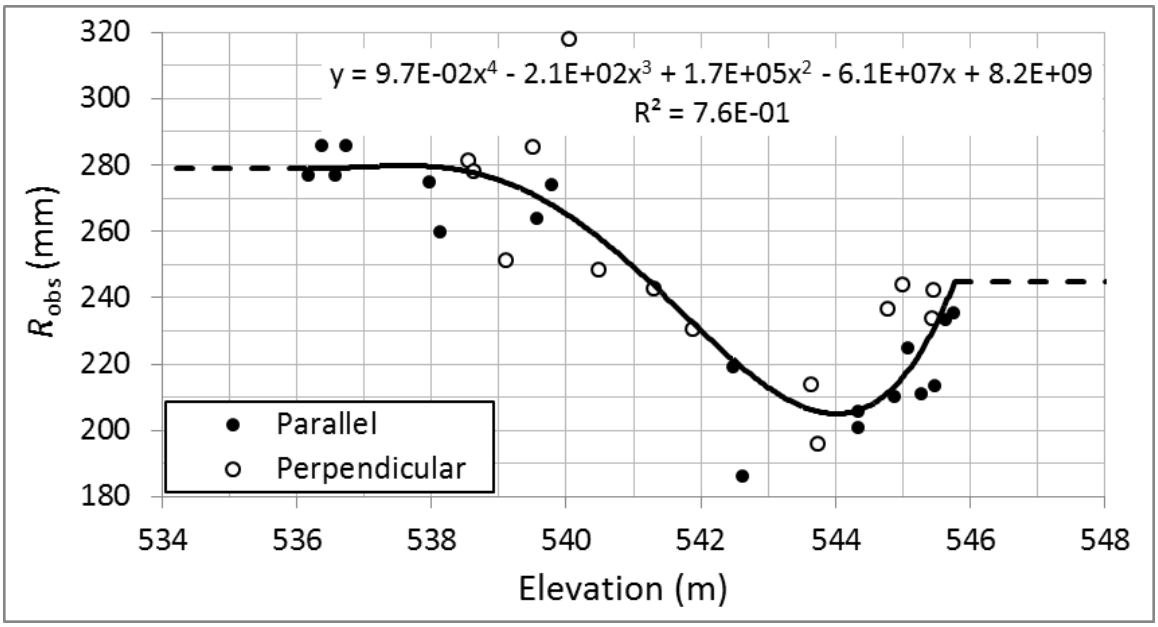

Figure 3.16. Elevation-based piecewise prediction function for *R* as determined by the observational method (R_{obs}); R_{obs} was assumed to follow the fourth-order polynomial (solid line) within the elevation range of the measurement locations (dots) but not to vary with elevation beyond this range (dashed lines).

The piecewise prediction function was applied to 1/9 arc-second NED DEM (USGS, 2014) to obtain a map of R_{obs} (fig. 3.16b). As pointed out earlier, the spatial trend in *R* as depicted by the field characterization method bore remarkable semblance to the spatial trend in *R* as depicted by gSSURGO (fig. 3.16a).

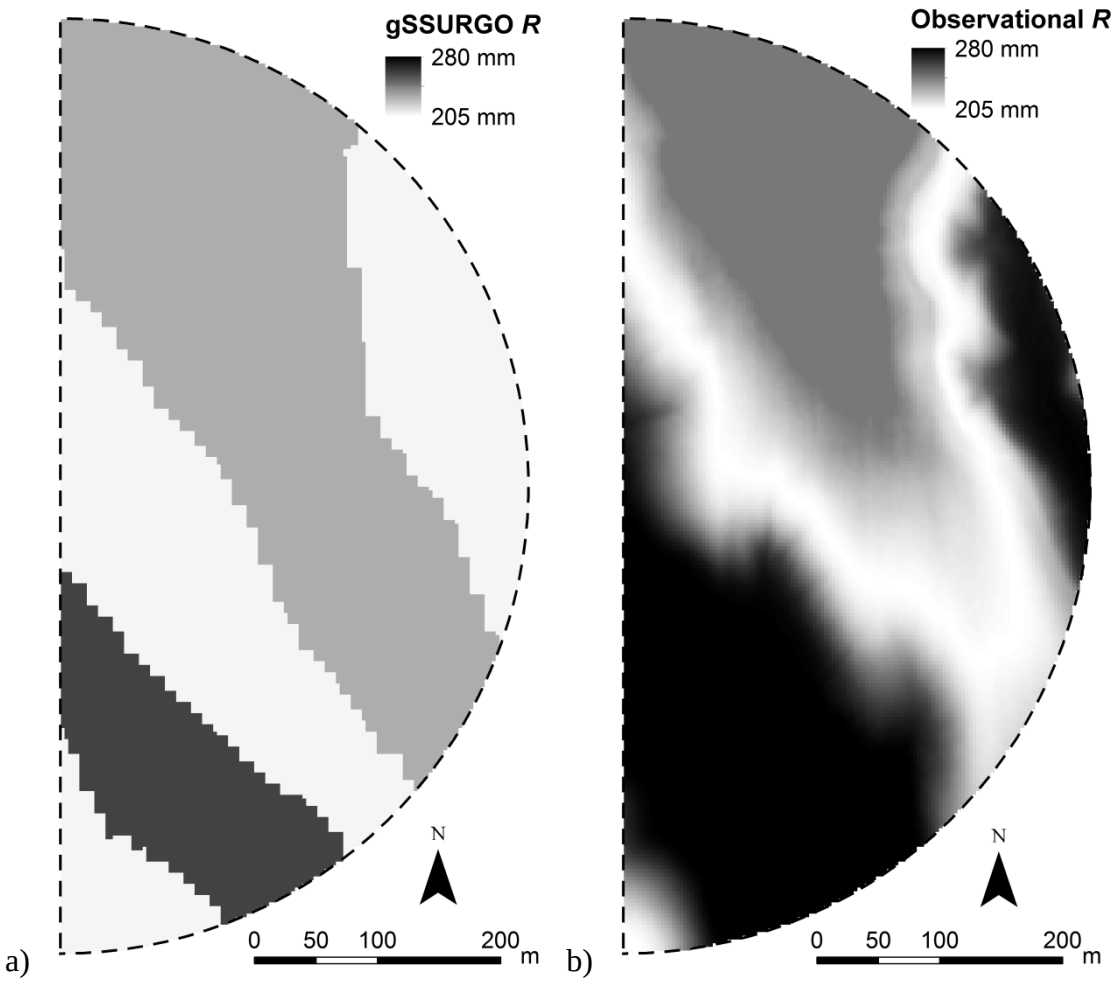

Figure 3.17. Map of a) soil map unit weighted average root zone water holding capacity (*R*) calculated from the gridded Soil Survey Geographic database (gSSURGO) and b) *R* determined by the observational method and then spatially predicted using the piecewise function shown in figure 3.16.

Just like gSSURGO, R_{obs} maps contain uncertainty from the point measurements of R_{obs} and from the process of spatial prediction. The issue of R_{obs} uncertainty becomes especially important when R_{obs} is measured at a small number of locations due to financial constraints and when overestimation of R may cause yield losses due to water stress. Readers are referred to Miller (2015) for an analysis of how R uncertainty in various data sources can affect the performance of adapting VRI to spatial heterogeneity of R. Further research can explore the change in R uncertainty and VRI performance with different numbers and placements of R_{obs} measurement locations.

Subsection Summary

Among the measurement locations, R_{obs} was found to relate well to elevation but poorly to EC_a variables. This observation demonstrated that selecting an auxiliary variable based on sound understanding of the particular field and careful examination of existing data could produce superior results as compared with always relying on a certain auxiliary variable. Since the best auxiliary variable for predicting R from point data is likely to be region-specific if not field-specific, practitioners are advised to exercise professional judgment and make use of all available resources.

3.4.4. Financial Implications

The R_{obs} map was first used to quantify the potential magnitude of irrigation cost reductions and agrochemical cost reductions from adapting VRI to spatial heterogeneity of R at the field site. The value of the field characterization of R was then quantified for this field site and for a typical center pivot irrigated field in Nebraska. Readers should bear in mind that all results in monetary terms are strongly dependent on the assumed prices of gross irrigation, N fertilizer, and VRI.

Private Benefit from Adapting VRI to Spatial Heterogeneity of *R*

The cumulative distribution functions of *R* from the R_{obs} map (fig. 3.16a) and the gSSURGO *R* map (fig. 3.16b) were shown in figure 3.17. Interestingly, R_p from both maps were within 0.1 mm of each other. In Chapter 2, gSSURGO R_p, which was based on coarsely discretized map units, was expected to exhibit greater sensitivity to the choice of *p* than would actual R_p. At this field site, gSSURGO R_p did not change as *p* varied between 5% and 15% at this field site. Observational R_p, relative to its value at the Chapter 2 choice of *p* = 10%, decreased by 2 mm at *p* = 5% and increased by 3 mm at *p* = 15% at this field site. For all subsequent calculations, *p* was held at 10%.

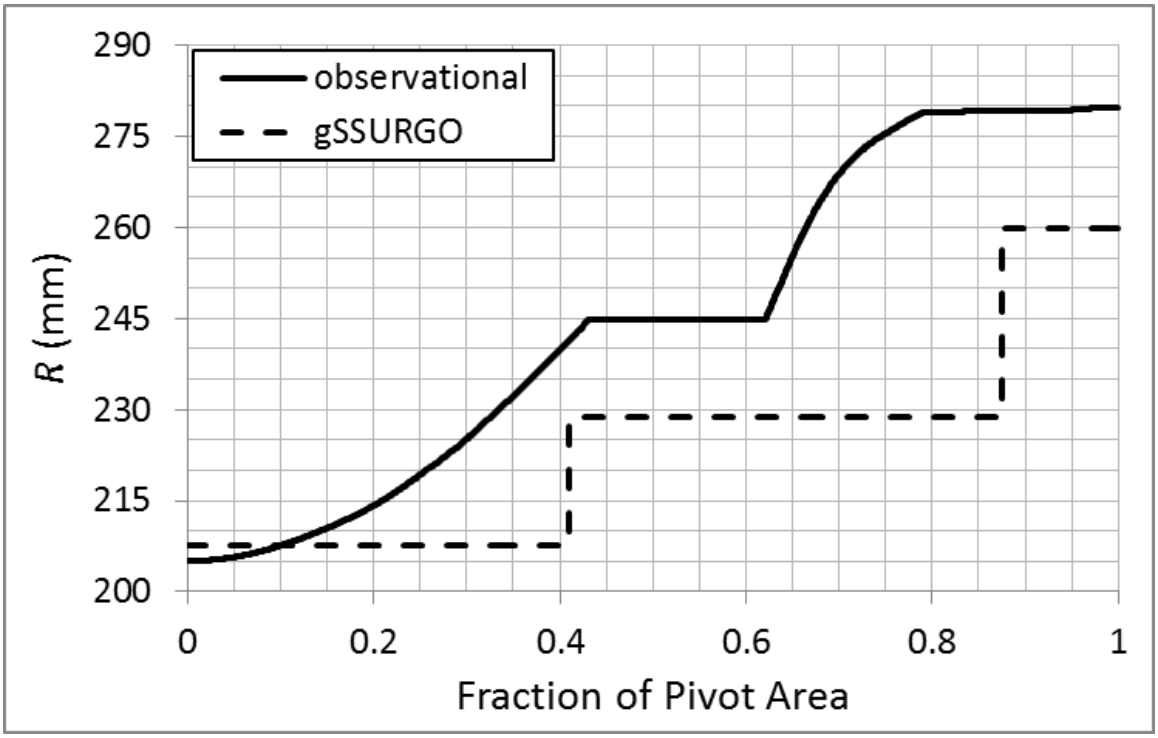

Figure 3.18. Cumulative distribution functions of root zone water holding capacity (*R*) from the gridded Soil Survey Geographic database (gSSURGO) *R* map (fig. 16a) and the observational *R* map (fig. 16b).

The basis of the subsequent calculations of the benefits from adapting VRI to spatial heterogeneity of *R* was the variable *U*, the unutilized R under CI (Chapter 2). The observational *U* was 37 mm, which corresponded to 22 mm or 4938 m^3 of gross irrigation

reductions. The gSSURGO *U* was 21 mm smaller and corresponded to 56% less gross irrigation reductions. It is important to remember that the magnitude of these reductions assumed the implementation of planned soil moisture depletion (Woodruff et al., 1972; as cited by Lamm et al., 1994) under CI.

As a comparison, enforcing an avoidance zone over the 0.6 ha uncropped area around the waterway (fig. 3.1a) would reduce gross irrigations by 3%. If the 138 mm of gross irrigation that the area was expected to have received during the 2014 growing season was withheld, the resultant volume of gross irrigation reduction would be 835 m^3. At this field site, the gross irrigation reductions from adapting VRI to spatial heterogeneity of *R* were more than four times those from avoiding the uncropped area.

Adapting VRI to spatial heterogeneity of *R* would reduce field-average deep percolation by 19 mm/y at this field site. The expected field-average N fertilizer reduction was 4 kg/ha.

From equation 3.6, q_r and PV_r were \$42.1/mm and \$1,555 at this field site. Despite the previous analyses and discussions surrounding spatial heterogeneity of *R* at this field site, the private benefits from this application of VRI constituted only about one-sixth of the estimated C_v of \$9,088.

Economic Value of the Field Characterization of *R*

The value of the field characterization of *R* was simplified as the profit forgone or the loss avoided by making decisions with perfect knowledge of the spatial distribution of *R* rather than with gSSURGO. The first scenario examined is where the VRI system is available irrespective of the magnitude of PV_r. For this field site, the value of the method was equal to the PV_r of \$1,555. For the typical field, the value of the method was equal

to q_r of \$79.4/mm multiplied by the actual U. The method would be profitable whenever PV_r exceeded the cost of the method.

The second scenario examined was where the purchase of the VRI system depended at least in part on the magnitude of PV_r. Because PV_o was unknown for both the field site and the typical field, the analysis below was limited to the special case where PV_o equaled zero. For this field site, U_b was 216 mm if PV_o was zero. Because gSSURGO U and actual U were both below U_b, VRI investment would not have been made with or without the field characterization of R. The value of the method was thus zero. For the typical field, U_b was 126 mm if PV_o is zero. The difference in U_b between the field site and the typical field is primarily explained by the disparity in irrigated area to center pivot length ratio. The field site is irrigated by a half-circle center pivot, whereas the typical field is irrigated by a full-circle center pivot. All things being equal, VRI investment is certainly favored by a high irrigated area to center pivot length ratio.

Although the empirical distribution of gSSURGO U among center pivot irrigated fields in Nebraska was known from Chapter 2, the statistical distribution of the differences between gSSURGO U and actual U is unknown. For the special case of the second scenario where PV_o equaled zero, the value of the field characterization of R for pairs of gSSURGO U and actual U was shown in table 3.3. If PV_o is non-zero, U_b would decrease linearly with increasing PV_o, and table 3.3 would consequently shift linearly to the top left.

Table 3.3. The value of the field characterization of root zone water holding capacity (*R*), for pairs of field-average unutilized *R* (*U*) expected from gSSURGO and actual *U*, when the VRI system has not been purchased and the benefits from adapting to spatial heterogeneity of *R* would need to pay for all of a $10,000 VRI system over 50 ha.

		actual *U* (mm)				
		0	50	100	150	200
gSSURGO *U* (mm)	0	$0	$0	$0	$1,909	$5,879
	50	$0	$0	$0	$1,909	$5,879
	100	$0	$0	$0	$1,909	$5,879
	150	$10,000	$6,030	$2,060	$1,909	$5,879
	200	$10,000	$6,030	$2,060	$1,909	$5,879

For the second scenario, the field characterization of *R* appeared to be beneficial whenever *U* was thought to be above U_b. If actual *U* was discovered to exceed U_b, then the producer is rewarded with increased profits. If actual *U* was discovered to be below U_b, then the producer has avoided an unprofitable VRI investment. The method would be profitable whenever $C_v - PV_r - PV_o$ exceeded the cost of the method if gSSURGO *U* was below U_b, or whenever $PV_r + PV_o - C_v$ exceeded the cost of the method if gSSURGO U was above U_b.

If gSSURGO *U* were an unbiased estimator of actual *U*, then results from Chapter 2 suggested that the financial benefits from adapting VRI to spatial heterogeneity of *R* alone may exceed C_v on the 0.1% of Nebraska center pivot irrigated fields with gSSURGO *U* above the U_b of 126 mm. The field characterization of *R* might be considered on these fields even without knowing the magnitude of other VRI benefits.

Subsection Summary

Based on the R_{obs} map of this field site, 22 mm of gross irrigation and 4 kg/ha of N fertilizer were potentially reduced by adapting VRI to spatial heterogeneity of *R*. The

private component of these benefits, totaling $1,555 over ten years, composed a small fraction of the estimated C_v at the field site. Where the VRI system is available regardless of the magnitude of PV_r, the field characterization of R would be beneficial if PV_r exceeds the cost of the method. Where the purchase of the VRI system depends partially on the magnitude of PV_r, the method would be beneficial if the profit gained or the loss avoided by implementing the method exceeds the cost of the method.

3.5. Conclusion and Recommendations

This study resulted in several interesting conclusions and recommendations related to the field characterization of R. First, spatial soil moisture patterns were found to be different in the topsoil and the subsoil at the field site, and drastic moisture differences occurred as the steepest stretch of the two hillslopes transitioned from convex to concave. For capturing spatial patterns in FC_{obs}, the entire managed root zone should be sampled, and densely spaced sampling locations should be considered where abrupt differences are suspected. Second, as compared with gSSURGO or the Saxton and Rawls (2006) PTF, the observational method was found to be the most effective source of FC values for accounting for measured soil water variability at the field site using a soil water balance model. This FC estimation method is recommended over the two other methods for characterizing spatial heterogeneity of R. Third, though EC_a has proven to be useful for predicting R in many circumstances, EC_a did not correlate well with R_{obs} at the field site. Practitioners should gain an understanding of the soil water pattern before selecting the most suitable auxiliary variable on a specific field. Fourth, the field characterization of R is recommended if the expected financial benefit from adapting VRI to spatial heterogeneity of R exceeds the cost of the method where VRI is available

irrespective of this benefit; it is also recommended if this benefit, subtracted by the cost of the method, is favorable for the purchase of VRI where the availability of the system depends on this benefit.

3.6. References

Allen, R. G., & Wright, J. L. (2002). Conversion of Wright (1981) and Wright (1982) alfalfa-based crop coefficients for use with the ASCE Standardized Penman-Monteith Reference Evapotranspiration Equation. Kimberly, Idaho: University of Idaho. Retrieved from http://www.kimberly.uidaho.edu/water/asceewri/Conversion_of_Wright_Kcs_2c.pdf

AMS. (2015). Iowa Production Cost Report (Bi-Weekly). Report No. NW_GR210. Washington, D.C.: United States Department of Agriculture. Retrieved from http://search.ams.usda.gov/mnsearch/mnsearch.aspx

ArcGIS. (2013). *ArcGIS Desktop*. Ver. 10.2. Redlands, Cal.: ESRI.

ASAE Standards. (2007). S526.3: Soil and Water Terminology. St. Joseph, Mich.: ASAE.

Brevik, E. C., Fenton, T. E., & Jaynes, D. B. (2003). Evaluation of the Accuracy of a Central Iowa Soil Survey and Implications for Precision Soil Management. *Precision Agric.*, 4(3), 331-342. doi: 10.1023/A:1024960708561

CPN International. (2013). CPN 503 Elite Hydroprobe: Operating Manual V1.0. Concord, Cal.: CPN International. Retrieved from http://instrotek.com/wordpress/wp-content/uploads/503-Elite-Op-Manual.pdf

Daccache, A., Knox, J. W., Weatherhead, E. K., Daneshkhah, A., & Hess, T. M. (2015). Implementing precision irrigation in a humid climate – Recent experiences and on-going challenges. *Agric. Water Mgmt.*, 147, 135-143. doi: 10.1016/j.agwat.2014.05.018

Deck, J. H. (2010). Hydraulic Conductivity, Infiltration, and Runoff from No-till and Tilled Cropland. MS thesis. Lincoln, Neb.: University of Nebraska-Lincoln, Department of Biological Systems Engineering.

Djaman, K., & Irmak, S. (2013). Actual Crop Evapotranspiration and Alfalfa-and Grass-Reference Crop Coefficients of Maize under Full and Limited Irrigation and Rainfed Conditions. *J. Irrig. Drainage Eng.*, 139(6), 433-446. doi: 10.1061/(ASCE)IR.1943-4774.0000559

Evans, R. G., LaRue, J., Stone, K. C., & King, B. A. (2013). Adoption of site-specific variable rate sprinkler irrigation systems. *Irrig. Sci.*, 31(4), 871-887.

Feinerman, E., & Voet, H. (2000). Site-specific management of agricultural inputs: an illustration for variable-rate irrigation. *European Rev. Agric. Economics*, 27(1), 17-37. doi: 10.1093/erae/27.1.17

FSA. (2014). National Agricultural Imagery Program. Washington, D.C.: United States Department of Agriculture. Retrieved from https://gdg.sc.egov.usda.gov/GDGOrder.aspx

Grisso, R. D., Alley, M. M., Holshouser, D. L., & Thomason, W. E. (2009). Precision Farming Tools: Soil Electrical Conductivity. Publication 442-508. Blacksburg,

Va.: Virginia Cooperative Extension. Retrieved from https://pubs.ext.vt.edu/442/442-508/442-508_pdf.pdf

Hanna, A. Y., Harlan, P. W., & Lewis, D. T. (1982). Soil Available Water as Influenced by Landscape Position and Aspect. *Agron. J.*, 74(6), 999-1004. doi: 10.2134/agronj1982.00021962007400060016x

Hedley, C. B., & Yule, I. J. (2009). A method for spatial prediction of daily soil water status for precise irrigation scheduling. *Agric. Water Mgmt.*, 96(12), 1737-1745. doi: 10.1016/j.agwat.2009.07.009

Hezarjaribi, A., & Sourell, H. (2007). Feasibility study of monitoring the total available water content using non-invasive electromagnetic induction-based and electrode-based soil electrical conductivity measurements. *Irrig. Drainage*, 56, 53-65. doi: 10.1002/ird.289

Hillyer, C. C., Higgins, C. W., & Kelly, J. (2013). Catch Can Testing of a Variable Rate Irrigation System and Evaluation Using a Time Varying Densogram. ASABE Paper No. 1620517. St. Joseph, Mich.: ASABE.

HPRCC. (2014). Classic Online Raw Data Report. Lincoln, Neb.: High Plains Regional Climate Center. Retrieved from http://hprcc6.unl.edu/cgi-hpcc/dr3.cgi

Hupet, F., & Vanclooster, M. (2002). Intraseasonal dynamics of soil moisture variability within a small agricultural maize cropped field. *J. Hydrology*, 261, 86-101. doi: 10.1016/S0022-1694(02)00016-1

Jenny, H. (1941). *Factors of Soil Formation: A System of Quantitative Pedology*. New York, N.Y.: McGraw-Hill.

Kincaid, D. C., & Heermann, D. F. (1974). Scheduling irrigations using a programmable calculator. USDA-ARS Rep. No. ARS-NC-12. Washington, D.C.: United States Department of Agriculture.

Kitchen, N. R., Sudduth, K. A., Myers, D. B., Drummond, S. T., & Hong, S. Y. (2005). Delineating productivity zones on claypan soil fields using apparent soil electrical conductivity. *Computers Electronics Agric.*, 46, 285-308. doi: 10.1016/j.compag.2004.11.012

Klocke, N. L., Watts, D. G., Schneekloth, J. P., Davison, D. R., Todd, R. W., & Parkhurst, A. M. (1999). Nitrate Leaching in Irrigated Corn and Soybean in a Semi-Arid Climate. *Trans. ASAE*, 42(6), 1621-1630. doi: 10.13031/2013.13328

Kranz, W. L. (2010). Updating the Nebraska Pumping Plant Performance Criteria. In Proc. 22nd Ann. Central Plains Irrig. Conf. Colby, Kans.: Central Plains Irrg. Assoc.

Kranz, W. L., Irmak, S., van Donk, S. J., Yonts, C. D., & Martin, D. L. (2008a). Irrigation Management for Corn. NebGuide G1850. Lincoln, Neb.: University of Nebraska–Lincoln. Retrieved from http://www.ianrpubs.unl.edu/epublic/live/g1850/build/g1850.pdf

Kranz, W. L., Martin, D. L., Irmak, S., van Donk, S. J., & Yonts, C. D. (2008b). Minimum Center Pivot Design Capacities in Nebraska. NebGuide G1851. Lincoln, Neb.: University of Nebraska–Lincoln. Retrieved from http://ianrpubs.unl.edu/live/g1851/build/g1851.pdf

Lamm, F. R., Rogers, D. H., & Manges, H. L. (1994). Irrigation Scheduling with Planned Soil Water Depletion. *Trans. ASAE*, 37(5), 1491-1497. doi: 10.13031/2013.28232

Martin, D. L., Stegman, E. C., & Fereres, E. (1990). Irrigation Scheduling Principles. In G. J. Hoffman, T. A. Howell, & K. H. Solomon (Eds.), *Management of Farm Irrigation Systems*, pp. 155-203. St. Joseph, Mich.: ASAE.

Merriam, J.L. (1966). A Management Control Concept for Determining the Economical Depth and Frequency of Irrigation. *Trans. ASAE*, 9(4), 492-498.

Miller, K. A. (2015). Estimating Potential Water Savings Based on Soil Water Content, Geospatial Data Layers, and VRI Pivot Control Resolution. MS thesis. Lincoln, Neb.: University of Nebraska-Lincoln, Department of Biological Systems Engineering.

Mortensen, I. I. (2011). Intraseasonal Management Strategies for Deficit Irrigation. MS thesis. Lincoln, Neb.: University of Nebraska-Lincoln, Department of Biological Systems Engineering.

NOAA. (2014). Global Historical Climatology Network – Daily. Washington, D.C.: National Oceanic and Atmospheric Administration. Retrieved from http://www.ncdc.noaa.gov/cdo-web/search

NPPD. (2014). Electric Service for Irrigation. Columbus, Neb.: Nebraska Public Power District. Retrieved from http://www.nppd.com/assets/irrigationbrochure.pdf

NRCS. (2015). Gridded Soil Survey Geographic (gSSURGO) by State. Washington, D.C.: Natural Resources Conservation Service. Retrieved from https://gdg.sc.egov.usda.gov/GDGOrder.aspx

R Core Team. (2015). *R: A language and environment for statistical computing*. Ver. 3.2.0. Vienna, Austria: R Foundation for Statistical Computing.

Rhoades, J. D., Manteghi, N. A., Shouse, P. J., & Alves, W. J. (1989). Soil Electrical Conductivity and Soil Salinity: New Formulations and Calibrations. *Soil Sci. Soc. America J.*, 53(2), 433-439. doi: 10.2136/sssaj1989.03615995005300020020x

Romano, N., & Santini, A. (2002). Field. In J. H. Dane & G. C. Topp (Eds.), Methods of Soil Analysis: Part 4 – Physical Methods, (pp. 721-738). Madison, Wisc.: Soil Science Society of America. doi: 10.2136/sssabookser5.4.c26

Rudnick, D. R., & Irmak, S. (2014). Implementation of a Soil Water Extraction Model on a Spatial Domain Using Field Capacity and Apparent Electrical Conductivity Relationships. *Trans. ASABE*, 57(5), 1359-1373. doi: 10.13031/trans.57.10515

Sadler, E. J., Evans, R.G., Stone, K. C., & Camp, C. R. (2005). Opportunities for conservation with precision irrigation. *J. Soil Water Cons.*, 60(6), 371-378.

Saxton, K. E., & Rawls, W. J. (2006). Soil Water Characteristic Estimates by Texture and Organic Matter for Hydrologic Solutions. *Soil Sci. Soc. America J.*, 70(5), 1569-1578. doi: 10.2136/sssaj2005.0117

Sinai, G., Zaslavsky, D., & Golany, P. (1981). The Effect of Soil Surface Curvature on Moisture and Yield: Beer Sheba Observation. *Soil Sci.*, 132(5), 367-375.

Starr, G. C. (2005). Assessing temporal stability and spatial variability of soil water patterns with implications for precision water management. *Agric. Water Mgmt.*, 72(3), 223-243. doi: 10.1016/j.agwat.2004.09.020

Sudduth, K. A., Kitchen, N. R., Wiebold, W. J., Batchelor, W. D., Bollero, G. A., Bullock, D. G., Clay, D.E., Palm, H. L., Pierce, F. J., Schuler, R. T., & Thelen, K. D. (2005). Relating apparent electrical conductivity to soil properties across the north-central USA. *Computers Electronics Agric.*, 46, 263-283. doi: 10.1016/j.compag.2004.11.010

USGS. (2014). 1/9 Arc-Second National Elevation Dataset. Reston, Va.: United States Geological Survey. Retrieved from https://gdg.sc.egov.usda.gov/GDGOrder.aspx

USGS. (n.d.). National Hydrography Dataset. Reston, Va.: United States Geological Survey. Retrieved from http://viewer.nationalmap.gov/viewer/nhd.html

Vachaud, G., Passerat de Silans, A., Balabanis, P., & Vauclin, M. (1985). Temporal Stability of Spatially Measured Soil Water Probability Density Function. *Soil Sci. Soc. America J.*, 49(4), 822-828. doi: 10.2136/sssaj1985.03615995004900040006x

Veris Technologies. (2002). Soil EC maps and NRCS soil surveys—how do they compare? Is an EC map worth the investment? Salina, Kans.: Veris Technologies. Retrieved from http://www.veristech.com/images/ecfaq/Soil%20EC%20Maps%20and%20soil%20surveys.pdf

Waine, T. W., Blackmore, B. S., & Godwin, R. J. (2000). Mapping available water content and estimating soil textural class using electromagnetic induction. Paper No. 00-SW-044. Silsoe, U.K.: EurAgEng.

Western, A. W., Grayson, R. B., Blöschl, G., Willgoose, G. R., & McMahon, T. A. (1999). Observed spatial organization of soil moisture and its relation to terrain indices. *Water Resources Res.*, 35(3), 797-810. doi: 10.1029/1998WR900065

Williams, B. G., & Hoey, D. (1987). The Use of Electromagnetic Induction to Detect the Spatial Variability of the Salt and Clay Contents of Soils. *Australian J. Soil Res.*, 25(1), 21-27. doi: 10.1071/SR9870021

Woodruff, C. M., Peterson, M. R., Schnarre, D. H., & Cromwell, C. F. (1972). Irrigation scheduling with planned soil moisture depletion. ASAE Paper No. 72-222. St. Joseph, Mich.: ASAE.

CHAPTER 4: GENERAL OBSERVATIONS AND FUTURE WORK

4.1. Yield Improvements Where Irrigation Water Supply is Non-Restrictive

Comparing the private component of the three categories of VRI benefits where irrigation water supply is non-restrictive in the Central Plains (Chapter 1), the increased revenue from higher corn yields stands out because it may have a large potential to drive financially-motivated adoption of VRI in this region. Merely achieving a small but consistent yield improvement would make VRI adoption profitable (Marek et al., 2001; Chapter 1). With low irrigation prices relative to corn prices, conventional irrigation (CI; i.e., non-site-specific irrigation) is expected to be most profitable when aiming for close to the maximum field total yield possible with CI (Martin et al., 1990). The primary goal for VRI in this context, therefore, might be to reduce yield losses related to excessive water rather than insufficient water, the former of which has received less research attention and is less understood than the latter (S. Irmak, personal communication, 2014; D. M. Heeren, personal communication, 2015).

Excessive water poses two problems that create opportunities for VRI. First, poor soil aeration, which can result after the root zone has been underwater and/or near saturation for an extended time, has been identified as the key mechanism by which excessive water damages crop health (Kanwar et al., 1988). Managing VRI to reduce deep percolation in areas with a shallow water table, to reduce application depths in areas with poor internal drainage, and to reduce irrigation runoff in areas with poor surface drainage may lower the potential for or the severity of poor soil aeration and consequent yield loss. Second, excessive water can increase nitrogen (N) losses due to accelerated

leaching and/or denitrification. Yield gains may be captured if the application of in-season supplementary N to small, scattered areas with especially large N losses is cost-effective with variable rate fertigation but not with other application methods. Future VRI research and extension for the parts of the Central Plains with a non-restrictive irrigation water supply can develop prediction methods for the potential magnitude of yield improvement, provide field demonstrations of the profitability of addressing with VRI the problems of excessive water, and educate producers and consultants on such VRI management.

4.2. Benefits from Mining of Unutilized Root Zone Water Holding Capacity

Analysis based on the gridded Soil Survey Geographic database (NRCS, 2014) indicates that annual mining of unutilized root zone water holding capacity would enable a large reduction in gross irrigation on a small fraction of center pivot irrigated fields in Nebraska (Chapter 2). The consequent reduction in irrigation costs may be substantial on fields with both high heterogeneity of R and high pumping costs. Instead of representing each soil survey map unit with a weighted average root zone water holding capacity (R), further research can consider R variability among the components of each soil survey map unit.

By decreasing deep percolation and the accompanied N leaching, adapting VRI to spatial heterogeneity of R would reduce not only N fertilizer expenses but also N loading into groundwater. Further research can verify these positive effects and provide simple methods of quantify the resulting public (i.e., societal and environmental) benefits. Strong evidence of significant achievable public benefits may lead to additional funding for VRI research and favorable policies for VRI adoption.

Lowering N leaching with VRI may be of particular interest to communities where groundwater with high nitrate concentrations is the source of drinking water and where the depth to the water table is small. In these settings, the lag time between changes in land management and changes in groundwater quality is expected to be relatively short. Therefore, VRI—in conjunction with other best management practices—may be likely to provide necessary improvements within an acceptable time frame.

4.3. Field Characterization of Root Zone Water Holding Capacity

Observational field capacity (FC_{obs}) is the estimate of field capacity determined by measuring soil water content as observed under "natural" (i.e., non-experimental) conditions rather than after experimental saturation according to the classical field measurement method. The concept of FC_{obs} is consistent with the suggestion by Martin et al. (1990) that "[a] good indication of the field capacity water content can be determined by sampling field soils one to three days after a thorough irrigation or rain and when crop water use is small". Expressed as a depth over the managed root zone, the difference between FC_{obs} and permanent wilting point (PWP) is observational R (R_{obs}).

The determination of FC_{obs} and PWP at specific locations, followed by the spatial prediction of R_{obs} with an auxiliary variable (Jiang et al., 2007; Miller, 2015; Chapter 3), can improve the characterization of R for informing VRI investment decisions and VRI management. The simplest and the most cost-effective method of determining FC_{obs} may be to obtain volumetric water content by oven-drying intact cores from soil sampling equipment such a Giddings probe (Windsor, Colo.). As for the selection of the auxiliary variable(s), other geospatial variables besides apparent soil electrical conductivity (EC_a)

should be considered as they may exhibit a stronger relationship with *R* than EC_a does on some fields (Chapter 3). The field characterization of *R* is recommended where the expected profit from adapting VRI to spatial heterogeneity of *R* exceeds the cost of the procedure (Chapter 3). If hesitant about the expected range of *R* and the choice of sampling locations, practitioners can first conduct a reconnaissance survey (Brevik et al., 2003) to obtain greater understanding of the field site before committing to the full procedure.

To minimize the cost of the field characterization of *R*, the accuracy of the resulting R map must be balanced with the number of sampling locations. Future research can offer practical guidance on this tradeoff. The decrease in the uncertainty of *R* with an increase in the number of sampling locations can be quantified, and the strategy for the optimal placement of a fixed number of sampling locations can be identified. Because the causes of *R* variability and the spatial patterns of *R* are expected to be shared among multiple fields in a region, regional archetypes could be defined. Then, research results on the number and placement of sampling locations and the selection of auxiliary variable(s) on a field of one archetype may be generalizable to other fields of the same archetype.

4.4. Operational Field Capacity

Pronounced topography exists within the field site in Chapter 3. Although the role of topography-driven hydrological processes was neither modeled explicitly nor ruled out, FC_{obs} values were effective in accounting for much of the observed soil water variability along the topographic transects (Chapter 3). Because hydrological modeling at the scale and with the precision necessary for VRI management is difficult, capturing

the effect of spatially heterogeneous hydrological processes in static parameters would be convenient for creating prescription maps. For transient lateral processes that only become significant when deep percolation is significant and whose net effect is similar to the augmentation or diminution of deep percolation, it might be possible to include their influence in an operational FC value for irrigation management. This static parameter, however, cannot represent spatial heterogeneity of vertical water fluxes such as infiltration, capillary rise, and evapotranspiration. Because the deep percolation-like lateral processes would not be activated throughout the field when only selected locations are saturated, operational FC must be determined by the FC_{obs} method instead of the classic field measurement method. Future research can evaluate the operational FC concept and test its utility in various topographically variable settings.

4.5. VRI Monitoring and Evaluation

Producers who have begun to implement VRI may be interested in knowing the magnitude of the achieved benefits and in assessing the performance of their VRI system and its management (D. M. Heeren, personal communication, 2015). For these purposes, the collection, storage, and analysis of data would be essential. The drawing of as-applied irrigation maps requires the synthesis of logged information on the measured system flow rate, the measured system pressure, the global position system (GPS) coordinates of one or more towers, and the fraction of time each sprinkler was turned on. The generation of annual summaries of the achieved pumping cost savings would need records of the price and consumption of electricity or fuel. The incorporation of such reporting functionalities into center pivot management software and web services may be possible in the short term.

In contrast, complex control functionalities may necessitate long-term development. One example is the valuable ability to detect problems with user inputs and irrigation equipment quickly by automatic comparisons between expected outcomes and measured data from sources such as irrigation system sensors, field sensors, and harvest machinery. Nonetheless, as the operation and assessment of VRI rely increasingly on continuous, behind-the-scenes feedback from sensors, establishing adequate checks for detecting malfunctioning sensors would be critical.

4.6. References

Brevik, E. C., Fenton, T. E., & Jaynes, D. B. (2003). Evaluation of the Accuracy of a Central Iowa Soil Survey and Implications for Precision Soil Management. *Precision Agric.*, 4(3), 331-342. doi: 10.1023/A:1024960708561

Jiang, P., Anderson, S. H., Kitchen, N. R., Sudduth, K. A., & Sadler, E. J. (2007). Estimating Plant-Available Water Capacity for Claypan Landscapes Using Apparent Electrical Conductivity. *Soil Sci. Soc. America J., 71*(6), 1902-1908. doi: 10.2136/sssaj2007.0011

Kanwar, R. S., Baker, J. L., & Mukhtar, S. (1998). Excessive Soil Water Effects at Various Stages of Development on the Growth and Yield of Corn. *Trans. ASAE,* 31(1), 133-141. doi: 10.13031/2013.30678

Marek, T., Cox, E., Almas, L., & Amosson, S. (2001). The Feasibility of Variable Rate Irrigation with Center Pivot Systems in the Northern Texas High Plains. ASAE Paper No. 011117. St. Joseph, Mich.: ASAE. doi: 10.13031/2013.3443

Martin, D. L., Stegman, E. C., & Fereres, E. (1990). Irrigation Scheduling Principles. In G. J. Hoffman, T. A. Howell, & K. H. Solomon (Eds.), *Management of Farm Irrigation Systems*, pp. 155-203. St. Joseph, Mich.: ASAE.

Miller, K. A. (2015). Estimating Potential Water Savings Based on Soil Water Content, Geospatial Data Layers, and VRI Pivot Control Resolution. MS thesis. Lincoln, Neb.: University of Nebraska-Lincoln, Department of Biological Systems Engineering.

NRCS. (2014). Gridded Soil Survey Geographic (gSSURGO) by State. Washington, D.C.: United States Department of Agriculture. Retrieved from http://datagateway.nrcs.usda.gov

APPENDIX A: PYTHON CODE FOR CHAPTER 2

```
# STATEWIDE VRI ANALYSIS
# version 2.2
# under Customize -> ArcMap Options -> Raster,
# increase the maximum number of unique values to 1,000,000

# import modules
import arcpy, arcpy.sa, csv, string

# define parameters for adding tables and layers
mxd = arcpy.mapping.MapDocument("CURRENT")
df = arcpy.mapping.ListDataFrames(mxd, "Layers")[0]

# identify input and output directory
indir = "//bsedom5/WEAI/StatewideVRI/"
outdir = "//bsedom5/WEAI/StatewideVRI/Results/"

# Part 1: obtain RZAWC for each map unit
# identify the directory of the gSSURGO file geodatabase
dir = "//bsedom5/WEAI/StatewideVRI/gSSURGO/soils/gssurgo_g_ne.gdb/"

# obtain and export info about shallowest bedrock layer within max root zone
rzdep_max = 120 # in cm
addTable = arcpy.mapping.TableView(dir + "corestrictions")
arcpy.mapping.AddTableView(df, addTable)
restrictions = arcpy.SearchCursor("corestrictions",
   "((reskind = 'Lithic bedrock') Or (reskind = 'Paralithic bedrock')) "
   "And (resdept_r < " + str(rzdep_max) + ")", "",
   "cokey; resdept_r; reskind; corestrictkey", "cokey A; resdept_r A")
res = [[0,0,"",0]]
resCount = 0
for restriction in restrictions:
   if restriction.cokey != res[resCount][0]: # different component
      res.append([restriction.cokey, restriction.resdept_r,
         restriction.reskind, restriction.corestrictkey]) # resdept_r in cm
      resCount += 1 # one more restriction
res.pop(0) # remove first entry
file = open(outdir + "restrictions.csv","wb")
writer = csv.writer(file)
writer.writerow(["COKEY", "RESDEPT_R", "RESKIND", "CORESKEY"])
writer.writerows(res)
file.close()

# store and export info about horizons starting within max root zone;
# store, calculate, and export info about components
addTable = arcpy.mapping.TableView(dir + "chorizon")
arcpy.mapping.AddTableView(df, addTable)
horizons = arcpy.SearchCursor("chorizon","hzdept_r < " + str(rzdep_max), "",
   "cokey; hzname; hzdept_r; hzdepb_r; awc_r; chkey", "cokey A; hzdept_r A")
lastCokey = 0
resNum = 0
rzdep_r = 0 # in cm
rzawc_r = 0 # in mm
hz = []
```

```
comp = []
for horizon in horizons:
   cokey = horizon.cokey
   if cokey != lastCokey: # gone through one more component
      # not gone through all restrictions and has the current restriction:
      if (resNum < resCount) and (lastCokey == res[resNum][0]):
         # sum of horizon depths not equal to restriction depth
         if rzdep_r != res[resNum][1]:
            rzdep_r = -9999 # error
         resNum += 1 # gone through one more restriction
      else: # no more restrictions or doesn't have the current restriction
         # sum of horizon depths not equal to max root zone depth
         if rzdep_r != rzdep_max:
            rzdep_r = -9999 # error
      if rzawc_r <= 0: # RZAWC error or zero RZAWC
         rzawc_r = -9999 # error
      comp.append([lastCokey, rzdep_r, rzawc_r])
      # new component
      lastCokey = cokey
      rzdep_r = 0 # in cm
      rzawc_r = 0 # in mm
      lastDep = 0 # in cm
      # not gone through all restrictions and has the current restriction:
      if (resNum < resCount) and (cokey == res[resNum][0]):
         maxDep = res[resNum][1] # in cm
      else: # no more restrictions or doesn't have the current restriction
         maxDep = rzdep_max # in cm
   hzname = horizon.hzname
   hzdept_r = horizon.hzdept_r # in cm
   hzdepb_r = horizon.hzdepb_r # in cm
   awc_r = horizon.awc_r # in cm3/cm3
   depErr = False
   # no top depth or top depth doesn't start where the previous horizon ends
   if (hzdept_r is None) or (hzdept_r != lastDep):
      hzdept_r = -9999 # error
      depErr = True
   # no bottom depth or bottom depth shallower than top depth
   if (hzdepb_r is None) or (hzdepb_r < hzdept_r):
      hzdepb_r = -9999 # error
      depErr = True
   else: # no depth error
      lastDep = hzdepb_r # in cm
   # no awc or negative awc
   if (awc_r is None) or (awc_r < 0):
      if "r" in hzname.lower(): # rock horizon
         awc_r = 0 # in cm3/cm3
      else: # not rock horizon
         awc_r = -9999 # error
   if depErr == True: # has depth error
      layerThickness_r = -9999 # error
      hz.append([cokey, hzdept_r, hzdepb_r, layerThickness_r,
         awc_r, horizon.chkey])
      rzdep_r += layerThickness_r # in cm
      rzawc_r += awc_r * layerThickness_r * 10 # in mm
   elif hzdept_r < maxDep: # top depth shallower than max depth
      if hzdepb_r > maxDep: # bottom depth deeper than max depth
```

```
            hzdepb_r = maxDep
        layerThickness_r = hzdepb_r – hzdept_r # in cm
        hz.append([cokey, hzdept_r, hzdepb_r, layerThickness_r,
            awc_r, horizon.chkey])
        rzdep_r += layerThickness_r # in cm
        rzawc_r += awc_r * layerThickness_r * 10 # in mm
# finish up last component
# not gone through all restrictions and has the current restriction:
if (resNum < resCount) and (lastCokey == res[resNum][0]):
    # sum of horizon depths not equal to restriction depth
    if rzdep_r != res[resNum][1]:
        rzdep_r = -9999 # error
    resNum += 1 # gone through one more restriction
else: # no more restrictions or doesn't have the current restriction
    # sum of horizon depths not equal to max root zone depth
    if rzdep_r != rzdep_max:
        rzdep_r = -9999 # error
if rzawc_r <= 0: # RZAWC error or zero RZAWC
    rzawc_r = -9999 # error
comp.append([lastCokey, rzdep_r, rzawc_r])
comp.pop(0) # remove first entry
file = open(outdir + "horizons.csv","wb")
writer = csv.writer(file)
writer.writerow(["COKEY", "HZDEPT_R", "HZDEPB_R", "HZTHK_R", "AWC_R", "CHKEY"])
writer.writerows(hz)
file.close()
addTable = arcpy.mapping.TableView(dir + "component")
arcpy.mapping.AddTableView(df, addTable)
components = arcpy.SearchCursor("component","","","","cokey; mukey; comppct_r",
    "cokey A; mukey A")
compNum = 0
for component in components:
    if component.cokey == comp[compNum][0]:
        comp[compNum] = [component.mukey, component.comppct_r
            if (component.comppct_r >= 0) and (component.comppct_r <= 100)
            else -9999] + comp[compNum]
        compNum += 1
comp.sort() # sort by mukey as string
file = open(outdir + "components.csv","wb")
writer = csv.writer(file)
writer.writerow(["MUKEY", "COMPPCT_R", "COKEY", "RZDEP_R", "RZAWC_R"])
writer.writerows(comp)
file.close()

# calculate and export info about map units
comp.insert(0, comp[0])
mu = []
knownPct_r = 0 # in %
unknownPct_r = 0 # in %
avgRZAWC_r = 0 # in mm
for I in xrange(1, compNum + 1):
    if comp[i][0] != comp[I – 1][0]: # gone through one more map unit
        # the unknown percent plus
        # the total percent's deviation from 100% is at least 10%
        if unknownPct_r + abs(100 – knownPct_r – unknownPct_r) >= 10:
            mu.append([comp[I – 1][0], knownPct_r, -9999]) # error
```

```
        else:
            if knownPct_r != 100: # known percent not 100%
                avgRZAWC_r = avgRZAWC_r / (float(knownPct_r) / 100)
            mu.append([comp[I – 1][0], knownPct_r, avgRZAWC_r])
        knownPct_r = 0 # in %
        unknownPct_r = 0 # in %
        avgRZAWC_r = 0 # in mm
    # component has no percent composition error
    if (comp[i][1] != -9999):
        # component has root zone depth error, RZAWC error, or zero RZAWC
        if (comp[i][3] == -9999) or (comp[i][4] == -9999):
            unknownPct_r += comp[i][1]
        else: # no such errors
            knownPct_r += comp[i][1]
            avgRZAWC_r += comp[i][4] * (float(comp[i][1]) / 100)
# finish up last map unit
# the unknown percent plus
# the total percent's deviation from 100% is at least 10%
if unknownPct_r + abs(100 – knownPct_r – unknownPct_r) >= 10:
    mu.append([comp[I – 1][0], knownPct_r, -9999]) # error
else:
    if knownPct_r != 100: # known percent not 100%
        avgRZAWC_r = avgRZAWC_r / (float(knownPct_r) / 100)
    mu.append([comp[I – 1][0], knownPct_r, avgRZAWC_r])
comp.pop(0)
addTable = arcpy.mapping.TableView(dir + "muaggatt")
arcpy.mapping.AddTableView(df, addTable)
mapunits = arcpy.SearchCursor("muaggatt", "", "", "mukey; musym, muname",
    "mukey A")
muNum = 0
for mapunit in mapunits:
    if mapunit.mukey == mu[muNum][0]:
        mu[muNum] = ([mu[muNum][0]] + [mapunit.musym, mapunit.muname] +
            mu[muNum][1:3])
        muNum += 1
file = open(outdir + "mapunits.csv","wb")
writer = csv.writer(file)
writer.writerow(["MUKEY", "MUSYM", "MUNAME", "KNOWNPCT_R", "AVGRZAWC_R"])
writer.writerows(mu)
file.close()

# Part 2: calculate RZAWC indicator for each pivot
# project state boundaries to the coordinate system of the map unit raster
arcpy.Project_management(indir + "StateCountiesBorders/state_nrcs_a_ne.shp",
    outdir + "Nebraska_proj.shp",
    arcpy.Describe("//bsedom5/WEAI/StatewideVRI/gSSURGO/soils/gssurgo_g_ne.gdb/"
        "MapunitRaster_NE_10m").spatialReference.exportToString())

# clip map unit raster by state boundaries
arcpy.Clip_management("//bsedom5/WEAI/StatewideVRI/gSSURGO/soils/"
    "gssurgo_g_ne.gdb/MapunitRaster_NE_10m", "",
    outdir + "mukey.tif", "Nebraska_proj", "", "ClippingGeometry")

# project pivots to the map unit key raster's coordinate system while
# clipping them to state boundaries
arcpy.env.outputCoordinateSystem = "mukey.tif"
```

```
arcpy.Clip_analysis(indir + "AllPivots/IrrigatedPivots2005.shp", "Nebraska_proj",
   outdir + "AllPivots_proj.shp")

# delete unnecessary fields and add a field with the vector-based areas
# for use as a priority field in PolygonToRaster
arcpy.DeleteField_management("AllPivots_proj",
   ["ACRES", "HECTARES", "Shape_area", "Shape_len"])
arcpy.AddField_management("AllPivots_proj", "VectorArea", "DOUBLE")
arcpy.CalculateField_management("AllPivots_proj",
   "VectorArea", "!shape.area@acres!", "PYTHON")

# convert pivot shapefile to equivalent raster which snaps to
# the map unit key raster and which has the pivot OBJECTIDs as its values;
# polygons with larger vector-based areas are prioritized
arcpy.env.snapRaster = "mukey.tif"
cellSize_m = int(arcpy.GetRasterProperties_management("mukey.tif",
   "CELLSIZEX").getOutput(0))
arcpy.PolygonToRaster_conversion("AllPivots_proj", "OBJECTID",
   outdir + "AllPivots_proj.tif", "MAXIMUM_AREA", "VectorArea", cellSize_m)

# store OBJECTID of each pivot with cell area at least 50 acres
cellSize_Acres = (cellSize_m / 0.3048) ** 2 / 43560
minCount = int(50 / cellSize_Acres) + 1
pivots = arcpy.SearchCursor("AllPivots_proj.tif", "", "",
   "Value; Count", "Value A")
OIDList = []
for pivot in pivots:
   if pivot.Count >= minCount:
      OIDList.append(pivot.Value)

# keep only the pivots with cell area at least 50 acres
arcpy.Select_analysis("AllPivots_proj", outdir + "LargePivots_proj.shp",
   "\"OBJECTID\" IN " + str(tuple(OIDList)))

# convert those pivots to equivalent raster; store OBJECTIDs and cell counts
arcpy.PolygonToRaster_conversion("LargePivots_proj", "OBJECTID",
   outdir + "LargePivots_proj.tif", "MAXIMUM_AREA", "VectorArea", cellSize_m)
pivots = arcpy.SearchCursor("LargePivots_proj.tif", "", "",
   "Value; Count", "Value A")
pivotTbl = []
for pivot in pivots:
   pivotTbl.append([pivot.Value, int(pivot.Count)])

# store cell area in acres
arcpy.AddField_management("LargePivots_proj", "Area_Acres", "DOUBLE")
pivots = arcpy.UpdateCursor("LargePivots_proj", "", "",
   "OBJECTID; Area_Acres", "OBJECTID A")
k = 0
for pivot in pivots:
   pivot.setValue("Area_Acres", pivotTbl[k][1] * cellSize_Acres)
   pivots.updateRow(pivot)
   k += 1

# make new raster that has a unique value for every different combination of
# pivot OBJECTID and RZAWC
arcpy.sa.Combine(["LargePivots_proj.tif",
```

```
   outdir + "mukey.tif"]).save(outdir + "combined.tif")

# match RZAWCs with their corresponding mukeys
arcpy.AddField_management(outdir + "combined.tif", "strMUKEY", "Text")
arcpy.CalculateField_management("combined.tif", "strMUKEY",
   "str(!mukey!)", "PYTHON")
arcpy.AddField_management("combined.tif", "RZAWC", "DOUBLE")
mapunits = arcpy.UpdateCursor("combined.tif", "", "",
   "strMUKEY; RZAWC", "strMUKEY A")
muNum = 0
for mapunit in mapunits:
   while mu[muNum][0] < mapunit.strMUKEY:
      muNum += 1
   if mu[muNum][0] == mapunit.strMUKEY:
      mapunit.setValue("RZAWC", mu[muNum][4])
   else:
      mapunit.setValue("RZAWC", -9999)
   mapunits.updateRow(mapunit)

# compute average known RZAWC, 10th percentile known RZAWC, and RZAWC indicator,
# and export results
combos = arcpy.SearchCursor("combined.tif", "", "",
   "LargePivot; RZAWC; Count", "LargePivot A; RZAWC A")
pivotOID = pivotTbl[0][0]
pivotNum = 0
unknownCount = 0
knownCount = 0
avgKnown = 0
tenthPctile = -9999
countErrOIDs = []
for combo in combos:
   # gone through one more pivot
   if combo.LargePivot != pivotOID:
      if knownCount != 0:
         avgKnown /= float(knownCount)
      else:
         avgKnown = -9999
      # known count is at least 90% of total count
      if knownCount * 10 >= pivotTbl[pivotNum][1] * 9:
         RZAWCInd = avgKnown – tenthPctile
      # known count is less than 90% of total count
      else:
         RZAWCInd = -9999
      pivotTbl[pivotNum] = (pivotTbl[pivotNum][:2] +
         [float(knownCount) / pivotTbl[pivotNum][1],
         float(unknownCount) / pivotTbl[pivotNum][1],
         avgKnown, tenthPctile, RZAWCInd] +
         pivotTbl[pivotNum][2:])
      # move to next pivotNum as long as the combo pivot OBJECTID is larger
      # than the pivotTbl pivot OBJECTID
      while combo.LargePivot > pivotTbl[pivotNum][0]:
         pivotNum += 1
      # reset variables
      pivotOID = pivotTbl[pivotNum][0]
      unknownCount = 0
      knownCount = 0
```

```
            avgKnown = 0
            tenthPctile = -9999
        # no RZAWCs yet or different from previous RZAWC
        if ((len(pivotTbl[pivotNum]) == 2) or
            (combo.RZAWC != pivotTbl[pivotNum][-2])):
            pivotTbl[pivotNum] += [combo.RZAWC, int(combo.Count)]
        # same as previous RZAWC
        else:
            pivotTbl[pivotNum][-1] += int(combo.Count)
        # unknown RZAWC
        if combo.RZAWC == -9999:
            unknownCount += int(combo.Count)
        # known RZAWC
        else:
            knownCount += int(combo.Count)
            avgKnown += combo.Count * combo.RZAWC
        # no 10th percentile RZAWC yet and known count is least 1/10 of total count
        if (tenthPctile == -9999) and (knownCount * 10 >= pivotTbl[pivotNum][1]):
            tenthPctile = combo.RZAWC
    # finish up last pivot
    if knownCount != 0:
        avgKnown /= float(knownCount)
    else:
        avgKnown = -9999
    # known count is at least 90% of total count
    if knownCount * 10 >= pivotTbl[pivotNum][1] * 9:
        RZAWCInd = avgKnown – tenthPctile
    # known count is less than 90% of total count
    else:
        RZAWCInd = -9999
    pivotTbl[pivotNum] = (pivotTbl[pivotNum][:2] +
        [float(knownCount) / pivotTbl[pivotNum][1],
        float(unknownCount) / pivotTbl[pivotNum][1],
        avgKnown, tenthPctile, RZAWCInd] +
        pivotTbl[pivotNum][2:])
    maxRZAWCNum = 0
    for pivot in pivotTbl:
        if len(pivot) > maxRZAWCNum:
            maxRZAWCNum = len(pivot)
    maxRZAWCNum = (maxRZAWCNum – 7) / 2
    file = open(outdir + “pivots.csv”,”wb”)
    writer = csv.writer(file)
    names = []
    for I in xrange(1, maxRZAWCNum + 1):
        names += [“RZAWC” + str(i), “COUNT” + str(i)]
    writer.writerow([“OBJECTID”, “TOTALCOUNT”, “KNOWNPCT”, “UNKNOWNPCT”,
        “AVGKNOWN”, “10THPCTILE”, “RZAWCIND”] + names)
    writer.writerows(pivotTbl)
    file.close()

    # Part 3: make an analyzed pivots shapefile and an analyzed centroids shapefile
    # match percent error of raster-based area relative to vector-based area and
    # RZAWC indicator to the corresponding analyzed pivot
    OIDList = []
    for pivot in pivotTbl:
        if (len(pivot) > 2) and (pivot[6] != -9999):
```

```
        OIDList.append(pivot[0])
arcpy.SelectLayerByAttribute_management("LargePivots_proj", "NEW_SELECTION",
    "\"OBJECTID\" IN" + str(tuple(OIDList)))
arcpy.CopyFeatures_management("LargePivots_proj", outdir + "AnalyzedPivots.shp")
arcpy.AddField_management("AnalyzedPivots", "RZAWCInd","DOUBLE")
pivots = arcpy.UpdateCursor("AnalyzedPivots", "", "",
    "OBJECTID; Area_Acres; RZAWCInd", "OBJECTID A")
pivotNum = 0
for pivot in pivots:
    while int(pivot.OBJECTID) > pivotTbl[pivotNum][0]:
        pivotNum += 1
    if int(pivot.OBJECTID) == pivotTbl[pivotNum][0]:
        pivot.setValue("RZAWCInd", pivotTbl[pivotNum][6])
        pivots.updateRow(pivot)
del pivots
arcpy.AddField_management("AnalyzedPivots", "CentroidX","DOUBLE")
arcpy.AddField_management("AnalyzedPivots", "CentroidY","DOUBLE")
arcpy.CalculateField_management("AnalyzedPivots", "CentroidX",
    "float(!shape.centroid!.split()[0])","PYTHON")
arcpy.CalculateField_management("AnalyzedPivots", "CentroidY",
    "float(!shape.centroid!.split()[1])","PYTHON")
arcpy.MakeXYEventLayer_management("AnalyzedPivots", "CentroidX", "CentroidY",
    "centroids", arcpy.Describe("combined.tif").spatialReference.exportToString())
arcpy.CopyFeatures_management("centroids", outdir + "AnalyzedCentroids.shp")

# Part 4: Spatial relationships between RZAWC indicator and counties
# project counties boundaries to the coordinate system of the combined raster
arcpy.Project_management(indir + "StateCountiesBorders/county_nrcs_a_ne.shp",
    outdir + "NebrCounties_proj.shp",
    arcpy.Describe("combined.tif").spatialReference.exportToString())

# delete unnecessary fields
allFields = arcpy.ListFields("NebrCounties_proj")
delFields = []
for f in allFields:
    if f.name not in ["FID", "Shape", "COUNTYNAME", "FIPSCO"]:
        delFields.append(f.name)
arcpy.DeleteField_management("NebrCounties_proj", delFields)

# make a new shapefile with data of both analyzed centroids and counties
arcpy.Intersect_analysis(["AnalyzedCentroids", "NebrCounties_proj"],
    outdir + "RZAWCIndByCounties.shp", "NO_FID")

# sort RZAWC indicator values by county of corresponding analyzed centroids, and
# store the minimum and maximum RZAWC indicator values for the state
centroids = arcpy.SearchCursor("RZAWCIndByCounties", "", "",
    "RZAWCInd; COUNTYNAME", "COUNTYNAME A; RZAWCInd A")
numCounties = int(arcpy.GetCount_management("NebrCounties_proj").getOutput(0))
counties = [["", 0]]
RZAWCIndByCounties = []
count = 0
minRZAWCInd = 9999
maxRZAWCInd = -9999
for centroid in centroids:
    if centroid.COUNTYNAME != counties[-1][0]:
        counties[-1][1] = count
```

```
      if len(counties) > 1:
         if RZAWCIndByCounties[0][(len(counties) – 2) * 2] < minRZAWCInd:
            minRZAWCInd = RZAWCIndByCounties[0][(len(counties) – 2) * 2]
         if RZAWCIndByCounties[count – 1][(len(counties) – 2) * 2] > maxRZAWCInd:
            maxRZAWCInd = RZAWCIndByCounties[count – 1][(len(counties) – 2) * 2]
      counties.append([centroid.COUNTYNAME, 0])
      count = 0
   count += 1
   # make space
   if count > len(RZAWCIndByCounties):
      RZAWCIndByCounties.append([“” for I in xrange(numCounties * 2)])
   RZAWCIndByCounties[count – 1][(len(counties) – 2) * 2] = centroid.RZAWCInd
counties[-1][1] = count
counties.pop(0)

# store the number of analyzed pivots in each county
arcpy.AddField_management(“NebrCounties_proj”, “N_Analyzed”, “SHORT”)
cs = arcpy.UpdateCursor(“NebrCounties_proj”, “”, “”,
   “COUNTYNAME; N_Analyzed”,”COUNTYNAME A”)
k = 0
for c in cs:
   c.setValue(“N_Analyzed”, counties[k][1])
   cs.updateRowI
   k += 1

# assign non-exceedance probabilities using the Weibull formula to
# each county’s ascending RZAWC indicator values
for j in xrange(len(counties)):
   for I in xrange(counties[j][1]):
      RZAWCIndByCounties[i][j * 2 + 1] = float(I + 1) / (counties[j][1] + 1)

# export the lists of RZAWC indicator values and probabilities for every county
file = open(outdir + “RZAWCIndByCounties.csv”,”wb”)
writer = csv.writer(file)
names1 = []
names2 = []
for county in counties:
   names1 += [county[0], “”]
   names2 += [“RZAWCInd”, “Prob”]
writer.writerow(names1)
writer.writerow(names2)
writer.writerows(RZAWCIndByCounties)
file.close()

# define upper bounds of each RZAWC indicator class
inTOmm = 25.4
if minRZAWCInd < 0: # negative minimum RZAWC indicator
   RZAWCIndClasses = [k * inTOmm for k in
      xrange(int(minRZAWCInd / inTOmm), int(maxRZAWCInd / inTOmm) + 2)]
else: # non-negative minimum RZAWC indicator
   RZAWCIndClasses = [k * inTOmm for k in
      xrange(int(minRZAWCInd / inTOmm) + 1, int(maxRZAWCInd / inTOmm) + 2)]

# summarize results by county using RZAWC indicator classes and export
RZAWCIndByCountiesSummary = []
for j in xrange(len(counties)):
```

```
    # make space
    RZAWCIndByCountiesSummary.append([counties[j][0]] +
      [“” for k in xrange((len(RZAWCIndClasses) + 1) * 2)])
    classNum = 0
    classCount = 0
    # count the number of RZAWC indicator values in each class
    for I in xrange(counties[j][1]):
      while RZAWCIndByCounties[i][j * 2] >= RZAWCIndClasses[classNum]:
        RZAWCIndByCountiesSummary[j][classNum + 1] = classCount
        RZAWCIndByCountiesSummary[j][len(RZAWCIndClasses) + classNum + 2] = (
          float(classCount) / counties[j][1])
        classNum += 1
        classCount = 0
      classCount += 1
    # finish up last non-empty class and go through the empty top classes
    while classNum < len(RZAWCIndClasses):
      RZAWCIndByCountiesSummary[j][classNum + 1] = classCount
      RZAWCIndByCountiesSummary[j][len(RZAWCIndClasses) + classNum + 2] = (
        float(classCount) / counties[j][1])
      classNum += 1
      classCount = 0
    # check total number of RZAWC indicator values for each county, then
    # record total counts and total fractions for each county
    if sum(RZAWCIndByCountiesSummary[j][1☹len(RZAWCIndClasses) + 1)]) == (
      counties[j][1]):
      RZAWCIndByCountiesSummary[j][len(RZAWCIndClasses) + 1] = counties[j][1]
      RZAWCIndByCountiesSummary[j][(len(RZAWCIndClasses) + 1) * 2] = (
        sum(RZAWCIndByCountiesSummary[j][(
        len(RZAWCIndClasses) + 2)☹(len(RZAWCIndClasses) + 1) * 2)]))
    else:
      RZAWCIndByCountiesSummary[j][len(RZAWCIndClasses) + 1] = -9999
      RZAWCIndByCountiesSummary[j][(len(RZAWCIndClasses) + 1) * 2] = -9999
      print “RZAWCInd count error for “ + counties[j][0] + “ County!”
file = open(outdir + “RZAWCIndByCountiesSummary.csv”,”wb”)
writer = csv.writer(file)
names = [“County”]
for classNum in xrange(len(RZAWCIndClasses)):
  names.append(“Count” + str(RZAWCIndClasses[classNum] – inTOmm) +
    “<<=” + str(RZAWCIndClasses[classNum]))
names.append(“CountTotal”)
for classNum in xrange(len(RZAWCIndClasses)):
  names.append(“Frac” + str(RZAWCIndClasses[classNum] – inTOmm) +
    “<<=” + str(RZAWCIndClasses[classNum]))
names.append(“FracTotal”)
writer.writerow(names)
writer.writerows(RZAWCIndByCountiesSummary)
file.close()

# Part 5: Spatial relationships between RZAWC indicator and soil associations
# project soil association map to the coordinate system of the combined raster
arcpy.Project_management(indir + “Other/soils_utm.shp”,
  outdir + “SoilAssoc_proj.shp”,
  arcpy.Describe(“combined.tif”).spatialReference.exportToString())

# delete unnecessary fields
arcpy.DeleteField_management(“SoilAssoc_proj”, “Id”)
```

```
# make a new shapefile with data of
# both analyzed centroids and soil associations
arcpy.Intersect_analysis(["AnalyzedCentroids", "SoilAssoc_proj"],
   outdir + "RZAWCIndBySoilAssoc.shp", "NO_FID")

# sort RZAWC indicator values
# by soil association of corresponding analyzed centroids
centroids = arcpy.SearchCursor("RZAWCIndBySoilAssoc", "", "",
   "RZAWCInd; MU_SYM; Assoc", "MU_SYM A; RZAWCInd A")
numAssocs = int(arcpy.GetCount_management("SoilAssoc_proj").getOutput(0))
assocs = [[0, "", 0]]
RZAWCIndBySoilAssoc = []
count = 0
for centroid in centroids:
   if centroid.MU_SYM != assocs[-1][0]:
      assocs[-1][2] = count
      assocs.append([centroid.MU_SYM, centroid.Assoc, 0])
      count = 0
   count += 1
   # make space
   if count > len(RZAWCIndBySoilAssoc):
      RZAWCIndBySoilAssoc.append(["" for I in xrange(numAssocs * 2)])
   RZAWCIndBySoilAssoc[count – 1][(len(assocs) – 2) * 2] = (
      centroid.RZAWCInd)
assocs[-1][2] = count
assocs.pop(0)

# assign non-exceedance probabilities using the Weibull formula to
# each soil association's ascending RZAWC indicator values
for j in xrange(len(assocs)):
   for I in xrange(assocs[j][2]):
      RZAWCIndBySoilAssoc[i][j * 2 + 1] = float(I + 1) / (assocs[j][2] + 1)

# export the lists of RZAWC indicator values and probabilities
# for every soil association
file = open(outdir + "RZAWCIndBySoilAssoc.csv","wb")
writer = csv.writer(file)
names1 = []
names2 = []
for assoc in assocs:
   names1 += [assoc[0], assoc[1], ""]
   names2 += ["RZAWCInd", "Prob"]
writer.writerow(names1)
writer.writerow(names2)
writer.writerows(RZAWCIndBySoilAssoc)
file.close()

# summarize results by soil association using RZAWC indicator classes and export
RZAWCIndBySoilAssocSummary = []
for j in xrange(len(assocs)):
   # make space
   RZAWCIndBySoilAssocSummary.append([assocs[j][0], assocs[j][1]] +
      ["" for k in xrange((len(RZAWCIndClasses) + 1) * 2)])
   classNum = 0
   classCount = 0
```

```
    # count the number of RZAWC indicator values in each class
    for I in xrange(assocs[j][2]):
        while RZAWCIndBySoilAssoc[i][j * 2] >= RZAWCIndClasses[classNum]:
            RZAWCIndBySoilAssocSummary[j][classNum + 2] = classCount
            RZAWCIndBySoilAssocSummary[j][len(RZAWCIndClasses) + classNum + 3] = (
                float(classCount) / assocs[j][2])
            classNum += 1
            classCount = 0
        classCount += 1
    # finish up last non-empty class and go through the empty top classes
    while classNum < len(RZAWCIndClasses):
        RZAWCIndBySoilAssocSummary[j][classNum + 2] = classCount
        RZAWCIndBySoilAssocSummary[j][len(RZAWCIndClasses) + classNum + 3] = (
            float(classCount) / assocs[j][2])
        classNum += 1
        classCount = 0
    # check total number of RZAWC indicator values for each soil association,
    # then record total counts and total fractions for each soil association
    if sum(RZAWCIndBySoilAssocSummary[j][2☹len(RZAWCIndClasses) + 2)]) == assocs[j][2]:
        RZAWCIndBySoilAssocSummary[j][len(RZAWCIndClasses) + 2] = assocs[j][2]
        RZAWCIndBySoilAssocSummary[j][(len(RZAWCIndClasses) + 1) * 2 + 1] = (
            sum(RZAWCIndBySoilAssocSummary[j][(
            len(RZAWCIndClasses) + 3)☹(len(RZAWCIndClasses) + 1) * 2 + 1)]))
    else:
        RZAWCIndBySoilAssocSummary[j][len(RZAWCIndClasses) + 2] = -9999
        RZAWCIndBySoilAssocSummary[j][(len(RZAWCIndClasses) + 1) * 2 + 1] = -9999
        print ("RZAWCInd count error for " +
            assocs[j][0] + " " + assocs[j][1] + " soil association!!!")
file = open(outdir + "RZAWCIndBySoilAssocSummary.csv","wb")
writer = csv.writer(file)
names = ["MU_SYM", "SoilAssoc"]
for classNum in xrange(len(RZAWCIndClasses)):
    names.append("Count" + str(RZAWCIndClasses[classNum] – inTOmm) +
        "<<=" + str(RZAWCIndClasses[classNum]))
names.append("CountTotal")
for classNum in xrange(len(RZAWCIndClasses)):
    names.append("Frac" + str(RZAWCIndClasses[classNum] – inTOmm) +
        "<<=" + str(RZAWCIndClasses[classNum]))
names.append("FracTotal")
writer.writerow(names)
writer.writerows(RZAWCIndBySoilAssocSummary)
file.close()

# Part 6: potential seasonal irrigation savings for the state and by NRD
# project NRD boundaries to the coordinate system of the combined raster
arcpy.Project_management(indir + "Other/NRDUTM.shp", outdir + "NRDs_proj.shp",
    arcpy.Describe("combined.tif").spatialReference.exportToString())

# delete unnecessary fields
arcpy.DeleteField_management("NRDs_proj",
    ["OBJECTID", "NRD_Name_A", "NRD_Num", "Shape_area", "Shape_len"])

# calculate irrigation savings in depth and volume for each analyzed centroid
# not in the skipped NRDs with NRD-wide allocations
numNRDs = int(arcpy.GetCount_management("NRDs_proj").getOutput(0))
skipNRDs = ["Lower Republican", "Middle Republican",
```

```
    "South Platte", "Upper Republican"]
arcpy.SelectLayerByAttribute_management("NRDs_proj", "NEW_SELECTION",
    "\"NRD_Name\" NOT IN" + str(tuple(skipNRDs)))
arcpy.SelectLayerByLocation_management("AnalyzedCentroids",
    "COMPLETELY_WITHIN", "NRDs_proj", "", "NEW_SELECTION")
arcpy.CopyFeatures_management("AnalyzedCentroids", outdir + "savings.shp")
acTOha = 43560 * 0.3048 ** 2 / 10000
arcpy.AddField_management("savings", "Area_ha", "DOUBLE")
MAD = 0.5
Ea = 0.85
arcpy.AddField_management("savings", "Savings_mm", "DOUBLE")
mmhaTOm3 = 10
arcpy.AddField_management("savings", "Savings_m3", "DOUBLE")
savs = arcpy.UpdateCursor("savings", "", "", "Area_Acres; RZAWCInd; "
    "Area_ha; Savings_mm; Savings_m3")
for sav in savs:
    sav.setValue("Area_ha", sav.Area_Acres * acTOha)
    sav.setValue("Savings_mm", sav.RZAWCInd * MAD / Ea)
    sav.setValue("Savings_m3", (sav.RZAWCInd * MAD / Ea) *
        (sav.Area_Acres * acTOha) * mmhaTOm3)
    savs.updateRow(sav)

# make a new shapefile with data of both analyzed centroids and NRDs
arcpy.Intersect_analysis(["savings", "NRDs_proj"],
    outdir + "SavingsByNRDs.shp", "NO_FID")

# output the irrigation savings info for the state and for each NRD;
# output the impact info for the state and for each NRD
savs = arcpy.SearchCursor("SavingsByNRDs", "", "",
    "OBJECTID; RZAWCInd; Area_ha; Savings_mm, Savings_m3; NRD_Name",
    "NRD_Name A; Savings_m3 A")
savings = []
savingsByNRD = []
j = -1
savingsClasses = [0] + [k * inTOmm for k in xrange(1, 3)]
m3TOML = 0.001
NRDs = [[""] + [0 for k in xrange(4 * len(savingsClasses) + 1)]]
for sav in savs:
    if sav.NRD_Name != NRDs[-1][0]:
        for k in xrange(len(savingsClasses)):
            if NRDs[-1][4 * k + 3] != 0:
                NRDs[-1][4 * k + 4] = ((NRDs[-1][4 * k + 5] / m3TOML / mmhaTOm3) /
                    NRDs[-1][4 * k + 3])
            else:
                NRDs[-1][4 * k + 4] = 0
        NRDs.append([sav.NRD_Name] +
            [0 for k in xrange(4 * len(savingsClasses) + 1)])
        j += 1
        I = 0
    I += 1
    NRDs[-1][1] += 1
    savings.append([sav.NRD_Name, sav.OBJECTID, sav.Area_ha, sav.RZAWCInd,
        sav.Savings_mm, sav.Savings_m3, 0])
    if I > len(savingsByNRD):
        savingsByNRD.append([" for k in xrange(6 * (numNRDs – len(skipNRDs)))])
    savingsByNRD[I – 1][(6 * j)☹6 * (j + 1) – 1)] = savings[-1][1:6]
```

```
    for k in xrange(len(savingsClasses)):
        if sav.Savings_mm > savingsClasses[k]:
            NRDs[-1][4 * k + 2] += 1
            NRDs[-1][4 * k + 3] += sav.Area_ha
            NRDs[-1][4 * k + 5] += sav.Savings_m3 * m3TOML
# finish up last NRD
for k in xrange(len(savingsClasses)):
    if NRDs[-1][4 * k + 3] != 0:
        NRDs[-1][4 * k + 4] = ((NRDs[-1][4 * k + 5] / m3TOML / mmhaTOm3) /
            NRDs[-1][4 * k + 3])
    else:
        NRDs[-1][4 * k + 4] = 0
NRDs.pop(0)
# tally for the state
NRDs.append([“All Nebraska”] + [0 for k in xrange(4 * len(savingsClasses) + 1)])
for I in xrange(numNRDs – len(skipNRDs)):
    NRDs[-1][1] += NRDs[i][1]
    for j in xrange(len(savingsClasses)):
        NRDs[-1][4 * j + 2] += NRDs[i][4 * j + 2]
        NRDs[-1][4 * j + 3] += NRDs[i][4 * j + 3]
        NRDs[-1][4 * j + 5] += NRDs[i][4 * j + 5]
for k in xrange(len(savingsClasses)):
    if NRDs[-1][4 * k + 3] != 0:
        NRDs[-1][4 * k + 4] = ((NRDs[-1][4 * k + 5] / m3TOML / mmhaTOm3) /
            NRDs[-1][4 * k + 3])
    else:
        NRDs[-1][4 * k + 4] = 0

# export impact info
file = open(outdir + “NRDs.csv”,”wb”)
writer = csv.writer(file)
names1 = [“”, “”]
names2 = [“NRD”, “CountTotal”]
for savingsClass in savingsClasses:
    names1 += [“Savings_mm>” + str(savingsClass), “”, “”, “”]
    names2 += [“Count”, “Area”, “Savings_mm”, “Savings_ML”]
writer.writerow(names1)
writer.writerow(names2)
writer.writerows(NRDs)
file.close()

# assign non-exceedance probabilities using the Weibull formula to
# pivots based on depth of irrigation savings; export savings info
# for the state
savings.sort(key = lambda saving: saving[5])
for k in xrange(len(savings)):
    savings[k][6] = (k + 1) / float(NRDs[-1][1] + 1)
file = open(outdir + “savings.csv”,”wb”)
writer = csv.writer(file)
writer.writerow([“NRD”, “OBJECTID”, “Area_ha”, “RZAWCInd”,
    “Savings_mm”, “Savings_m3”, “Prob”])
writer.writerows(savings)
file.close()
# for each NRD
for j in xrange(numNRDs – len(skipNRDs)):
    for I in xrange(NRDs[j][1]):
```

```
        savingsByNRD[i][6 * (j + 1) – 1] = float(I + 1) / (NRDs[j][1] + 1)
file = open(outdir + “savingsByNRDs.csv”,”wb”)
writer = csv.writer(file)
names1 = []
names2 = []
for NRD in NRDs:
   names1 += [NRD[0]] + [“” for k in xrange(5)]
   names2 += [“OBJECTID”, “Area_ha”, “RZAWCInd”,
      “Savings_mm”, “Savings_m3”, “Prob”]
writer.writerow(names1)
writer.writerow(names2)
writer.writerows(savingsByNRD)
file.close()

# Part 7: Sensitivity
# 5th percentile
pivots = arcpy.SearchCursor(“LargePivots_proj.tif”, “”, “”,
   “Value; Count”, “Value A”)
pivotTbl = []
for pivot in pivots:
   pivotTbl.append([pivot.Value, int(pivot.Count)])
combos = arcpy.SearchCursor(“combined.tif”, “”, “”,
   “LargePivot; RZAWC; Count”, “LargePivot A; RZAWC A”)
pivotOID = pivotTbl[0][0]
pivotNum = 0
unknownCount = 0
knownCount = 0
avgKnown = 0
fifthPctile = -9999
countErrOIDs = []
for combo in combos:
   # gone through one more pivot
   if combo.LargePivot != pivotOID:
      if knownCount != 0:
         avgKnown /= float(knownCount)
      else:
         avgKnown = -9999
      # known count is at least 90% of total count
      if knownCount * 10 >= pivotTbl[pivotNum][1] * 9:
         RZAWCInd = avgKnown – fifthPctile
      # known count is less than 90% of total count
      else:
         RZAWCInd = -9999
      pivotTbl[pivotNum] = (pivotTbl[pivotNum][:2] +
         [float(knownCount) / pivotTbl[pivotNum][1],
         float(unknownCount) / pivotTbl[pivotNum][1],
         avgKnown, fifthPctile, RZAWCInd] +
         pivotTbl[pivotNum][2:])
      # move to next pivotNum as long as the combo pivot OBJECTID is larger
      # than the pivotTbl pivot OBJECTID
      while combo.LargePivot > pivotTbl[pivotNum][0]:
         pivotNum += 1
      # reset variables
      pivotOID = pivotTbl[pivotNum][0]
      unknownCount = 0
      knownCount = 0
```

```
        avgKnown = 0
        fifthPctile = -9999
    # no RZAWCs yet or different from previous RZAWC
    if ((len(pivotTbl[pivotNum]) == 2) or
        (combo.RZAWC != pivotTbl[pivotNum][-2])):
        pivotTbl[pivotNum] += [combo.RZAWC, int(combo.Count)]
    # same as previous RZAWC
    else:
        pivotTbl[pivotNum][-1] += int(combo.Count)
    # unknown RZAWC
    if combo.RZAWC == -9999:
        unknownCount += int(combo.Count)
    # known RZAWC
    else:
        knownCount += int(combo.Count)
        avgKnown += combo.Count * combo.RZAWC
    # no 5th percentile RZAWC yet and known count is least 1/20 of total count
    if (fifthPctile == -9999) and (knownCount * 20 >= pivotTbl[pivotNum][1]):
        fifthPctile = combo.RZAWC
# finish up last pivot
if knownCount != 0:
    avgKnown /= float(knownCount)
else:
    avgKnown = -9999
# known count is at least 90% of total count
if knownCount * 10 >= pivotTbl[pivotNum][1] * 9:
    RZAWCInd = avgKnown – fifthPctile
# known count is less than 90% of total count
else:
    RZAWCInd = -9999
pivotTbl[pivotNum] = (pivotTbl[pivotNum][:2] +
    [float(knownCount) / pivotTbl[pivotNum][1],
    float(unknownCount) / pivotTbl[pivotNum][1],
    avgKnown, fifthPctile, RZAWCInd] +
    pivotTbl[pivotNum][2:])
maxRZAWCNum = 0
for pivot in pivotTbl:
    if len(pivot) > maxRZAWCNum:
        maxRZAWCNum = len(pivot)
maxRZAWCNum = (maxRZAWCNum – 7) / 2
file = open(outdir + “pivots5.csv”,”wb”)
writer = csv.writer(file)
names = []
for I in xrange(1, maxRZAWCNum + 1):
    names += [“RZAWC” + str(i), “COUNT” + str(i)]
writer.writerow([“OBJECTID”, “TOTALCOUNT”, “KNOWNPCT”, “UNKNOWNPCT”,
    “AVGKNOWN”, “5THPCTILE”, “RZAWCIND”] + names)
writer.writerows(pivotTbl)
file.close()

# 15th percentile
pivots = arcpy.SearchCursor(“LargePivots_proj.tif”, “”, “”,
    “Value; Count”, “Value A”)
pivotTbl = []
for pivot in pivots:
    pivotTbl.append([pivot.Value, int(pivot.Count)])
```

```
combos = arcpy.SearchCursor("combined.tif", "", "",
   "LargePivot; RZAWC; Count", "LargePivot A; RZAWC A")
pivotOID = pivotTbl[0][0]
pivotNum = 0
unknownCount = 0
knownCount = 0
avgKnown = 0
fifteenthPctile = -9999
countErrOIDs = []
for combo in combos:
   # gone through one more pivot
   if combo.LargePivot != pivotOID:
      if knownCount != 0:
         avgKnown /= float(knownCount)
      else:
         avgKnown = -9999
      # known count is at least 90% of total count
      if knownCount * 10 >= pivotTbl[pivotNum][1] * 9:
         RZAWCInd = avgKnown – fifteenthPctile
      # known count is less than 90% of total count
      else:
         RZAWCInd = -9999
      pivotTbl[pivotNum] = (pivotTbl[pivotNum][:2] +
         [float(knownCount) / pivotTbl[pivotNum][1],
         float(unknownCount) / pivotTbl[pivotNum][1],
         avgKnown, fifteenthPctile, RZAWCInd] +
         pivotTbl[pivotNum][2:])
      # move to next pivotNum as long as the combo pivot OBJECTID is larger
      # than the pivotTbl pivot OBJECTID
      while combo.LargePivot > pivotTbl[pivotNum][0]:
         pivotNum += 1
      # reset variables
      pivotOID = pivotTbl[pivotNum][0]
      unknownCount = 0
      knownCount = 0
      avgKnown = 0
      fifteenthPctile = -9999
   # no RZAWCs yet or different from previous RZAWC
   if ((len(pivotTbl[pivotNum]) == 2) or
      (combo.RZAWC != pivotTbl[pivotNum][-2])):
      pivotTbl[pivotNum] += [combo.RZAWC, int(combo.Count)]
   # same as previous RZAWC
   else:
      pivotTbl[pivotNum][-1] += int(combo.Count)
   # unknown RZAWC
   if combo.RZAWC == -9999:
      unknownCount += int(combo.Count)
   # known RZAWC
   else:
      knownCount += int(combo.Count)
      avgKnown += combo.Count * combo.RZAWC
   # no 15th percentile RZAWC yet and known count is least 3/20 of total count
   if (fifteenthPctile == -9999) and (knownCount * 20 >= pivotTbl[pivotNum][1] * 3):
      fifteenthPctile = combo.RZAWC
# finish up last pivot
if knownCount != 0:
```

```
   avgKnown /= float(knownCount)
else:
   avgKnown = -9999
# known count is at least 90% of total count
if knownCount * 10 >= pivotTbl[pivotNum][1] * 9:
   RZAWCInd = avgKnown – fifteenthPctile
# known count is less than 90% of total count
else:
   RZAWCInd = -9999
pivotTbl[pivotNum] = (pivotTbl[pivotNum][:2] +
   [float(knownCount) / pivotTbl[pivotNum][1],
   float(unknownCount) / pivotTbl[pivotNum][1],
   avgKnown, fifteenthPctile, RZAWCInd] +
   pivotTbl[pivotNum][2:])
maxRZAWCNum = 0
for pivot in pivotTbl:
   if len(pivot) > maxRZAWCNum:
      maxRZAWCNum = len(pivot)
maxRZAWCNum = (maxRZAWCNum – 7) / 2
file = open(outdir + “pivots15.csv”,”wb”)
writer = csv.writer(file)
names = []
for I in xrange(1, maxRZAWCNum + 1):
   names += [“RZAWC” + str(i), “COUNT” + str(i)]
writer.writerow([“OBJECTID”, “TOTALCOUNT”, “KNOWNPCT”, “UNKNOWNPCT”,
   “AVGKNOWN”, “15THPCTILE”, “RZAWCIND”] + names)
writer.writerows(pivotTbl)
file.close()
```

APPENDIX B: 120 CM ROOT ZONE WATER HOLDING CAPACITY MAP OF NEBRASKA

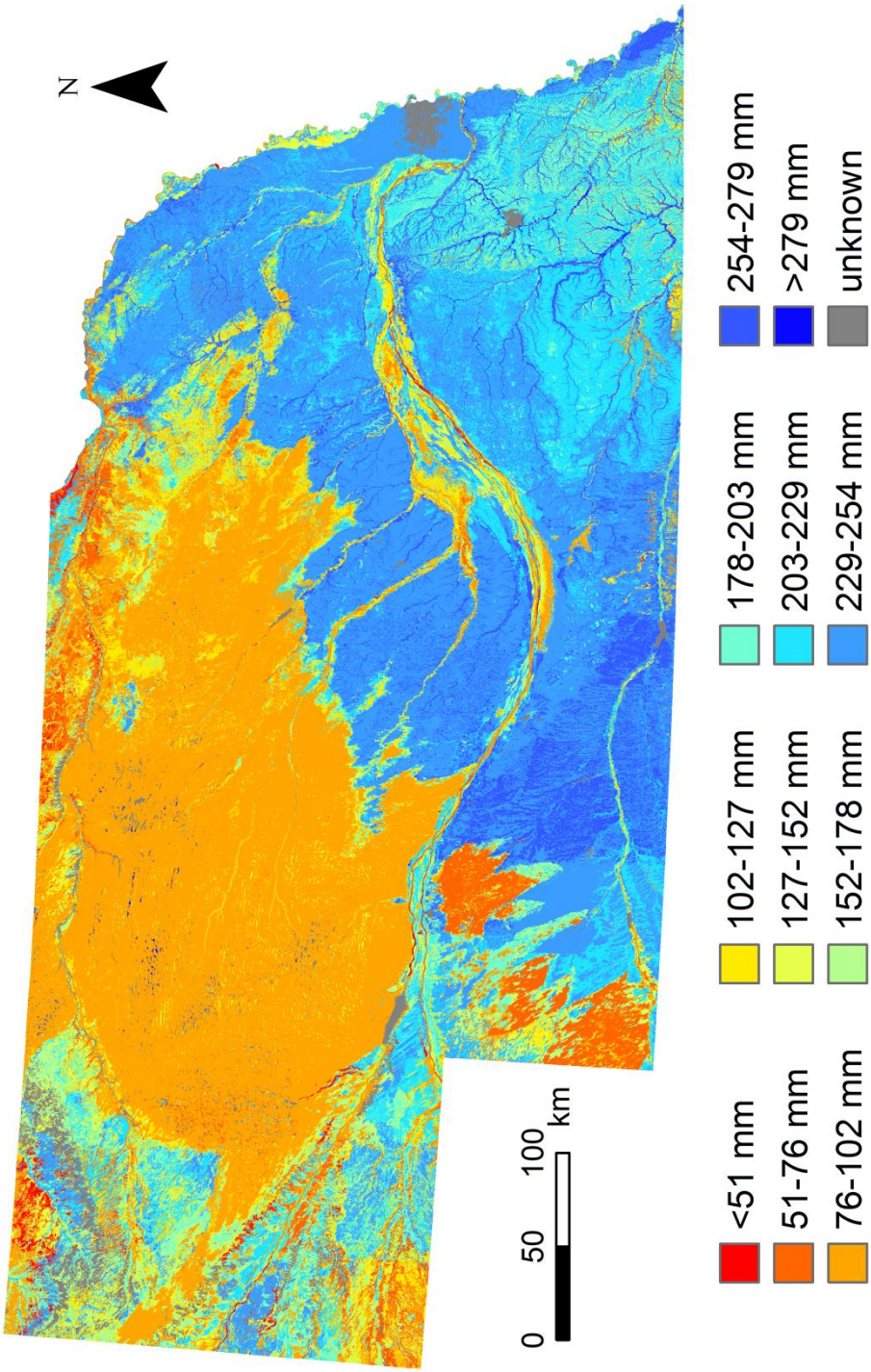

Figure B.1. 120 cm root zone water holding capacity map of Nebraska based on gSSURGO (NRCS, 2015)

APPENDIX C: SOIL WATER, CHANGES IN SOIL WATER, AND VRI APPLICATIONS IN A TOPOGRAPHICALLY VARIABLE FIELD

C.1. Methods

C.1.1. $TW - I_n$

At this field site (Chapter 3) during the 2014 growing season, irrigation presented two problems for direct comparison of soil moisture between measurement locations. First, the pump did not always supply sufficient pressure to meet the pressure requirement of the sprinklers. The irrigation application was thus systematically non-uniform throughout the field. Second, due to abundant in-season rainfall, center pivot revolutions were often interrupted. Some measurement locations consequently received an additional irrigation application as compared with the others at the time of neutron gauge readings.

$TW - I_n$ is defined as the total amount of soil water in the top 122 cm (TW; relative to $\theta_v = 0$) subtracted by the cumulative net irrigation I_n (assuming a constant and uniform application efficiency E_a) at that location up to the time of measurement. This quantity attempts to adjust for the effects of irrigation differences by completely removing the amount of soil water that may be attributed to irrigation. Its goal is to isolate the natural (vs. artificial) effects of topography on soil water.

On any measurement date, the biggest difference in expected cumulative gross irrigation was 30 mm. When E_a is not known, as in this study, Kranz et al. (2008) suggested 0.85 as an estimate. If the actual E_a is spatially uniform and between 0.75 and

0.95, then the maximum error in I_n due to assuming an E_a of 0.85 is within 3 mm. Therefore, only the results that assumed an E_a of 0.85 were reported here.

C.1.2. Statistical Analyses

Following Vachaud et al. (1985), Spearman's rank correlation coefficient ρ was used as an indicator of the temporal rank stability of soil moisture among measurement locations. In this study, soil moisture was expressed as $TW - I_n$ instead of soil water storage, the choice in Vachaud et al. (1985). A large ρ between two dates reveals that measurement locations are ranked similarly on both dates based on $TW - I_n$.

Differences between topographic groups will almost always be observed, but the Student's t-test and the non-parametric Mann-Whitney test were used to assess the statistical significance of the observed differences. The results of these tests help identify the comparisons in which the topographic groups are most likely to truly differ from each other. Because the bottom of the hillslopes is assumed to be wetter than the top of the hillslopes, one-sided alternative hypotheses (H_a) were used for comparisons of $TW - I_n$. As for comparisons of temporal changes in $TW - I_n$, a two-sided H_a was used.

All three statistical procedures were conducted using functions in the stats package of the statistical computing system R (R Core Team, 2015). The functions were cor.test for Spearman's ρ, t.test for t-tests, and wilcox.test for Mann-Whitney tests.

C.2. Results and Discussion

C.2.1. $TW - I_n$

The stability and significance of the soil water differences along the topographic transects were evaluated by both parametric and non-parametric statistical methods. The

$TW - I_n$ was used to correct for disparities in gross irrigation among measurement locations and represents the total water within the managed root zone in the absence of irrigation. $TW - I_n$ along the parallel and perpendicular transects on seven measurement dates was shown in figures C.1a-b.

a)

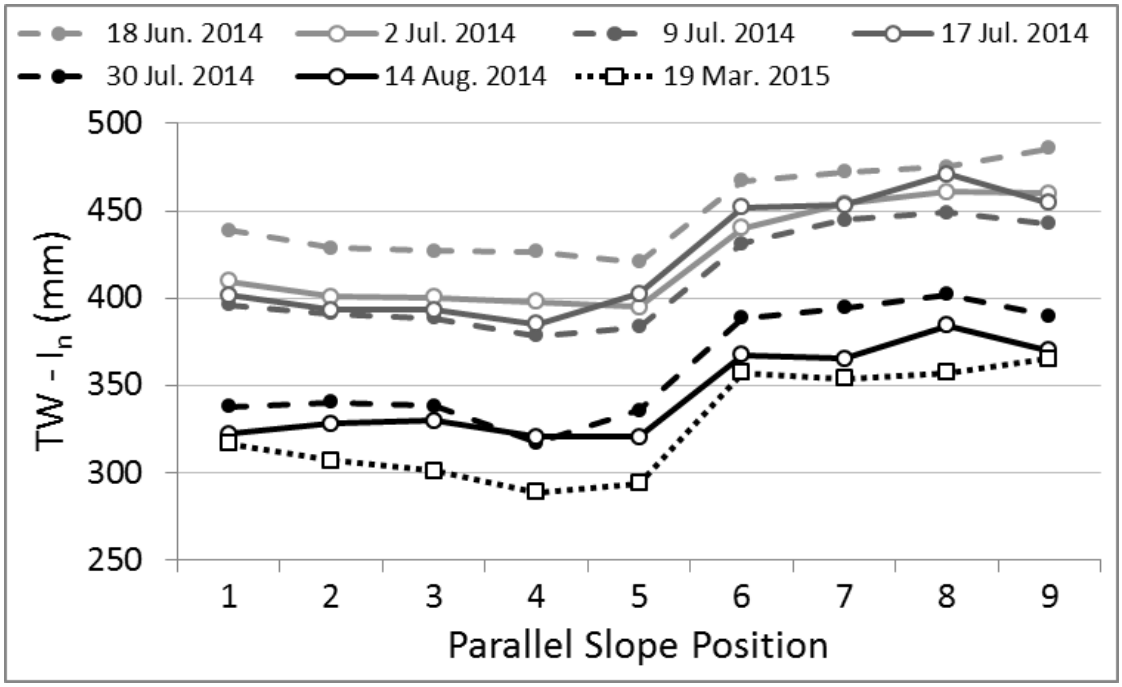

b)

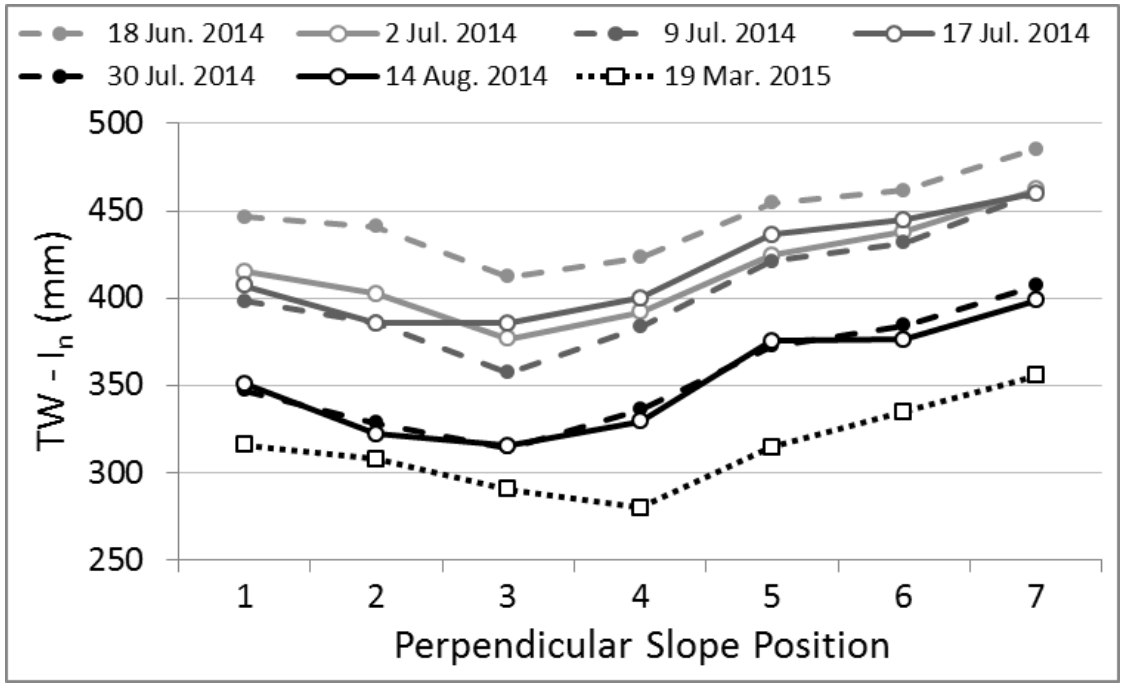

Figure C.1. Total soil water in the top 122 cm subtracted by cumulative net irrigation ($TW - I_n$) on seven dates along the topographic transects that are a) parallel or b) perpendicular to corn rows (slope position numbers increase with decreasing elevation); each data point represents the average between two replicate measurement locations.

The rank stability of $TW - I_n$ over the monitoring period is supported by large Spearman's ρ values for $TW - I_n$ between measurement dates (table C.1). Along the

parallel transects, about half of the Spearman ρ values were between 0.8 and 0.9 whereas the rest were roughly equally distributed between the ranges of 0.7-0.8 and 0.9-1. Along the perpendicular transects, two-thirds of the Spearman's ρ values were between 0.9 and 1; the remainder were mostly in the 0.8-0.9 range, and a couple were in the 0.7-0.8 range. Furthermore, all of the calculated Spearman's ρ values were greater than 0 at a p-value less than 0.002.

Table C.1. Spearman's rank correlation coefficient ρ for total soil water in the top 122 cm subtracted by cumulative net irrigation ($TW - I_n$) between measurement dates; ρ was calculated separately along the topographic transects parallel to corn rows (18 locations) and along the topographic transects perpendicular to corn rows (14 locations).

Date	18 Jun. 2014	2 Jul. 2014	9 Jul. 2014	17 Jul. 2014	30 Jul. 2014	14 Aug. 2014	19 Mar. 2015
18 Jun. 2014	1	0.98	0.95	0.80	0.93	0.93	0.94
2 Jul. 2014	0.95	1	0.96	0.82	0.96	0.93	0.91
9 Jul. 2014	0.90	0.97	1	0.89	0.99	0.96	0.87
17 Jul. 2014	0.80	0.82	0.87	1	0.92	0.93	0.75
30 Jul. 2014	0.83	0.89	0.95	0.91	1	0.98	0.86
14 Aug. 2014	0.78	0.78	0.75	0.78	0.82	1	0.87
19 Mar. 2015	0.92	0.88	0.86	0.76	0.85	0.85	1

parallel transects

perpendicular transects

The significance of $TW - I_n$ differences between topographic groups is supported by results from two-sample t-tests and Mann-Whitney tests (table C.2). On all seven dates and for both parallel and perpendicular transects, $TW - I_n$ was larger in the bottom group than in the top group, with p-values of less than 0.05. The difference in group mean $TW - I_n$ averaged 53 mm along the parallel transects and 46 mm along the perpendicular transects over the monitoring period. Such differences are comparable in

magnitude to the amount of stored soil water expected from two typical center pivot irrigation applications in Nebraska.

Table C.2. Results from two-sample t-tests and Mann-Whitney tests comparing, on seven measurement dates, total soil water in the top 122 cm subtracted by cumulative net irrigation ($TW - I_n$) at the locations at the top of the topographic transects parallel or perpendicular to corn rows and at the locations at the bottom of the same transects.

Date	Top group mean TW $- I_n$ (mm)	Bottom group mean TW $- I_n$ (mm)	t-test p-value (H_a: $\mu_{top} < \mu_{bottom}$)	Mann-Whitney test p-value (H_a: top < bottom)
parallel transects				
18 Jun. 2014	431	478	7E-06	1E-03
2 Jul. 2014	404	458	9E-07	1E-03
9 Jul. 2014	392	445	9E-06	1E-03
17 Jul. 2014	396	459	7E-05	1E-03
30 Jul. 2014	339	396	2E-05	1E-03
14 Aug. 2014	327	373	1E-03	1E-03
19 Mar. 2015	308	359	1E-05	1E-03
perpendicular transects				
18 Jun. 2014	444	473	8E-03	1E-02
2 Jul. 2014	409	450	5E-03	1E-02
9 Jul. 2014	392	446	3E-03	1E-02
17 Jul. 2014	396	452	2E-03	1E-02
30 Jul. 2014	338	396	1E-03	1E-02
14 Aug. 2014	337	388	5E-03	1E-02
19 Mar. 2015	312	345	4E-03	1E-02

Ultimately, these analyses give weight to the claim that the soil water differences along the topographic transects are stable and both practically and statistically significant. The top and bottom topographic groups in this study are more homogeneous than the three EC zones in Hedley and Yule (2009), which shared similar mean θ_v and frequently had similar standard deviations of θ_v as the population of all 50 measurement locations in the field. Indeed, on all seven measurement dates in this study, all top locations on either hillslope had less $TW - I_n$ than all bottom locations on the same hillslope. 14 August

2014 was the only measurement date when some top locations on one hillslope had more $TW - I_n$ than some bottom locations on the other hillslope.

C.2.2. $\Delta(TW - I_n)$

The temporal changes in $TW - I_n$ along the parallel and the perpendicular transects between seven measurement dates were shown in figures C.2a-d. Between all pairs of adjacent measurement dates except 9 July and 17 July 2014, $\Delta(TW - I_n)$ was generally negative along entire transects. The managed root zone throughout the hillslopes would have been drying overall during the monitoring period if no irrigation had been applied.

a)

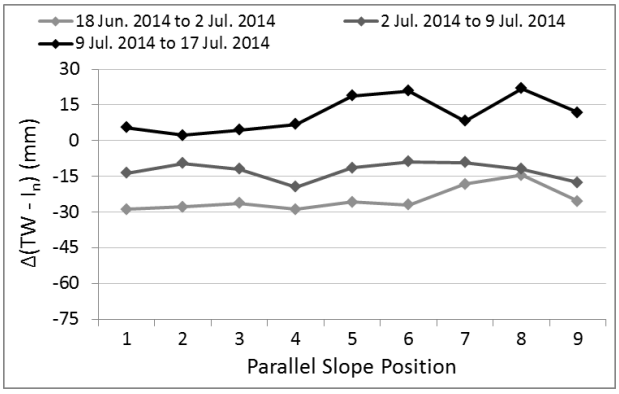

b)

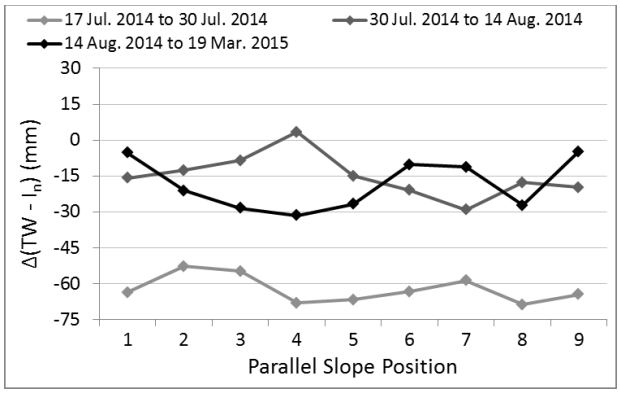

c)

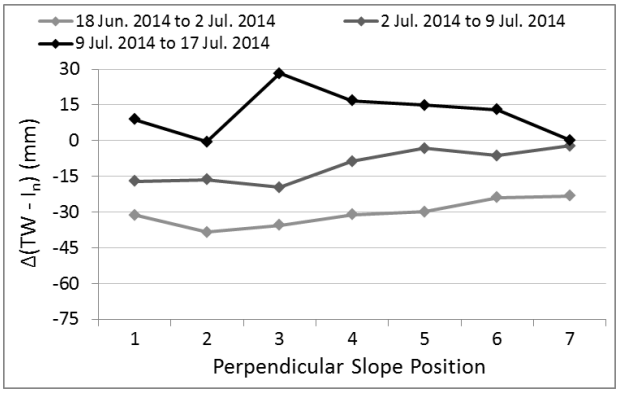

d)

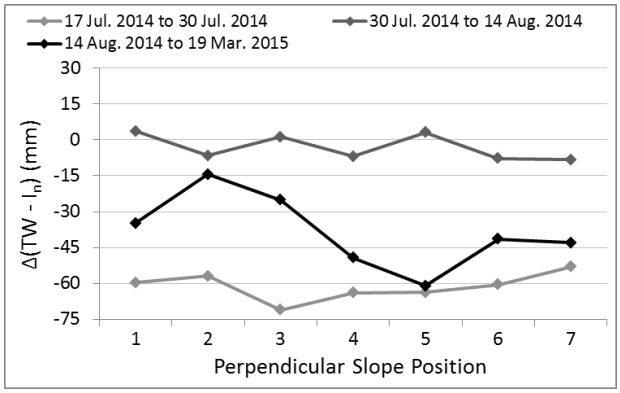

Figure C.2. $\Delta(TW - I_n)$, change in total soil water in the top 122 cm subtracted by cumulative net irrigation, over six intervals along the topographic transects parallel or perpendicular to corn rows (slope position numbers increase with decreasing elevation); each data point represents the average between two replicate measurement locations.

Unlike $TW - I_n$, however, there is not one $\Delta(TW - I_n)$ pattern that is present across all time intervals. Instead, slope positions have above-average $\Delta(TW - I_n)$ during some time intervals but below-average $\Delta(TW - I_n)$ during other time intervals. This lack of strong, stable spatial trends is evident from both parametric and non-parametric statistical comparisons of $\Delta(TW - I_n)$ between the top and bottom groups (table C.3). The differences in group mean $\Delta(TW - I_n)$ often reverse signs, and many of the p-values are large.

Table C.3. Results from two-sample t-tests and Mann-Whitney tests comparing, over six intervals, change in total soil water in the top 122 cm subtracted by cumulative net irrigation ($\Delta(TW - I_n)$) at the locations at the top of the topographic transects parallel or perpendicular to corn rows and at the locations at the bottom of the same transects.

Date	Top group mean $\Delta(TW - I_n)$ (mm)	Bottom group mean $\Delta(TW - I_n)$ (mm)	t-test p-value (H_a: $\mu_{top} \neq \mu_{bottom}$)	Mann-Whitney test p-value (H_a: top ≠ bottom)
parallel transects				
18 Jun. 2014 to 2 Jul. 2014	-28	-19	3E-02	3E-02
2 Jul. 2014 to 9 Jul. 2014	-12	-13	7E-01	7E-01
9 Jul. 2014 to 17 Jul. 2014	4	14	2E-01	3E-01
17 Jul. 2014 to 30 Jul. 2014	-57	-64	6E-02	1E-01
30 Jul. 2014 to 14 Aug. 2014	-12	-22	2E-01	3E-01
14 Aug. 2014 to 19 Mar. 2015	-18	-14	7E-01	9E-01
perpendicular transects				
18 Jun. 2014 to 2 Jul. 2014	-35	-24	4E-02	3E-02
2 Jul. 2014 to 9 Jul. 2014	-17	-4	4E-02	6E-02
9 Jul. 2014 to 17 Jul. 2014	4	7	7E-01	9E-01
17 Jul. 2014 to 30 Jul. 2014	-58	-57	6E-01	7E-01
30 Jul. 2014 to 14 Aug. 2014	-1	-8	1E-01	1E-01
14 Aug. 2014 to 19 Mar. 2015	-25	-42	8E-02	6E-02

On parallel transects, 18 June to 2 July 2014 was the time interval during which $\Delta(TW - I_n)$ was confidently larger in the bottom group than in the top group, with an 8 mm difference in group means. 17 July to 30 July 2014 was the time interval during which $\Delta(TW - I_n)$ was confidently larger in the top group than in the bottom group, with a 7 mm difference in group means.

On perpendicular transects, both 18 June to 2 July 2014 and 2 July to 9 July 2014 were the time intervals during which $\Delta(TW - I_n)$ was confidently larger in the bottom group than in the top group, with 11 mm and 13 mm differences in group means, respectively. 14 August 2014 to 19 March 2015 was the time interval during which $\Delta(TW - I_n)$ was confidently larger in the top group than in the bottom group, with an 18 mm difference in group means.

Interestingly, for both the parallel and perpendicular transects, $\Delta(TW - I_n)$ was smaller in the bottom group than in the top group during the non-irrigated period. By 19 March of the next year, nevertheless, cumulative $\Delta(TW - I_n)$ had become approximately the same among topographic groups.

C.2.3. Other Applications of Variable Rate Irrigation in Variable Topography

Besides adapting to spatial heterogeneity of *R* that results from soil formation differences, variable rate irrigation (VRI) has other applications in variable topography. One such application is the improvement of infiltration uniformity. With a conventional irrigation (CI; i.e., non-site-specific irrigation) center pivot, infiltration of irrigation water is managed by lateral length, sprinkler wetted diameter, system capacity, and timer setting. If there is a small part of the field that is a steep eroded slope with especially low infiltration capacity, a VRI center pivot can slow down over this part and turn off one out of every several of its sprinklers to apply the same depth of water but over a longer time (fig. C.3.; L. Mateos, personal communication, 2014). A negative consequence is an increase in energy consumption for the same volume of water pumped as the operation point shifts away from the best efficiency point. However, if extra amounts of water had been applied under CI to this part or to the whole field to avoid drought stress in this part

of the field, then implementing this application of VRI could lead to a net decrease in energy consumption. Without variable frequency drive (VFD) technology, an additional negative consequence is a reduction in system capacity, which can be precious during peak evapotranspiration periods. In short, this application of VRI might be useful for addressing small areas with particular infiltration problems, but it is by no means a replacement of proper design and management currently recommended for minimizing irrigation runoff.

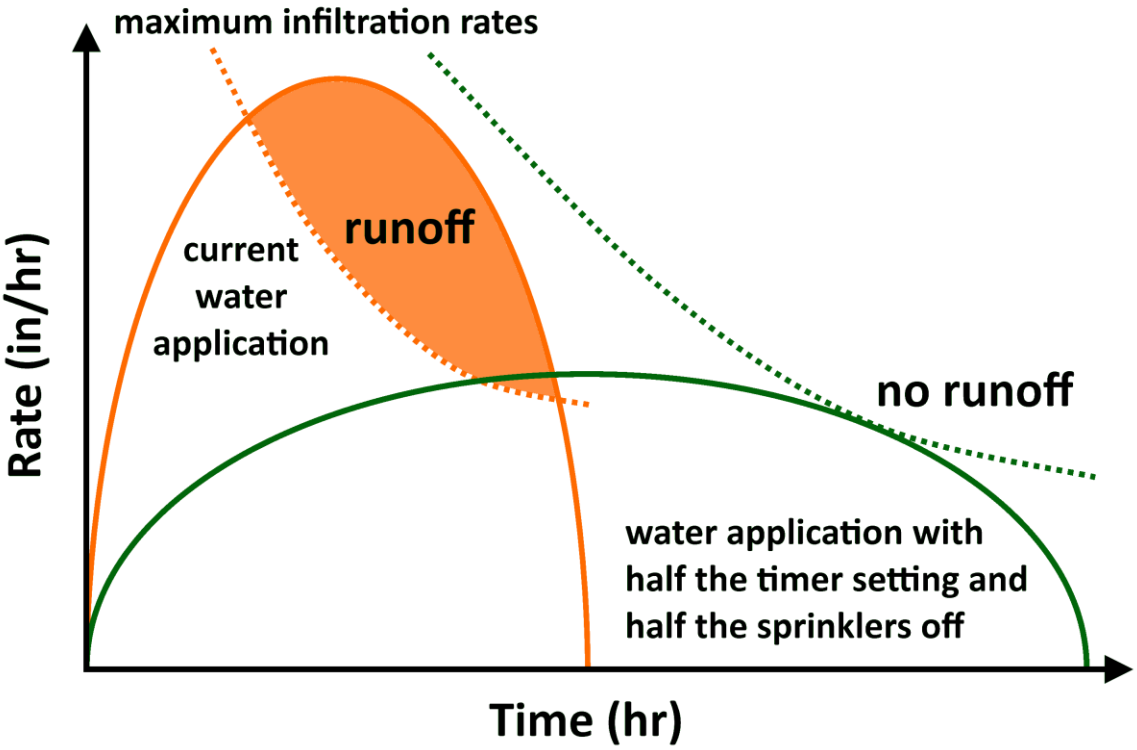

Figure C.3. Conceptual diagram illustrating the use of VRI to apply the same irrigation depth but at lower intensities (e.g., sprinklers pulse with a 50% duty cycle while center pivot lateral travels at half of its normal speed) for reducing runoff in areas with high runoff potential.

Another application of VRI in variable topography is the maintenance of irrigation uniformity in the absence of pressure regulators. Elevation changes are a main source of pressure fluctuations as a center pivot makes its revolution. Conventionally, the strategy has been to supply a constant pressure at the pivot point that is sufficient to

meet the pressure requirement where the minimum lateral pressure in the field occurs. Then, everywhere else in the field with higher lateral pressure, pressure regulators reduce the pressure to the design pressure of the sprinklers. The idea of controlling sprinkler flow rates using the solenoid valves for VRI zone control instead of pressure regulators has been proposed (D. L. Martin, personal communication, 2014). The fraction of time that sprinklers are turned off can be adjusted to maintain the design flow rate despite pressure fluctuations due to elevation changes. A current problem for this application of VRI is the durability of the solenoid valves, which has been mentioned as a challenge faced by center pivot manufacturers (Evans et al., 2013). Also, if the minimum lateral pressure in the field is much lower than the minimum lateral pressure at most angles, the fundamental issue of wasted energy is not resolved. Thus, whereas pressure regulators or solenoid valves can provide uniformity, technologies such as VFD can provide energy savings in fields with topographic variability. Readers are referred to Brar (2015) on the topic of how VFD can reduce pumping energy requirements for center pivots.

C.3. References

Brar, D. (2015). Conservation of Energy Using Variable Frequency Drive for Center Pivot Irrigation Systems in Nebraska. MS thesis. Lincoln, Neb.: University of Nebraska-Lincoln, Department of Biological Systems Engineering.

Evans, R. G., LaRue, J., Stone, K. C., & King, B. A. (2013). Adoption of site-specific variable rate sprinkler irrigation systems. *Irrig. Sci.*, 31(4), 871-887.

Hedley, C. B., & Yule, I. J. (2009). A method for spatial prediction of daily soil water status for precise irrigation scheduling. *Agric. Water Mgmt.*, 96(12), 1737-1745. doi: 10.1016/j.agwat.2009.07.009

Kranz, W. L., Martin, D. L., Irmak, S., van Donk, S. J., & Yonts, C. D. (2008). Minimum Center Pivot Design Capacities in Nebraska. NebGuide G1851. Lincoln, Neb.: University of Nebraska–Lincoln. Retrieved from http://ianrpubs.unl.edu/live/g1851/build/g1851.pdf

Vachaud, G., Passerat de Silans, A., Balabanis, P., & Vauclin, M. (1985). Temporal Stability of Spatially Measured Soil Water Probability Density Function. *Soil Sci. Soc. America J.*, 49(4), 822-828. doi: 10.2136/sssaj1985.03615995004900040006x

APPENDIX D: SOIL AND TOPOGRAPHIC VARIABILITY WITHIN CENTER PIVOTS IN SOME WESTERN NEBRASKA COUNTIES [2]

D.1. Introduction and Methods

Soil and topographic variability within > 60 ac. center pivot irrigated fields of western Nebraska was examined. One hundred pivots of this size, as mapped by CALMIT (2007), were randomly sampled without replacement from seven counties (fig. D.1 and table D.1) spanning seven Natural Resources Districts (NRDs; NARD, 2012). Three statistics indicating degree of soil complexity and three statistics indicating propensity for lateral redistribution of water were calculated in each of these sampled pivots.

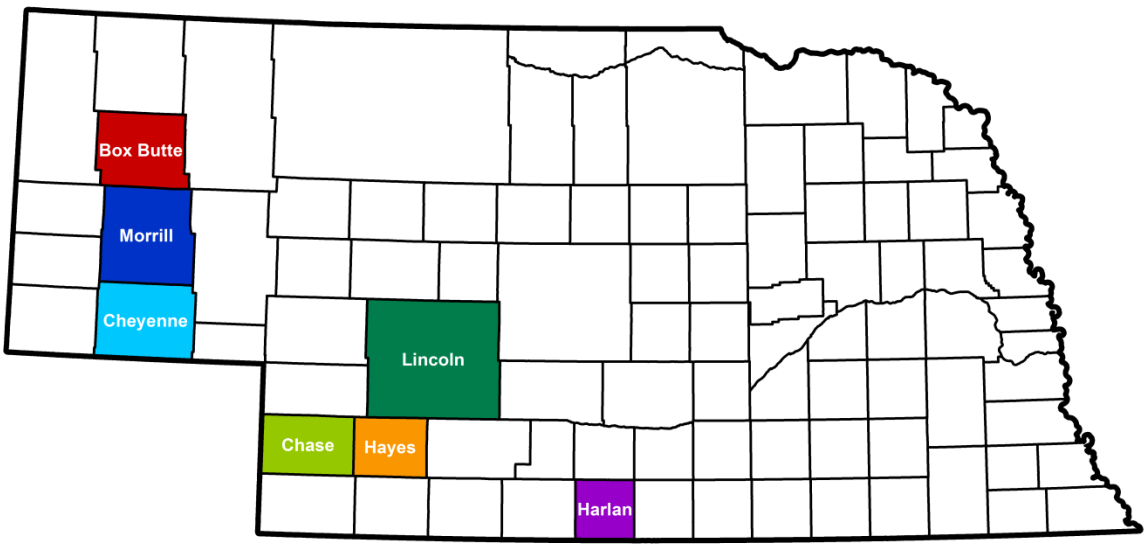

Figure D.1. The seven selected counties of Nebraska (NRCS, 2009).

[2] Previous version submitted as a class project for AGEN 896 Site-Specific Crop Management in the fall semester of 2013

Table D.1. The seven selected counties of Nebraska.

County	Natural Resources District(s)	# of Pivots > 60 ac.	Area Under Allocation
Box Butte	Upper Niobrara White	1152	Most
Chase	Upper Republican	1325	All
Cheyenne	South Platte	447	All
Harlan	Lower Republican	539	All
Hayes	Middle Republican	442	All
Lincoln	Twin Platte and Middle Republican	1508	Some
Morrill	North Platte	671	Some

Other data inputs are a Nebraska counties' boundaries shapefile (NRCS, 2009), National Elevation Dataset digital elevation models (DEMs; USGS, n.d.), and Soil Survey Geographic database (SSURGO; NRCS, 2012) spatial and tabular data.

The textural classes of the soil map units were extracted from their names (e.g. "Hastings silt loam, 0 to 1% slope" → "silt loam"). Whenever a sampled pivot contains a map unit whose textural class was not recognized from its name, this pivot is discarded and replaced by a newly sampled pivot. This procedure may have resulted in a bias for pivots with simpler soil map units.

The 10 m DEMs were used because the 3 m DEMs did not completely cover the state of Nebraska at the time the files were downloaded, so some microtopographic details might be lost due to the coarse grid size. The cumulative probabilities were assigned to observed values of the three topographic statistics using the Gringorten formula with a = 0.40 because the underlying distributions are unknown (Chin, 2006).

D.2. Degree of Soil Complexity

The first two statistics presented are the number of map units and unique map units within the pivot area. They could be related to the magnitude of management scale and the number of management treatments. Line graphs rather than bar graphs were used

because the relatively large range of observed values would make the latter format difficult to read.

Three categories of counties based on the most common number of map units within the pivot area are suggested by figure D.2. Box Butte, Cheyenne, Hayes, and Morrill Counties have distributions that are roughly centered at around eight map units per pivot, and significant proportion of the sampled pivots in these counties have even more map units within them. In contrast, the sampled pivots in Chase and Harlan Counties tend to have fewer map units, and the distributions peak between three to five map units per pivot. Lincoln County is the unusual one here, with a distribution that peaks at one map unit per pivot and follows a generally declining trend beyond that.

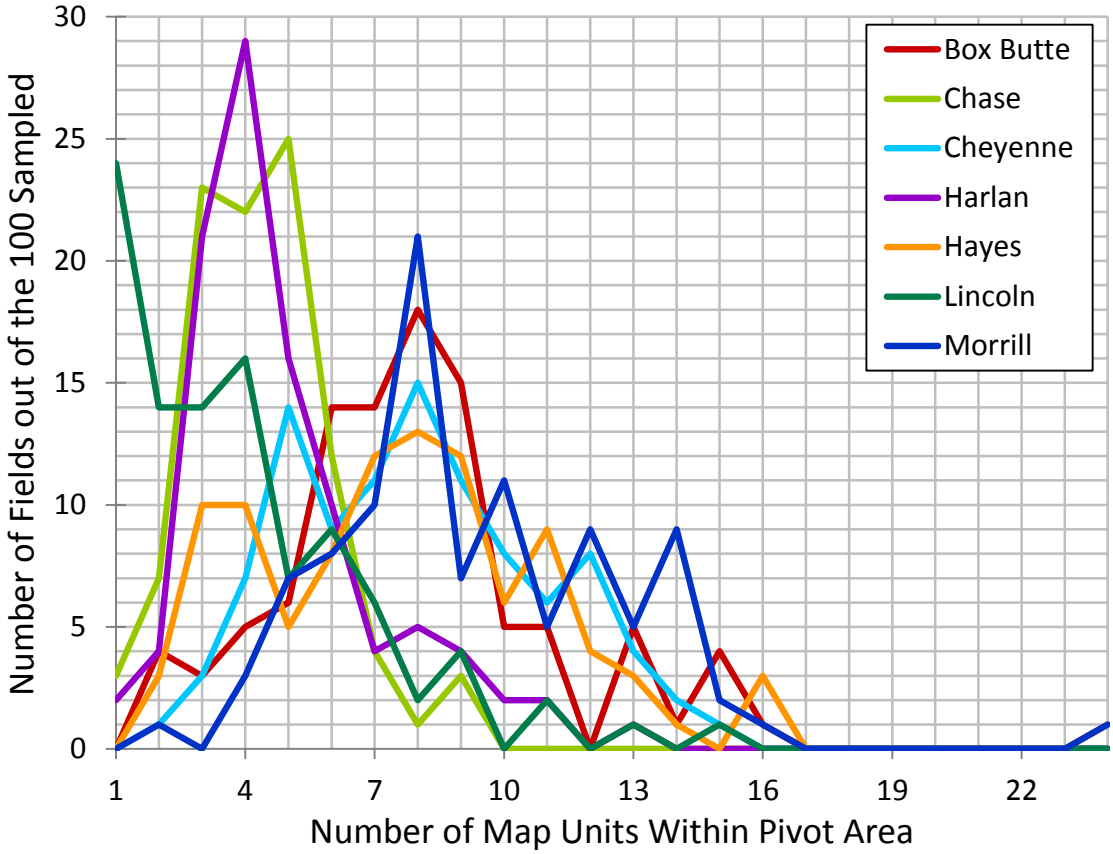

Figure D.2. Frequency distribution of the number of map units within pivot area.

Lincoln County stands out in figure D.3 as well. Its distribution steadily decreases as the number of unique map units per pivot area increases. The other six counties form a continuum of distributions. The progression of shortening peaks and rightward shifting is especially evident from Harlan to Chase to Hayes to Box Butte/Cheyenne to Morrill Counties.

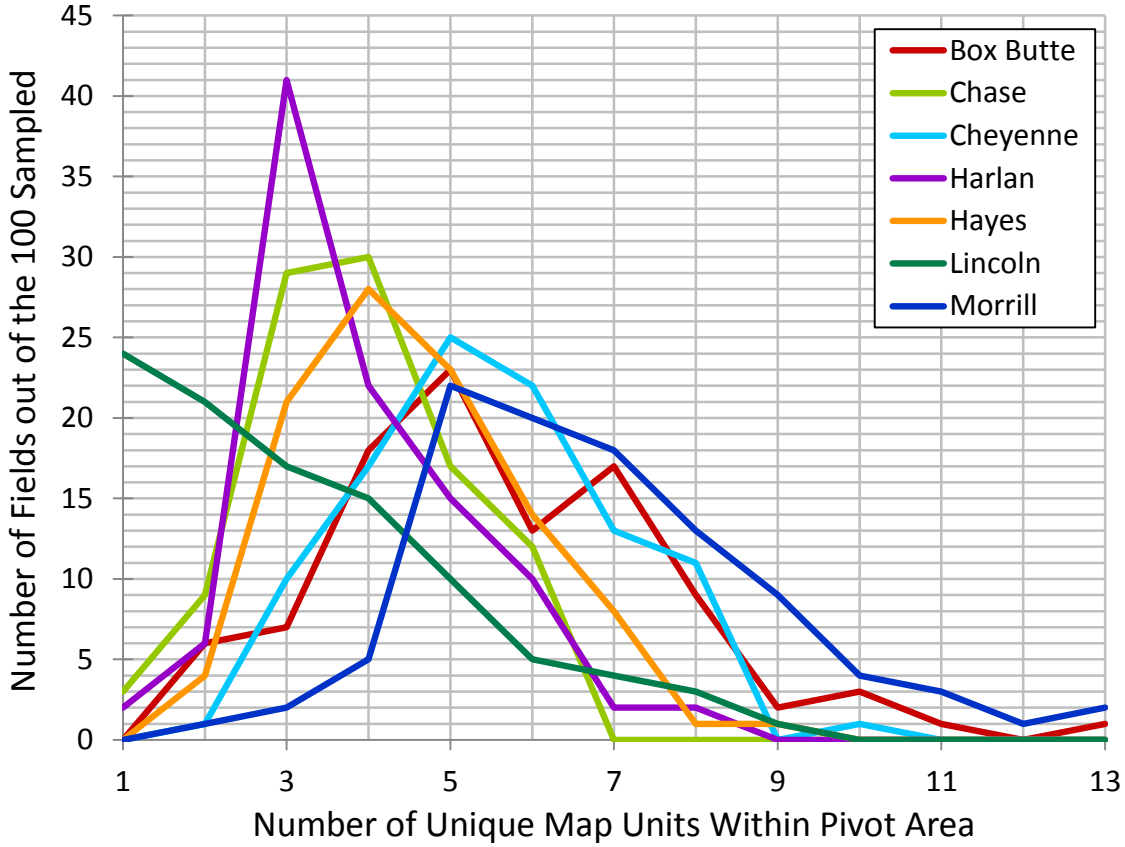

Figure D.3. Frequency distribution of the number of unique map units within pivot area.

The third statistic presented is the number of textural classes within the pivot area (fig. D.4). The sand-silt-clay composition of a soil affects its infiltration capacity and water retention, so fields with more textural classes may exhibit greater variability in plant-available moisture content (Famiglietti et al., 1998). With VRI, farmers can take advantage of this discrepancy and irrigate differentially (i.e. primarily targeting the lighter textured soils) during the early and late season. Based on the first two statistics,

readers might have expected Lincoln County's pivots to contain the fewest number of textural classes. Yet in order of decreasing textural diversity, the counties are Morrill, Chase/Hayes, Box Butte, Cheyenne, Lincoln, and Harlan. Highlighting the extremes, more than 80% of the sampled pivots in Morrill County have more than one textural class in them, whereas almost all of the sampled pivots in Harlan County contain just one textural class.

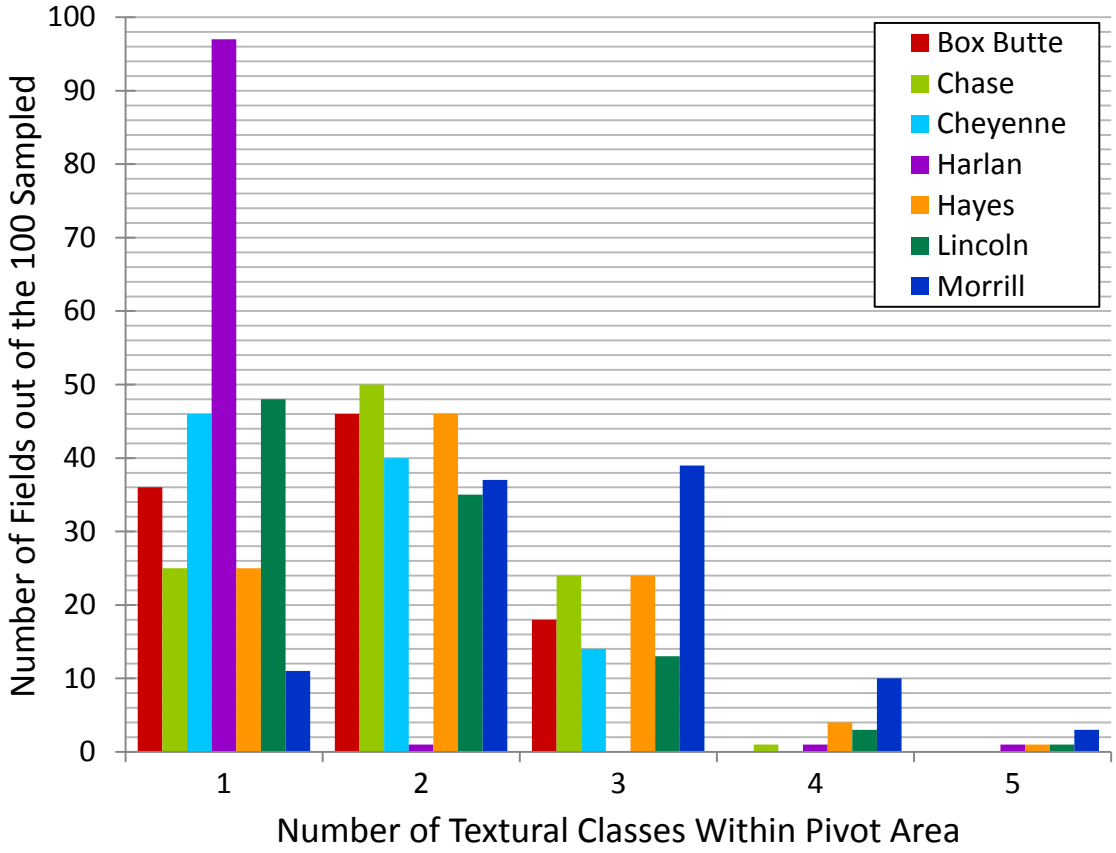

Figure D.4. Histogram of the number of textural classes within pivot area.

Even though it is important to remember that variable rate irrigation requires site-specific decision-making and management, this study seems to suggest that some counties have greater degrees of soil complexity than other counties. The three largest contiguous map units in the Lincoln County soil survey comprise about 22%, 18%, and 4% of the total survey area, respectively (fig. D.5a). In contrast, the three largest contiguous

map units in the Morrill County soil survey comprise about 6%, 1%, and 0.9% of the total survey area, respectively (fig. D.5b). This information might contribute to the explanation of why Lincoln County pivots appear to contain fewer map units and unique map units.

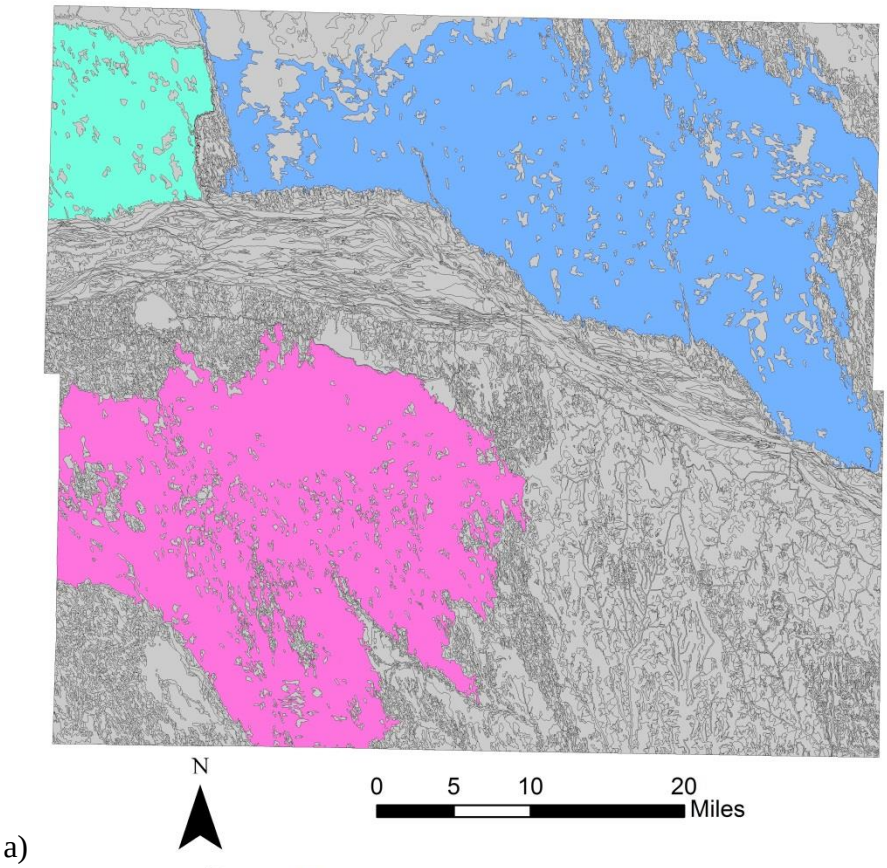

a)

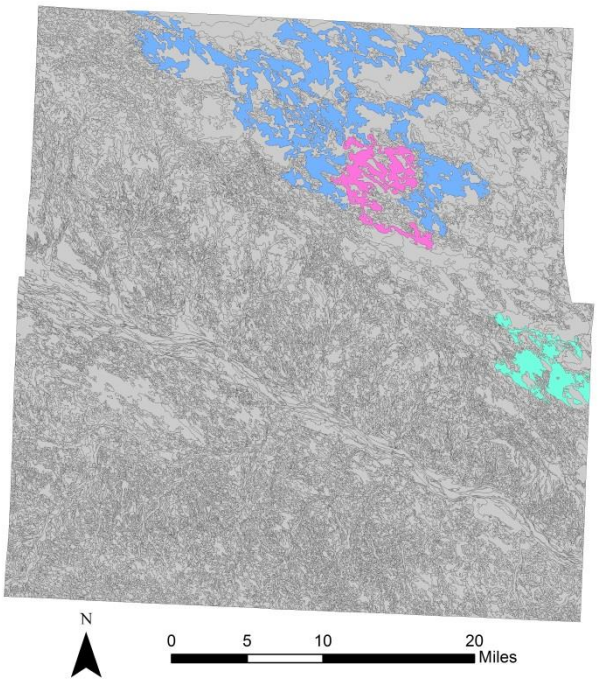

b)

Figure D.5. The first (blue), second (pink), and third (green) largest contiguous map units in a) Lincoln and b) Morrill Counties (NRCS, 2012); the counties are drawn to scale.

On one hand, over 95% of Harlan County is composed of soil associations dominated by silt loam soils (i.e. the Holdrege, Holdrege-Coly-Uly, and Hord-Cozad-Hall associations) (SCS, 1974; fig. D.6a). On the other hand, a mix of loamy sand and sandy loam (coexisting in almost 70% of sampled pivots) predominates in Morrill County except in a mostly sand region in the northeast occupying roughly 30% of the county area (fig. D.6b). A deep understanding of the local soil forming factors (Jenny, 1941) may facilitate the prediction of the degree of soil complexity within center pivot irrigated fields in different counties.

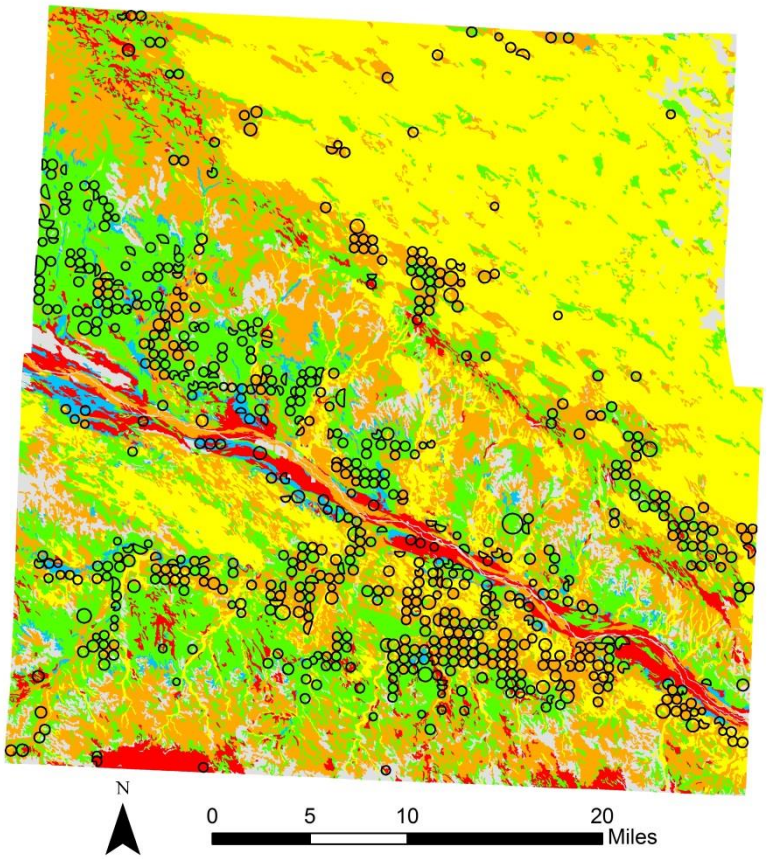

a)

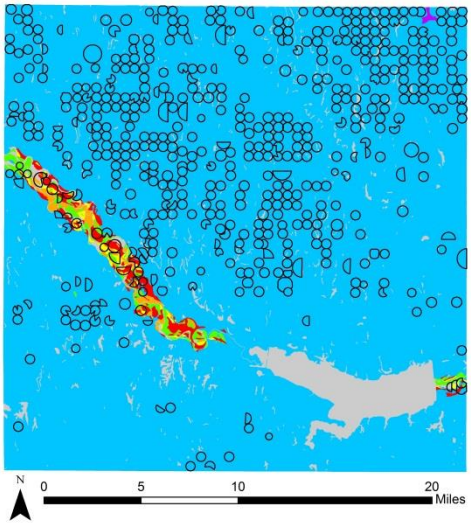

b)

Figure D.6. Geographic distribution of various soil textural classes throughout a) Morrill and b) Harlan Counties: loam (red), loamy sand (orange), sand (yellow), sandy loam (green), silt loam (blue), silty clay loam (purple), and not recognized (grey); the counties are drawn to scale.

D.3. Propensity for Lateral Redistribution of Water

Topography plays a major role in influencing the lateral redistribution of water through surface and subsurface flow. For surface runoff, terrain affects the opportunity time for infiltration as well as the direction, speed, and depth of flow.

The fourth statistic presented is the standard deviation in slope within the pivot area (fig. D.7). Slope steepness can alter the volume of depression storage (Onstad, 1984) and the speed of the surface flow (cf. Manning's equation for open channel flow). Assuming infiltration excess to be the dominant mechanism for runoff generation (Horton, 1933), perhaps the standard deviation in slope within the pivot area would hint at the magnitude of the variability in runoff and erosion propensity inside a field. The standard deviations in slope within the sampled pivot areas in Cheyenne County were generally the least and also had the narrowest spread. Half of the sampled pivots in this county had a standard deviation in slope between 0.75% and 1.25%. In order of generally increasing standard deviation in slope within the sampled pivot areas, the counties were Cheyenne, Box Butte, Chase, Morrill, Hayes, Lincoln, and Harlan. Notably, the sampled pivot area with the smallest standard deviation in slope as well as the sampled pivot area with the largest standard deviation in slope are both found in Harlan County.

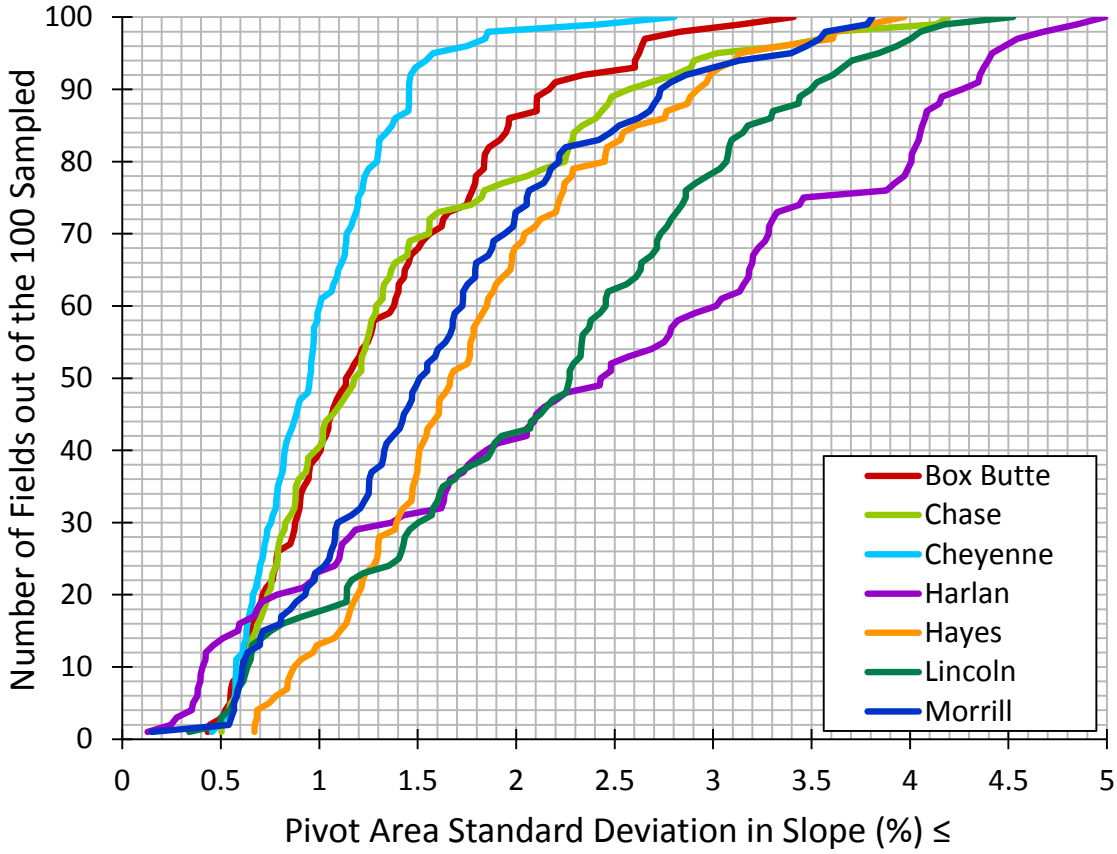

Figure D.7. Cumulative distribution functions for pivot area standard deviation in slope.

The fifth statistic presented is the standard deviation in flow accumulation within the pivot area (fig. D.8). Here, one flow accumulation unit is equal to 100 m^2 of upslope contributing area because the DEM grid size was 10 m (USGS, n.d.). When the soil is relatively wet, flow to areas of topographic convergence may be substantial and might cause the moisture content there to rise significantly (Grayson et al., 1997). The standard deviation in flow accumulation would, therefore, relate to the soil moisture variability inside a field. In the graph, Chase, Cheyenne, Box Butte, Lincoln, and Morrill Counties form a cluster characterized by relatively small standard deviations in flow accumulation within the sampled pivot areas. In contrast, the sampled pivot areas in Hayes County and even more so in Harlan County have larger standard deviations in flow accumulation.

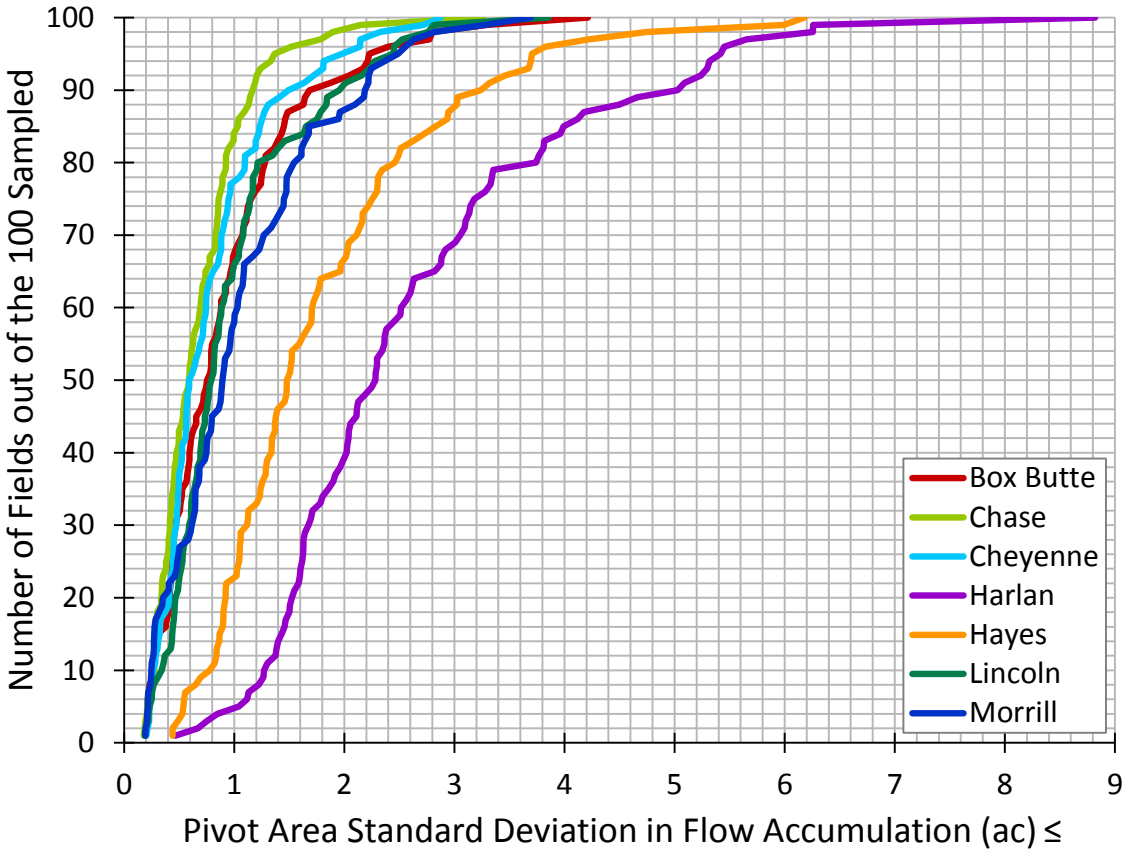

Figure D.8. Cumulative distribution functions for pivot area standard deviation in flow accumulation.

The last statistic presented is the standard deviation in flow length within the pivot area (fig. D.9). Here, upstream locations have small values whereas downstream locations have high values. The scientific literature suggests that longer slopes may infiltrate a larger fraction of the incoming precipitation/irrigation. This phenomenon can be because more areas are underwater and infiltrating at their maximum capacity or because rainfall rate is not constant throughout the infiltration/runoff process (Van de Giesen et al., 2011). Regardless, slope length is expected to affect runoff and the spatial distribution of soil moisture. The sampled pivot areas of Chase, Cheyenne, Lincoln, Box Butte, and Morrill Counties were observed to possess generally smaller standard deviations in flow length than those of Hayes and Harlan Counties.

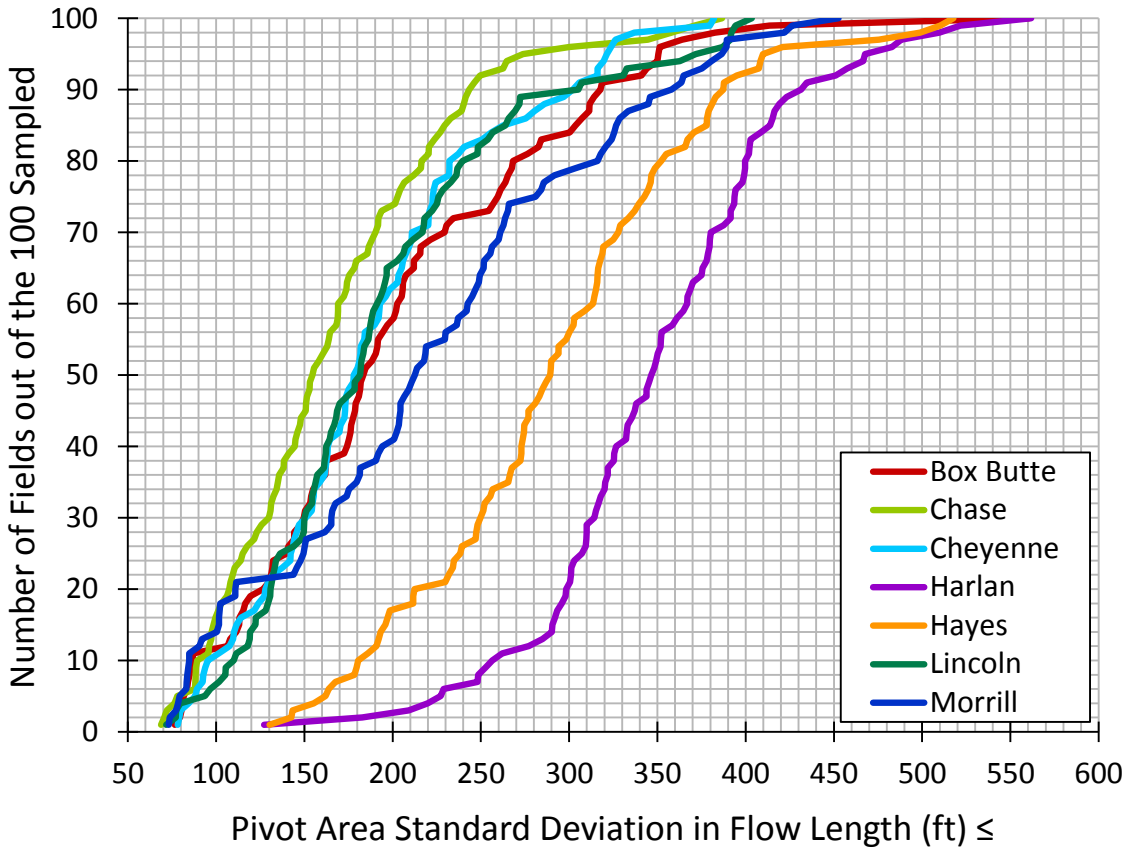

Figure D.9. Cumulative distribution functions for pivot area standard deviation in flow length.

The sampled pivots areas that demonstrate the largest value among all sampled pivots for each of the three statistics of topographic attributes were shown in figure D.10. Surprisingly, the three fields are all in Harlan County. The one with the highest standard deviation in slope shows quite a number of sharp distinct drainageways (fig. D.10a). The one with the highest standard deviation in flow accumulation has a half-mile radius and one main drainageway (fig. D.10c). The one with the highest standard deviation in flow length contains many flow paths that converge after relatively long distance (fig. D.10b). Although these patterns are not the only ways to score high for the three topographic statistics, they might be good archetypes for fields where VRI might be particularly beneficial.

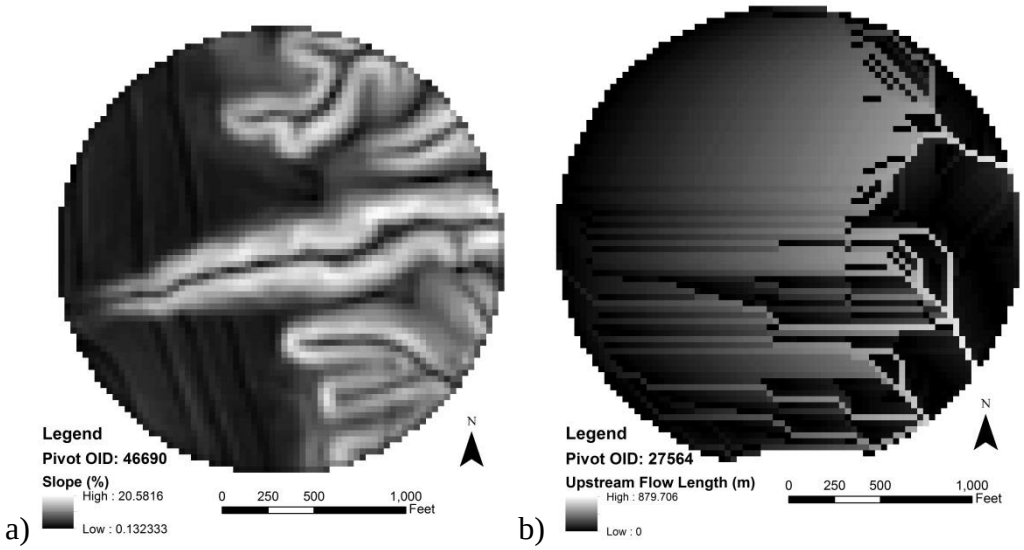

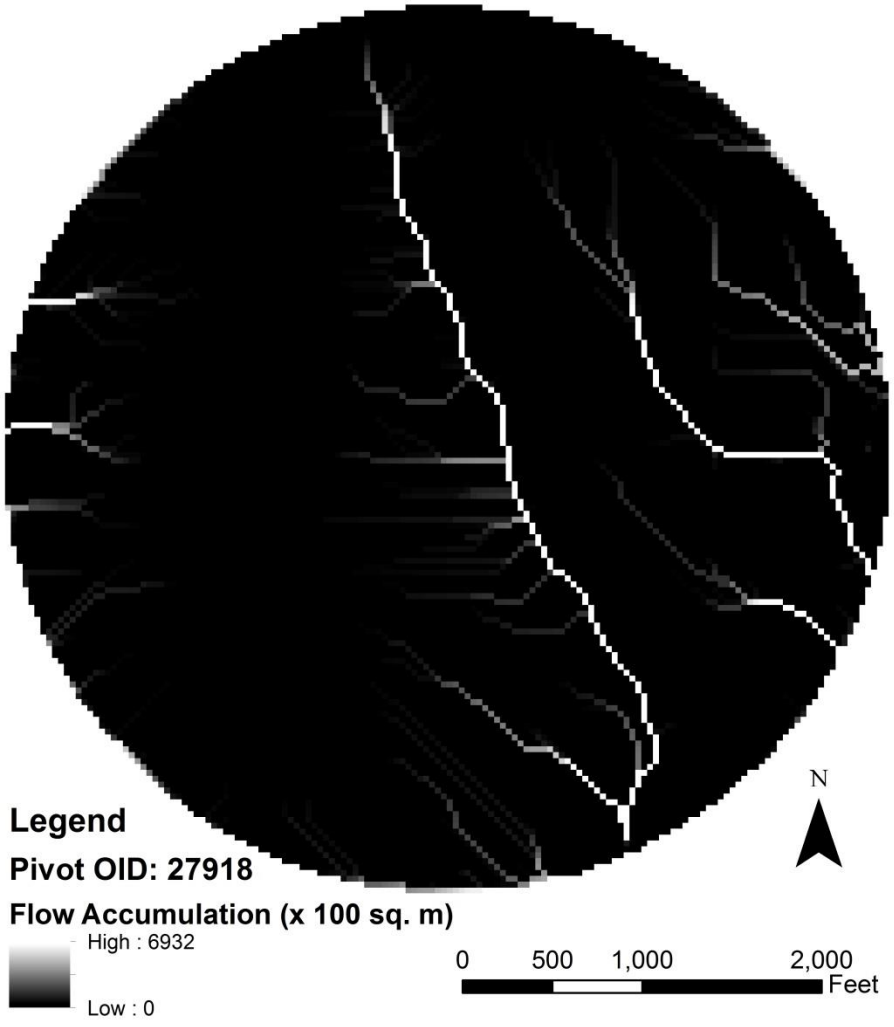

Figure D.10. The sampled pivot areas with the largest standard deviation in a) slope, b) flow length, and c) flow accumulation; the pivot areas are drawn to scale, with the diameter of the pivot area in figure D.10c being twice as long as the diameter of the pivot areas in figures D.10a and D.10b.

Finally, the DEMs (USGS, n.d.) reveal that Harlan County (fig. D.11a), whose sampled pivots scored high on all three topographic statistics, has considerably more convergent topographic features than both Chase (fig. D.11b) and Cheyenne (fig. D.11c) Counties, whose sampled pivots generally scored low on the three topographic statistics.

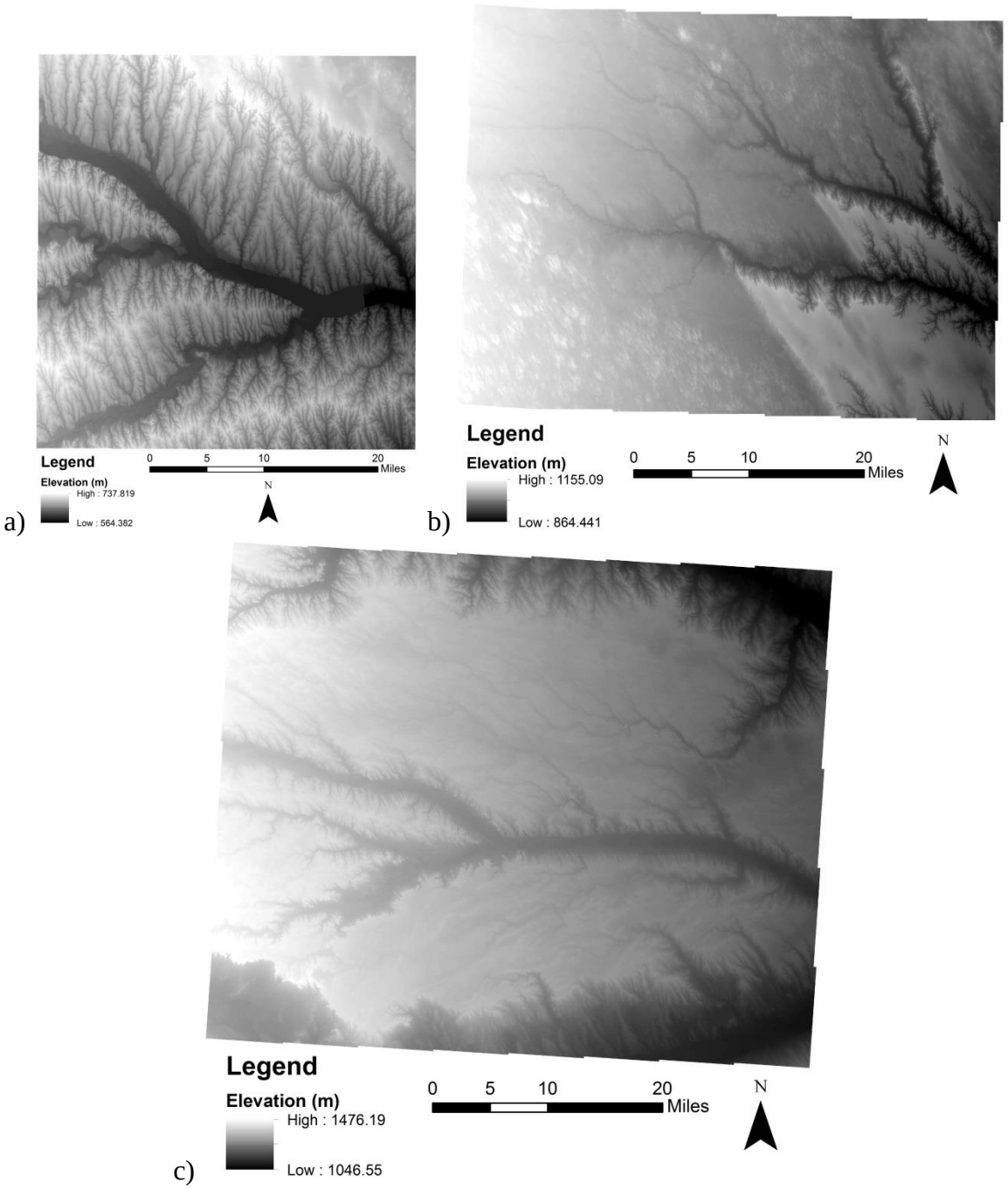

Figure D.11. Digital elevation models of a) Harlan, b) Chase, and c) Cheyenne Counties (USGS, n.d), drawn to scale.

D.4. References

CALMIT. (2007). 2005 Nebraska Center Pivot Irrigation Systems. Lincoln, Neb.: University of Nebraska–Lincoln. Retrieved from ftp://dnrftp.dnr.ne.gov/pub/data/state/IrrigatedPivots2005.zip

Chin, D. A. (2006). *Water Resources Engineering*. 2nd ed. Upper Saddle River, N.J.: Pearson Education.

Dunne, T., Zhang, W., & Aubry, B. F. (1991). Effects of Rainfall, Vegetation, and Microtopography on Infiltration and Runoff. *Water Resources Res*., 27(9), 2271-2285. doi: 10.1029/91WR01585

Famiglietti, J. S., Rudnicki, J. W., & Rodell, M. (1998). Variability in surface moisture content along a hillslope transect: Rattlesnake Hill, Texas. *J. Hydrology*, 210, 259-281. doi: 10.1016/S0022-1694(98)00187-5

Grayson, R. B., Western, A. W., Chiew, F. H., & Blöschl, G. (1997). Preferred states in spatial soil moisture patterns: Local and nonlocal controls. Water Resources Res., 33(12), 2897-2908. doi: 10.1029/97WR02174

Horton, R. E. (1933). The Rôle of Infiltration in the Hydrologic Cycle. *Trans., American Geophysical Union*, 14, 446-460. doi: 10.1029/TR014i001p00446

Jenny, H. (1941). *Factors of Soil Formation: A System of Quantitative Pedology*. New York, N.Y.: McGraw-Hill.

NARD. (2012). 2012 NRD Groundwater Management Summary. Lincoln, Neb.: Nebraska Association of Resources Districts. Retrieved from http://nrdnet.org/DOCS/FILE/groundwater%20managment%20summary%202012-reduced%20size.pdf

NRCS. (2009). Processed TIGER 2002 Counties plus NRCS additions. Washington, D.C.: United States Department of Agriculture. Retrieved from http://datagateway.nrcs.usda.gov

NRCS. (2012). Soil Survey Geographic (SSURGO) database. Washington, D.C.: United States Department of Agriculture. Retrieved from http://datagateway.nrcs.usda.gov

Onstad, C. A. (1984). Depressional Storage on Tilled Soil Surfaces. *Trans. ASAE*, 27(3), 729-732. doi: 10.13031/2013.32861

SCS. (1974). Soil Survey of Harlan County. Washington, D.C.: United States Department of Agriculture. Retrieved from http://www.nrcs.usda.gov/Internet/FSE_MANUSCRIPTS/nebraska/harlanNE1974/HarlanNE1974.pdf

USGS. (n.d). National Elevation Dataset. Retrieved from http://datagateway.nrcs.usda.gov

Van de Giesen, N., Stomph, T. J., Ajayi, A. E., & Bagayoko, F. (2011). Scale effects in Hortonian surface runoff on agricultural slopes in West Africa: Field data and models. *Agric., Ecosystems & Environ.,* 142(1-2), 95-101. doi: 10.1016/j.agee.2010.06.006